THE EFFECT OF FIXATION ON THE MORPHOLOGY OF THE LATE PREMOLT AND EARLY POSTMOLT CUTICLE OF THE BLUE CRAB, *CALLINECTES SAPIDUS*

SHANNON MODLA

A Thesis Submitted to the
University of North Carolina Wilmington in Partial Fulfillment
Of the Requirements for the Degree of
Master of Science

Department of Biology and Marine Biology

University of North Carolina Wilmington

2006

Approved by

Advisory Committee

Robert D. Roer Thomas H. Shafer

Richard M. Dillaman
Chair

Accepted by

Robert D. Roer
Dean, Graduate School

This thesis has been prepared in the style and format

consistent with the journal

Journal of Morphology

TABLE OF CONTENTS

ABSTRACT

The dorsal carapace from late premolt (D_3) and early postmolt (1 hr) blue crabs (*Callinectes sapidus*) was used to study the effects of fixation on the morphology of the epicuticle, exocuticle, and hypodermis. Tissues were freshly dissected, quick-frozen in liquid nitrogen, or lyophilized. They were then treated with a standard fixation consisting of sequential fixation in glutaraldehyde, osmium tetroxide, tannic acid and uranyl acetate or with a uranyl acetate primary fixative. Lyophilized-unfixed and lyophilized-rehydrated tissues were also examined. Treatments were viewed using transmission and scanning electron microscopy. Standard fixation preserved both cuticle fibers and cellular elements. Results varied due to the impervious nature of cuticle and the formation of a permeability barrier by 1 hr postmolt. Uranyl acetate fixation greatly improved the contrast of fibers and enhanced the visualization of calcification initiation sites at the epicuticle-exocuticle interface and along the interprismatic septa (IPS), but it did not preserve the hypodermis. The IPS varied in staining intensity among samples, but overall fixation was more uniform than standard fixation. Both treatments revealed a diverse collection of fiber types. Anaglyphs showed that horizontal fibers, oriented parallel to the cuticle surface, rotated in successive planes while vertical fibers were oriented perpendicular to the cuticle surface. Of the vertical fiber types observed, some were associated with pore canals, others were not, and certain ones were restricted to specialized regions of the cuticle. Quick-freezing caused voids to occur between horizontal fibers. Voids were accentuated by lyophilization. The cuticle was more distorted by voids when it was quick-frozen or lyophilized and treated with standard fixation than with uranyl acetate fixation. Unfixed lyophilized samples had a unique tubular morphology that exhibited a lamellar periodicity. Rehydration of lyophilized cuticles reconstituted the fibrous matrix, with all fiber types being preserved except

the IPS. Fibers in this treatment appeared most similar to uranyl acetate fixations but were more dispersed. Although the tubular morphology of unfixed, lyophilized samples appears to be an artifact of quick-freezing, it speaks to the highly hydrated nature of the cuticle at the time of ecdysis.

ACKNOWLEDGEMENTS

I would like to thank the members of my committee, Dr. Dillaman, Dr. Shafer, and Dr. Roer, for their welcomed advice and constructive criticism. Also, a special thanks to Mark Gay, who not only taught me all the skills in the microscopy lab but also was a good friend outside of the lab. He was always willing to help and solve any problems that I may have encountered along the way.

My parents, John and Shannon Modla, were continuously encouraging me and offering their support during my transition to graduate school and throughout the past two years.

I would also like to thank my fellow graduate students, especially Lindsay Faircloth, Al Nyack, and Samantha Johnson, whose friendship and humor made the last two years a fun and enjoyable experience.

Finally, my thanks go to Tracie, Lori, Debbie, Eleanor, and Carol who welcomed my baking obsession and were always willing to test new recipes.

LIST OF TABLES

LIST OF FIGURES

INTRODUCTION

The crustacean integument consists of a mineralized extracellular matrix overlaying a simple epithelium called the hypodermis that is columnar when actively depositing cuticle. The matrix, or cuticle, is subdivided into four layers: epicuticle, exocuticle, endocuticle, and membranous layer (Green & Neff, 1972). The outermost epicuticle is composed of lipids and proteins and forms a thin barrier that separates the matrix from the external environment (Travis, 1963). The remainder of the cuticle, or procuticle, is a composite of chitin fibers embedded in a proteinacous ground substance (Weis-Fogh, 1970). In the dorsal carapace, the epicuticle, exocuticle, and endocuticle are impregnated with calcium carbonate crystals in the form of calcite and/or amorphous calcium carbonate (Travis, 1963; Dillaman et al., 2005).

Although the dorsal carapace is the region most often studied, cuticle from other anatomical locations varies in its composition, deposition, and degree of mineralization. For instance, the arthodial membrane is the cuticle that forms the joints of the appendages. Although the arthrodial membrane has the same layers and is synthesized concurrently with the dorsal carapace, it remains uncalcified to maintain the flexibility and mobility of the appendages (Williams et al., 2003). Both the cuticle that lines the branchial chamber and the gill epithelium are also unmineralized. However, unlike the arthrodial membrane, they are only composed of epicuticle and exocuticle and fail to deposit new cuticle after ecdysis (Andrews & Dillaman, 1993; Elliot & Dillaman, 1999). In the gill epithelium, the onset of new cuticle synthesis is delayed relative to the dorsal carapace so as to prolong efficient gas exchange by maintaining a minimal diffusion distance (Andrews & Dillaman, 1993). Regional variations in cuticle morphology

demonstrate that the exoskeleton is a heterogeneous structure, selectively modified to accommodate the physiological demands of the organism.

The chitin-protein fibers that constitute the procuticle are organized in a hierarchical fashion. At the molecular level, polymers of α-chitin crystals (N-acetyl-β-D-glucosamine) are arranged in an anti-parallel configuration to form microfibrils consisting of approximately 20 chitin chains stabilized by hydrogen bonds (Merzendorfer & Zimoch, 2003). The chitin rods are surrounded by a sheath of protein subunits that form a helix around the chitin core (Blackwell & Weih, 1980). The chitin-protein microfibrils then bundle together and form larger fibrils. In the exocuticle, fibrils coalesce to create a reticular structure, whereas in the endocuticle, they form a fibrillar structure (Giraud-Guille, 1984). At the microscopic level, fibrils oriented parallel to the surface of the cuticle continuously rotate in successive planes so as to form a helicoidal or plywood-like arrangement. As a result, distinct lamellae are observed when the cuticle is cross-sectioned. When sectioned at an oblique angle, fibrils form a series of nested arcs, which have been considered a sectioning artifact caused by the overlap of fibrils in adjacent planes (Bouligand, 1972; Giraud-Guille, 1994). Although this interpretation is generally accepted, some researchers contend that the arcs are created when fibrils within a plane curve upward to interconnect adjacent lamellae (Locke, 1961; Travis, 1963; Mutvei, 1974).

While fibers constitute the bulk of the procuticle, other specializations can also be found. Penetrating the matrix are numerous pore canals, cytoplasmic extensions arising from the hypodermis. They are considered to be conduits that deliver the components necessary for tanning and mineralization (Travis & Friberg, 1963; Compère & Goffinet,

1987; Dillaman et al., 2005). Over the course of the molt cycle, the pore canals undergo a periodic growth and degeneration so as to exhibit a heterogeneous spatial distribution throughout the time course of cuticle deposition (Compère & Goffinet, 1987).

Although pore canals can be found throughout the cuticle, the interprismatic septa (IPS) are specializations restricted to the exocuticle. The IPS are polygonal outlines presumed to be left by the receding hypodermal cells during cuticle synthesis. Histochemical techniques have demonstrated that the IPS are distinct entities within the cuticle that contain anionic glycosaminoglycans and possibly carbonic anhydrase (Giraud-Guille, 1984). Evidence strongly suggests that they play a critical role during biomineralization (Travis, 1963; Giraud-Guille, 1984; Dillaman et al., 2005). At the onset of mineralization in the blue crab, calcium is first deposited in a stable amorphous phase along the most proximal and distal margins of the exocuticle and the IPS. At later stages, amorphous calcium carbonate is converted into calcite (Dillaman et al., 2005). Consequently, the IPS must inhibit crystallization pre-ecdysis, promote the nucleation of an amorphous phase post-ecdysis and, finally, initiate the conversion of amorphous calcium carbonate into calcite.

The crustacean integument is not a static structure but, rather, it changes regularly with the molt cycle. In order to accommodate growth, reproduction, and larval metamorphosis, crustaceans must shed their old cuticle, synthesize and deposit the organic components of the new cuticle, and mineralize many portions of the nascent exoskeleton during a highly regulated sequence of events. To standardize the processes that occur before, during, and after ecdysis, the molt cycle has been divided into stages (A through E) developed by Drach (1939). Stages D_0-D_4 correspond to a premolt animal

that is preparing for exuviation. At stage E, or ecdysis, the animal crawls out of its old exoskeleton, or exuvia. Stages A_1 and A_2, B_1 and B_2, and C_1-C_3 refer to a postmolt crab that is mineralizing and continuing to deposit post-exuvial cuticle. Finally, stage C_4 is an intermolt crab that exhibits minimal synthetic activity.

Prior to the onset of the molt, the old exoskeleton separates from the underlying hypodermis in a process known as apolysis (D_0), and a molting fluid is released. The molting fluid contains enzymes that digest portions of the old cuticle, giving the animal room to grow and begin the synthesis of the new cuticle (O'Brien & Skinner, 1987, 1988; Compère & Goffinet, 1998). The underlying hypodermal cells undergo a period of mitotic activity to expand the epithelium, causing the epidermis and pre-exuvial cuticle to become highly convoluted under the old exoskeleton (Tchernigovtzeff, 1965). As the new epicuticle and exocuticle are deposited under the old, the organic and inorganic constituents are simultaneously reabsorbed from the old membranous layer and endocuticle (Travis, 1963; Roer, 1980; Greenway et al., 1995). Since the new epicuticle and exocuticle are formed before ecdysis, they are collectively called the pre-exuvial cuticle (Drach, 1939). At ecdysis, the animal sheds its old cuticle and takes up water to expand the highly folded pre-exuvial cuticle (Mykles, 1980; Taylor & Kier, 2003). During the postmolt stages, the pre-exuvial layers are tanned and then mineralized with calcium salts (Roer & Dillaman, 1993). The endocuticle is calcified as it is deposited and, lastly, the unmineralized membranous layer is synthesized (Travis, 1963). The completion of the membranous layer marks the transition to intermolt (C_4) wherein the cuticle is fully formed and calcified, and the hypodermal cells exhibit minimal synthetic activity.

In order for the cuticle to provide crustaceans support and protection, it is transformed into a rigid structure by tanning and calcification. Since the pre-exuvial layers are deposited before the molt but not mineralized until after the molt, a mechanism must exist that allows the animal to control when and where calcification is initiated and how it proceeds. Studies have strongly suggested that the control mechanism is in the cuticle matrix itself and not entirely due to calcium salts being supplied through the cytoplasmic processes of the underlying hypodermal cells (Roer et al., 1988; Roer & Dillaman, 1993). Since the matrix constituents are involved in regulating crystal growth, knowing the morphology and distribution of the cuticle components is of utmost importance. With a clear understanding of the diversity of fibers, their location, and orientation, a spatial relationship can be assigned to the proteins and glycoproteins (Coblentz et al., 1998; Inoue et al., 2001, 2003, 2004) that have been implicated in the control of nucleation and crystal growth.

Previous observations by Dillaman et al. (2005) have revealed that unfixed lyophilized cuticle assumes a morphology unlike cuticle that has been fixed by traditional methods. Lyophilized cuticles display a tubular latticework organization with no semblance of the fibrous matrix generated by fixation. Consequently, the true structure of the cuticle was brought into question, and it became paramount to resolve whether the tubular morphology was an artifact of lyophilization or whether the traditionally accepted fibrous matrix was, itself, an artifact of fixation.

Chemical fixation involves the introduction of agents that preserve molecules through either cross-linkages or coagulation. Since fixatives are limited in their ability to preserve every organic component, a degree of extraction may occur, which can alter the

true structure of the tissue (Hayat, 2000). Moreover, the types and combinations of fixatives used can greatly alter the appearance of tissue by either masking or accentuating particular components (Brodie et al., 1982; Afzelius, 1992; Locke, 1994). For instance, the use of uranyl acetate as a primary fixative greatly enhances the contrast of skeletal muscle and, when used after aldehyde fixation, uranyl acetate allows for the visualization of structures not seen by osmication (Locke, 1994; Fassel & Greaser, 1997). Additionally, tannic acid functions as a mordant to enhance the contrast of glycogen and collagen, but it also masks sites that would otherwise be reactive toward uranyl acetate (Afzelius, 1992).

Lyophilization, on the other hand, is a two stage process whereby samples are quick-frozen and then the vitrified ice is sublimated (Hayat, 2000). Although freezing can introduce possible artifacts through the creation of ice crystals, lyophilization will dehydrate the specimen in a manner that will circumvent the extraction of ionic and organic constituents. Consequently, a larger fraction of the tissue will be retained.

The purpose of this study was to determine the effect of both physical and chemical fixation on the morphology of the late premolt and early postmolt dorsal carapace of the blue crab. Cuticle pieces were freshly fixed, quick-frozen in liquid nitrogen, or quick-frozen and lyophilized. They were then either fixed by standard methods involving sequential fixation in glutaraldehyde, osmium tetroxide, tannic acid, and uranyl acetate or by a uranyl acetate primary fixative or with acetone. Some were left unfixed. By using a combination of treatments, the component fibers making up the crustacean dorsal carapace were revealed, permitting a greater understanding of its overall organization. By providing an enhanced perspective on cuticle morphology, this

study can give a structural framework in which the physiological and biochemical processes governing cuticle deposition and calcification of the dorsal carapace can be understood.

MATERIALS AND METHODS

Cuticle samples from male and female blue crabs (*Callinectes sapidus*; carapace width 9.5-14.5 cm) were obtained from Endurance Seafood in Kill Devil Hills, NC in May 2005 for analysis with transmission (TEM) and scanning electron microscopy (SEM). Cuticle was dissected from the dorso-lateral carapace of late premolt (D_3) and early postmolt (1 hr post-ecdysis) crabs. Premolt crabs were staged as D_3 when light pressure broke the ecdysial suture on the anterior aspect of the ventral carapace. For D_3 crabs, only the pre-exuvial cuticle was sampled. Ten pieces of dorsal carapace were collected from each crab and subjected to different physical and chemical treatments (Table 1). Three pieces were freshly fixed on site, and the remaining seven were placed in cryotubes and quick-frozen in liquid nitrogen. Of the freshly fixed samples, two were fixed with 2.5% glutaraldehyde in 0.2 M sodium cacodylate buffer adjusted to 870 mOsm, pH 7.4, and held in that fixative until further processing. The remaining sample was fixed in 2% aqueous uranyl acetate for two hours and then transferred to 70% acetone. Frozen samples were stored in a -70˚ C freezer until further processing. Five of the frozen samples were lyophilized in a Labconco Freeze Dryer 4.5 and stored in a dessicator.

TEM Specimen Preparation

A summary of tissue treatments is seen in table 1. Briefly, one frozen and one lyophilized sample from each crab were fixed by standard means in 2.5% glutaraldehyde

Table 1. Summary of treatments for premolt and postmolt cuticle prepared for transmission electron microscopy (+ denotes experimental groups).

Chemical Treatment	**Physical Treatment**		
	Freshly Dissected	Quick-Frozen	Lyophilized
Standard	+	+	+
Uranyl Acetate	+	+	+
None			+
Water-Acetone			+

in 0.2 M sodium cacodylate buffer (pH 7.4) overnight. Fresh, frozen, and lyophilized samples fixed in glutaraldehyde were rinsed in 0.2 M cacodylate buffer (pH 7.4) for 15 min before being fixed in 0.5% osmium tetroxide in 0.2 M sodium cacodylate buffer (pH 7.4) for 2 hours. Samples were rinsed in 0.2 M cacodylate buffer (pH 7.4) for 15 min and fixed in 0.15% tannic acid in 0.2 M cacodylate buffer (pH 7.4) for 15 min. The tissue was rinsed in 0.2 M cacodylate buffer (pH 7.4) and distilled water, 15 min each, before being fixed with 2% aqueous uranyl acetate for two hours. They were then dehydrated in an ascending acetone series (50%, 70%, 90%, 100%, 100%; 15 min each) prior to embedding.

One frozen and one lyophilized sample from each crab was fixed for 2 hours in 2% aqueous uranyl acetate and transferred to 70% acetone overnight. Fresh, frozen, and lyophilized samples fixed in uranyl acetate were then dehydrated in an ascending acetone series (90%, 100%, 100%, 15 min each) prior to embedding.

Samples preserved by standard or uranyl acetate fixations were infiltrated with a 1:1 mixture of 100% Spurr's epoxy resin (Spurr, 1969) and 100% acetone for an hour on a rotator. The mixture was replaced with fresh 100% Spurr's epoxy resin, which infiltrated overnight on a rotator. Tissue samples were then placed in fresh 100% Spurr's epoxy resin and polymerized in a 70˚ C oven for 8 hours.

One lyophilized sample from each crab was placed directly in 100% Spurr's epoxy resin without fixation. After the tissue had settled in the resin, it was polymerized for 8 hours in a 70˚ C oven. A second lyophilized sample was rehydrated in distilled water on a rotator for 30 min, then dehydrated in an ascending acetone series (50%, 70%, 90%, 100%, 100%, 15 min each), and infiltrated for one hour with a 1:1 mixture of 100%

Spurr's epoxy resin and 100% acetone on a rotator. These samples were then covered with fresh 100% Spurr's epoxy resin and polymerized in a 70˚ C oven for 8 hours.

The samples were sectioned both tangentially and transversely with a diamond knife on a Reichert-Jung Ultracut E ultramicrotome. Both thin sections (90-100 nm) and thick sections (800 nm) were cut. Thin and thick sections were post-stained with 2% uranyl acetate in 50% ETOH and with Reynolds' lead citrate (Reynolds, 1963).

The tissue was examined with a Philips CM 12 transmission electron microscope in TEM bright field mode at 80 kV for thin (90-100 nm) sections and 100 kV for thick (800 nm) sections. Anaglyphs of thick sections were made by tilting the eucentric specimen with a goniometer and photographing the image at 0˚ and 7˚ or –5˚ and +5˚ tilt angles. Micrographs were taken using Kodak 4489 EM film and developed. Negatives were scanned on a Microtek Scanmaker 8700, and digital images were processed with Adobe Photoshop 7.0.

SEM Specimen Preparation

Tissue pieces fixed on site with 2.5% glutaraldehyde in 0.2 M cacodylate buffer (pH 7.4) were processed as described above for standard fixation with the exception of infiltration with resin. Following dehydration in acetone, the tissue was placed in HMDS (Hexamethyldisilazone) for 15 min and then air-dried on filter paper in a fume hood. Samples were then fractured, mounted fracture-side up on aluminum stubs with colloidal graphite, and sputter-coated with 6 nm platinum/palladium (80/20) in a Cressington 208HR Sputter Coater. One lyophilized sample from each crab was not fixed and was fractured, mounted on aluminum stubs, and sputter-coated as described above. Samples were viewed with a Philips XL30S FEG scanning electron microscope using either the

secondary electron (SE) or through-the-lens detector (TLD) modes with a 5 kV beam, spot size 3.0. Whole cuticle pieces treated by standard fixation for the SEM were also viewed and photographed with a RT SPOT (Diagnostics Instruments Inc.) camera mounted on a Zeiss StemiSV6 polarizing dissecting microscope.

RESULTS

TEM Observations

Throughout all phases of this investigation, comparisons were made between premolt (D_3) and postmolt (1 hr) cuticle. Descriptions of features are the same for both stages, except in a few noted instances. Furthermore, since cuticles from premolt crabs were more highly folded than those from postmolt crabs, obtaining the proper sectioning angle was easier in premolt than in postmolt samples. Consequently, while both premolt and postmolt stages were equally examined, all micrographs presented here were taken from postmolt crabs unless otherwise noted.

Fresh, Standard Fixed Tissue

When dorsal carapace was fixed by standard methods, all regions of the epicuticle, exocuticle, and hypodermis were well preserved. In cross-section, the epicuticle averaged 2.5 μm in thickness and consisted of two distinct layers: (1) a thin 70 nm outer epicuticle and (2) the remaining thick 1.5-2 μm inner epicuticle (Fig. 1a-c). The morphology of the outer epicuticle varied among samples, with some displaying a trilaminar and others a pentalaminar structure. Those with a trilaminar outer epicuticle had a fuzzy surface coat, an electron dense middle layer, and an electron lucent inner layer (Fig. 1a, b, e), and the thickness of the middle and inner layers varied among

Figure 1. TEM of fresh, standard fixed (a, b, c, e, f, g, h) and quick-frozen, standard fixed (d) dorsal carapace. a, b, c. Cross-sections through the epicuticle. Note the variation in the outer epicuticle (oe) and epicuticular roots (er). d. Anaglyph of a tangential section through the inner epicuticle. e, f. Higher magnification of the epicuticle in a and c respectively. Note the variation in the outer epicuticle (oe). g, h. Tangential section through the inner epicuticle (g) and distal exocuticle (h). dense vertical fibers, dvf; epicuticular canal, ec; epicuticular fibers, ef; epicuticular roots, er; exocuticle, Exo; inclusion, i; inner epicuticle, ie; saw-tooth border, arrowhead; termination of filaments within er, arrow

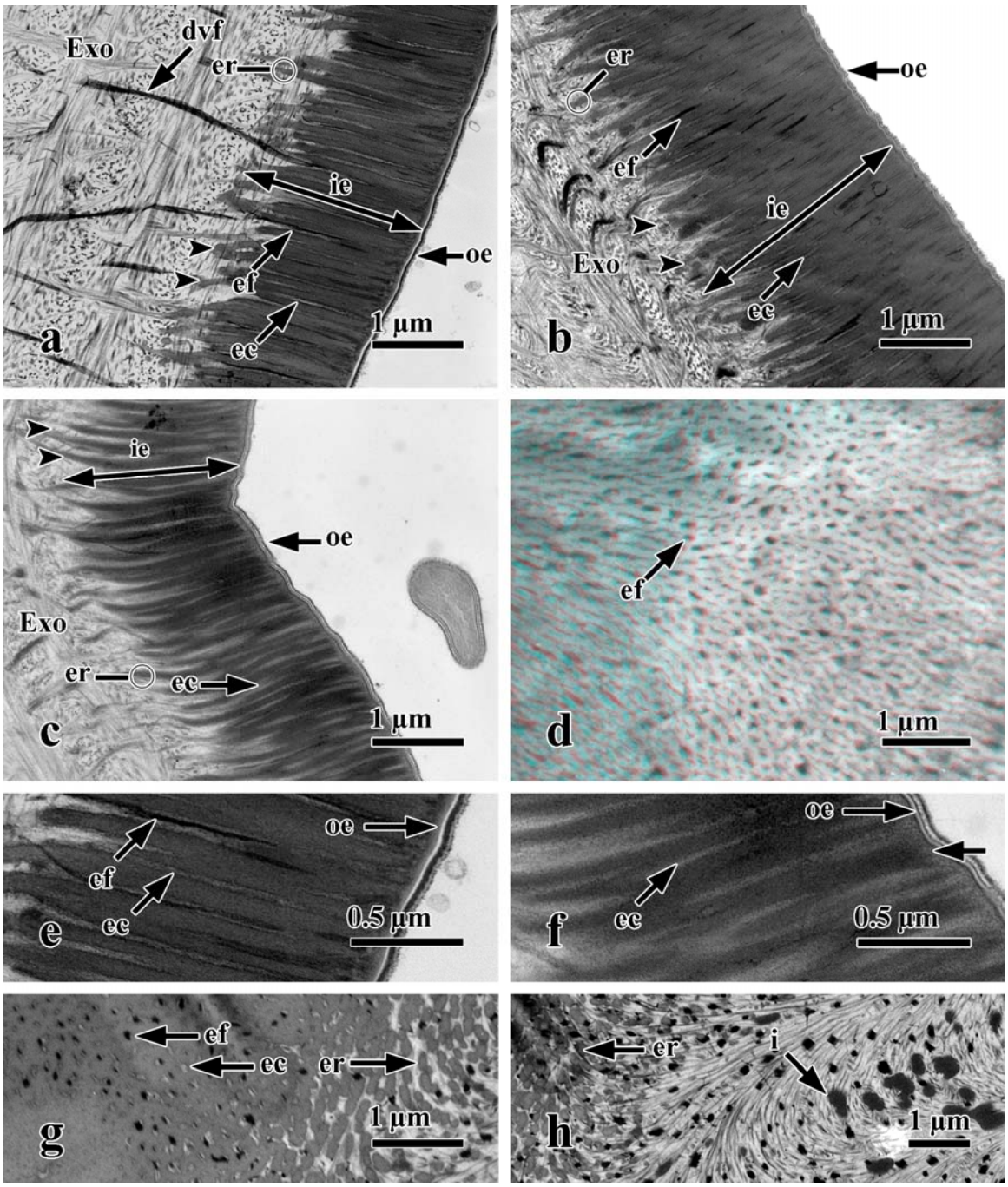
Exo
dvf
er
ie
oe
ef
ec
1 µm
a
er
oe
ef
ie
Exo
ec
1 µm
b
ie
oe
Exo
er
ec
1 µm
c
ef
1 µm
d
oe
ef
ec
0.5 µm
e
oe
ec
0.5 µm
f
ef
ec
er
1 µm
g
er
i
1 µm
h

samples (Fig. 1a, b). Those with a pentalaminar outer epicuticle had three electron dense layers separated from one another by two equal electron lucent layers (Fig. 1c, f).

The morphology of the inner epicuticle also varied among crabs. In some, the inner epicuticle had distinct vertical epicuticular roots (er) oriented perpendicular to the surface and approximately 0.1 μm across (Table 2, Group A). The roots were often separated from one another by a canal-like region of lower electron density (Fig. 1c, f). In other samples, the roots were very closely apposed resulting in a thin canal, thereby giving the inner epicuticle a more homogeneous appearance (Fig. 1a, b, e). The canal often contained an electron dense fiber (Table 2, Group A; ef), some being confined to the epicuticle while others extended into the exocuticle (Fig. 1a, b, e). Anaglyphs of tangential sections through the inner epicuticle revealed that ef's varied in both size and density and were very numerous and randomly spaced (Fig. 1d). At high magnifications, the roots had a faint striated appearance, being composed of bundles of vertical filaments (Fig. 1e). The filaments were sometimes seen terminating about 50 nm from the bottom of the outer epicuticle (Fig. 1f; arrow). Proximal to the exocuticle, the roots tapered conically, creating a saw-tooth border (Fig. 1a-c; arrowheads). Individual horizontal fibers from the exocuticle, oriented parallel to the surface, were seen among the conical ends of the roots.

In tangential sections of the epicuticle, the inner epicuticle appeared as a homogeneous matrix of moderate electron density. In distal regions, the matrix was penetrated by numerous round pores, which corresponded to cross-sections of epicuticular canals (Figs. 1g; 7f). Some pores contained electron dense epicuticular fibers (Fig. 1g). As the epicuticle entered the exocuticle, the homogeneous matrix

became fragmented into discrete round or oblong aggregates, consistent with cross-sections of the vertical epicuticular roots that were located between horizontal fibers of the exocuticle (Fig. 1g, h). Occasionally, irregularly-spaced, electron dense inclusions were observed embedded within the fibrous matrix of the distal exocuticle adjacent to the epicuticle (Figs.1h; 2a; 4a).

The exocuticle consisted of a fibrous network penetrated by cellular pore canals from the hypodermis. Six widespread and two more specialized fiber types were observed in the exocuticle with standard fixation (Table 2). Fiber types were differentiated based on their morphology, orientation, and distribution. The first type of fiber, referred to as bundles of horizontal fibers (bhf), ran parallel to the surface of the cuticle, and these fibers were arranged in a helical pattern. In transverse sections, bhf in successive vertical planes rotated relative to one another so that fibers were cut longitudinally, in cross-section, and at various intermediate angles (Fig. 2a-f). Consequently, for every 180˚ rotation of planes of successive fibers, a single lamella was formed (Fig. 2a, c, e). In transverse sections, lamellae near the epicuticle were noticeably narrower than those located more proximally (Fig. 2a). The bhf within the lamellae in the distal exocuticle were more widely spaced (Fig. 2a, b), whereas those in the medial (Fig. 2c, d) and proximal exocuticle (Fig. 2e, f), especially those closest to the hypodermis (Fig. 3a, b), were more closely packed and therefore appeared more homogeneous. Often found embedded within the first several lamellae adjacent to the hypodermis were round, electron dense bodies 1-1.5 µm in diameter (Figs. 3a; 7b). These round bodies may be pigment granules that were incorporated into the exocuticle during cuticle deposition.

Table 2. Summary of fiber types observed in the epicuticle exclusively (Group A), exocuticle (Group B), or special structures (Group C).

Group	Fiber Type	Abbreviation	Orientation relative to cuticle surface	Location
A	Epicuticular roots	er	perpendicular	Epicuticle
	Epicuticular fibers	ef	perpendicular	Epicuticle
B	Dense vertical fibers	dvf	perpendicular	Epicuticle and upper exocuticle
	Bundles of horizontal fibers	bhf	parallel	Entire exocuticle
	Vertical fibers	vf	perpendicular	Distal and medial exocuticle
	Pore canal sheath	pcs	perpendicular	Medial and proximal exocuticle
	Pore canal fiber	pcf	perpendicular	Proximal exocuticle
	Anchoring fiber	af	perpendicular	Medial and proximal exocuticle
C	Interprismatic septa*	IPS	perpendicular	Distal and medial exocuticle
	Tonofibers**	tf	perpendicular	Entire exocuticle; possibly epicuticle
	Electron dense rods**	r	perpendicular	Distal exocuticle; possibly epicuticle

*Only observed in uranyl acetate fixations

**Limited to specialized regions of the dorsal carapace

Figure 2. TEM of fresh, standard fixed dorsal carapace. Low (a, c, e) and higher (b, d, f) magnifications of cross-sections through the cuticle. Note that lamellae width and the density of horizontal fibers increases from the distal (a) to proximal (e) exocuticle. anchoring fiber, af; bundles of horizontal fibers cut longitudinally, arrowhead; inclusion, i; dense vertical fibers, dvf; exocuticle, Exo; inner epicuticle, ie; lamella, L; pore canal, pc; pore canal fiber, pcf; vertical fibers, vf

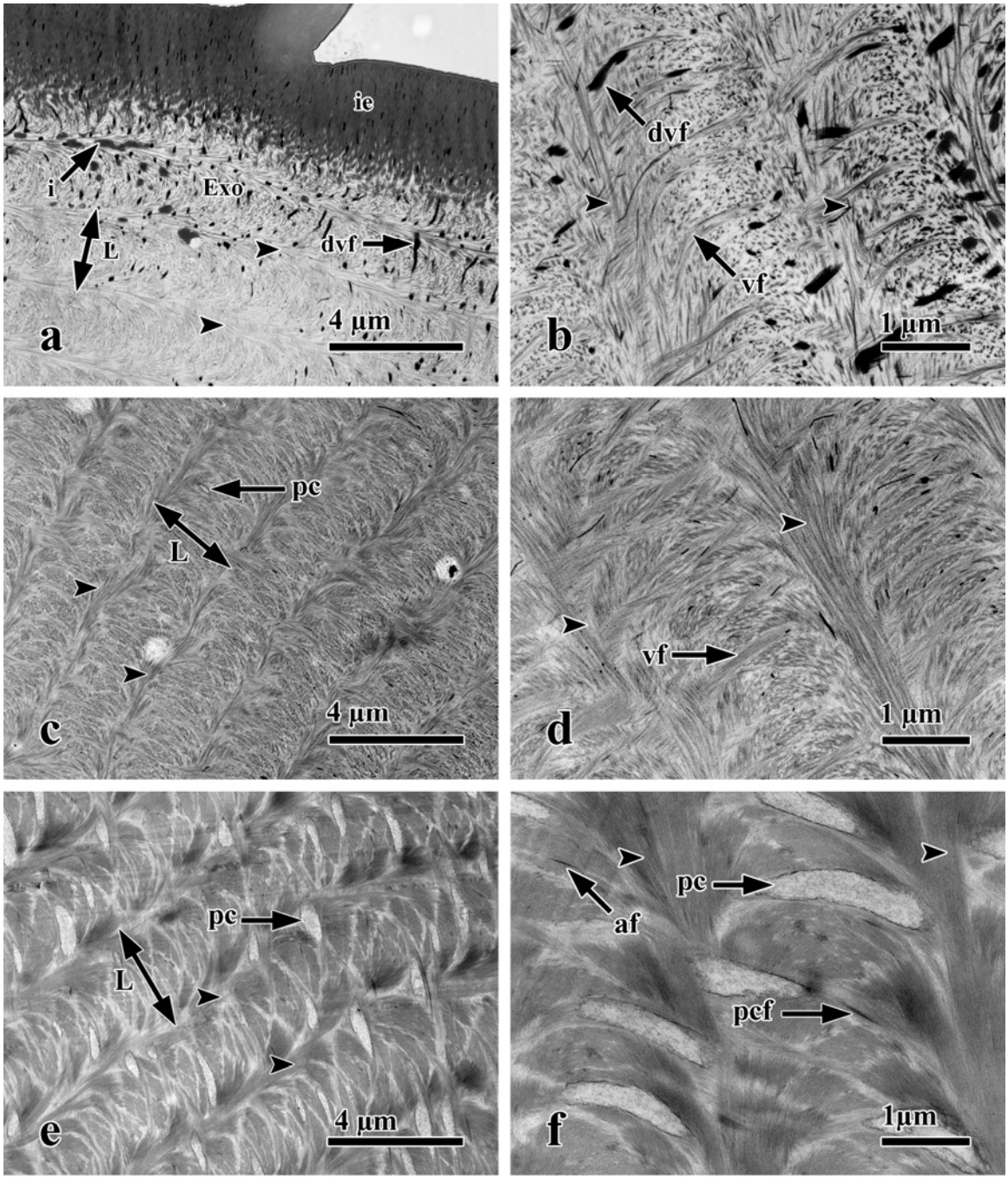
ie
i
Exo
L
dvf
4 µm
a
dvf
vf
1 µm
b
pc
L
4 µm
c
vf
1 µm
d
pc
L
4 µm
e
pc
af
pcf
1µm
f

Figure 3. TEM of fresh, standard fixed dorsal carapace. Low (a) and higher (b) magnifications of cross-sections through the proximal exocuticle and hypodermis. anchoring fiber, af; hypodermis, H; mitochondria, mc; microvilli, mv; pigment granule, pg; pore canal, pc; pore canal fiber, pcf; electron dense vesicle, v

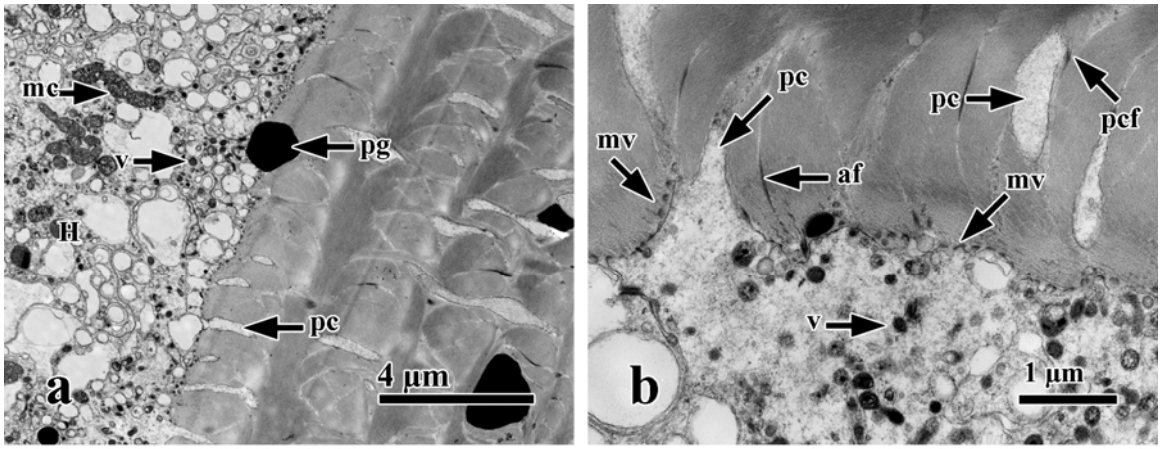
mc
v
pg
H
pc
4 µm
a
pc
pc
pcf
mv
af
mv
v
1 µm
b

When observed in tangential sections, the horizontal fibers were organized into bundles that increased in diameter from the epicuticle toward the hypodermis (Fig. 4a-f). Horizontal fibers near the epicuticle (Fig. 4b) tended to occur as small bundles or individual fibers whereas more proximally, bundles became larger with a diameter of 50-100 nm (Fig. 4c). The bhf became progressively larger in successive planes, increasing from 140-200 nm thickness in the medial exocuticle (Fig. 4d, e) to a maximum thickness of 500 nm near the hypodermis (Fig. 4f). With an increase in width, bhf also increased in electron density with the result that individual fibers became less distinct.

When sectioned tangential to the surface of the cuticle, bhf were organized roughly parallel to one another within a plane but tended to split and merge with adjacent bundles as they navigated around pore canals and vertical fibers (Fig. 4f; arrowheads). When sectioned obliquely, the bhf formed an arcing pattern (Fig. 4d; arrows). The diameter of the arc varied with the sectioning plane such that large arcs were created when sectioned close to parallel to the surface of the cuticle and small arcs when sectioned more obliquely to the surface.

The second type of fibers observed were electron dense vertical fibers (dvf) in the distal exocuticle (Table 2, Group B). These fibers occurred in thick bundles and could be seen in transverse sections as arising from either within the epicuticle or at the epicuticle-exocuticle interface and extending approximately 8 µm into the exocuticle (Figs. 1a, 2a, b). The dvf were approximately 100 nm in diameter. When viewed in tangential sections, the dvf were organized into discrete, round groups, approximately 5 µm across near the epicuticle (Fig. 4a; bracket). Deeper into the exocuticle, the diameters of both the groups and dvf themselves became progressively smaller until the fibers disappeared

Figure 4. TEM of fresh, standard fixed dorsal carapace. Tangential sections through the distal (a, b), medial (c, d, e), and proximal (f) exocuticle. Note the groupings (brackets) of dense vertical fibers (dvf; a, b) and pore canals (pc; d, e). Also note the increase in width of the bundles of horizontal fibers (bhf) from the distal (a, b) to the medial (c, d, e) to the proximal (f) exocuticle and the increase in size of the pore canals from the medial (d, e) to proximal (f) exocuticle. anchoring fibers, af; arc, arrows; dense vertical fibers, dvf; inclusion, i; inner epicuticle, ie; pore canals, pc; pore canal sheath, pcs; splitting of bhf; arrowheads

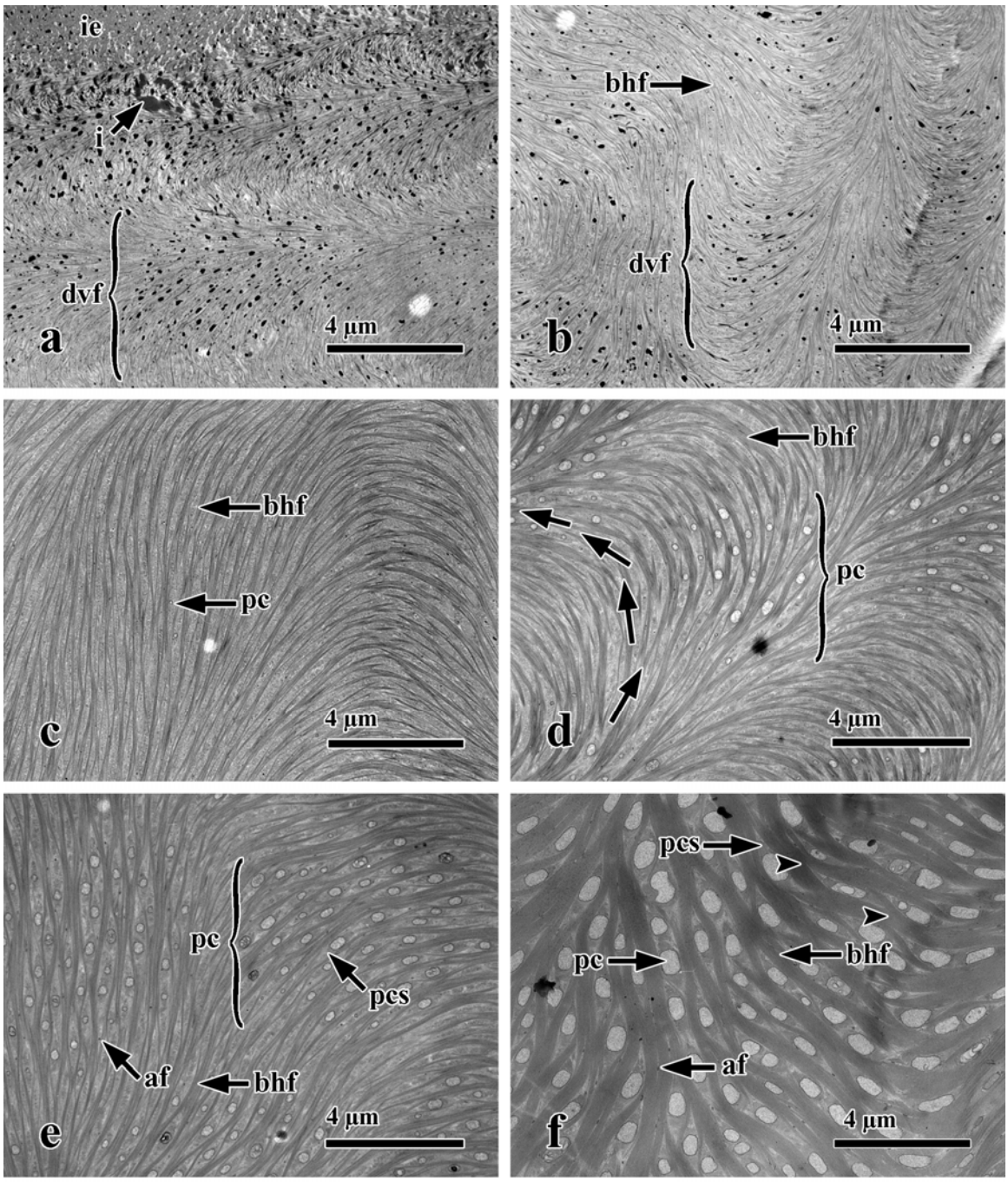
ie
i
dvf
a
4 µm
bhf
dvf
b
4 µm
bhf
pc
c
4 µm
bhf
pc
d
4 µm
pc
pcs
af
bhf
e
4 µm
pcs
pc
bhf
af
f
4 µm

completely (Fig. 4b; bracket). Therefore, the groups of dvf seemed to taper conically with depth.

The third type of fibers observed were vertical fibers (vf) that traversed most of the exocuticle (Table 2, Group B). These vf stained less intensely than the dvf but were more abundant and widespread. In transverse sections, they crossed lamellae vertically, appearing more prominent in the distal and medial regions of the exocuticle while virtually disappearing near the hypodermis (Fig. 2b, d). In tangential sections, the vf appeared as either a granular or fibrous material between the bhf (Fig. 5e). In sections taken near the hypodermis, vf were absent, and the spaces between bhf were instead occupied by numerous pore canals and their associated pore canal sheaths (Fig. 5f).

The pore canals are cytoplasmic extensions arising from the underlying hypodermis, which undergo a periodic growth and regression during cuticle deposition (Compère and Goffinet, 1987). In transverse sections, the pore canals were membrane-bound, finger-like processes that emanated from the hypodermis and crossed lamellae vertically (Figs. 2c, e, f; 3a, b). No branching of pore canals was observed in transverse sections. Pore canals were completely absent in the distal exocuticle (Fig. 2a, b) but became more numerous near the hypodermis (Fig. 2e, f).

In tangential sections, pore canals first appeared where the groups of dvf were diminishing (Fig. 4d), and they increased in both size and abundance from the medial exocuticle toward the hypodermis. Initially, pore canals, approximately 140 nm in diameter, arose in small groups about 3.8 µm across (Fig. 4d; bracket). More proximally, the size of the groups increased from 4.4 µm to 6 µm, and pore canals increased in diameter from 200 nm to 250-350 nm (Fig. 4e; bracket). As pore canals became more

Figure 5. TEM of fresh, standard fixed dorsal carapace. a, b, c, d. Comparison of pore canal size between premolt (a, b) and postmolt (c, d) crabs in cross-sections (a, c) and tangential sections (b, d). e, f. Tangential sections of pore canals from the medial (e) and proximal (f) exocuticle. Note the increase in size of pore canals from the medial (e) to the proximal (f) exocuticle. g. Anaglyph of a tangential section through the proximal exocuticle showing the orientation of pore canals in the top (A) and bottom (B) of the section. anchoring fiber, af; hypodermis, H; pore canal, pc; pore canal fiber, pcf; pore canal sheath; pcs

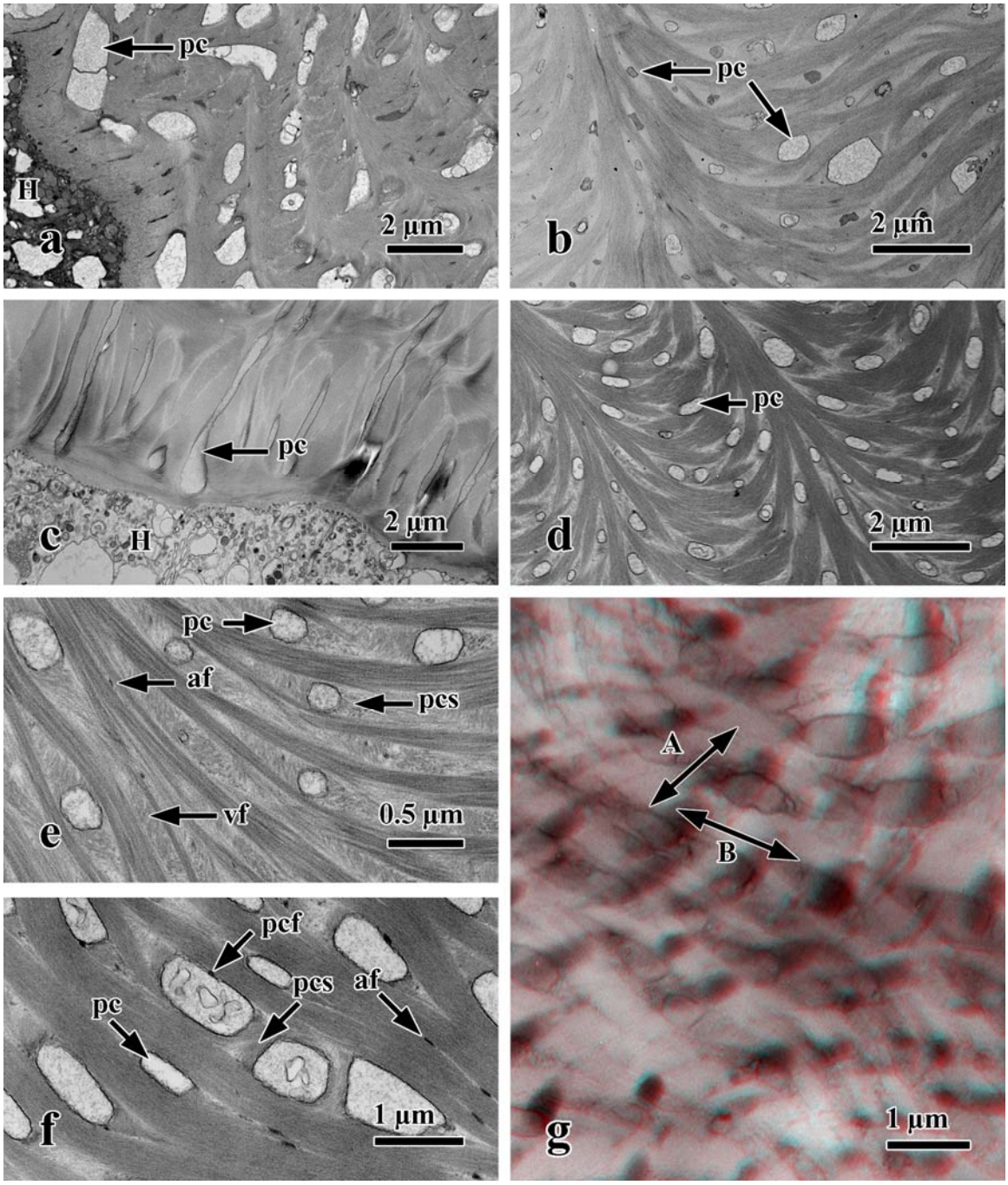
pc
H
a
2 µm
pc
b
2 µm
pc
c
H
2 µm
pc
d
2 µm
pc
af
pcs
vf
e
0.5 µm
A
B
g
1 µm
pcf
pcs
af
pc
f
1 µm

numerous, they appeared in rows between the bhf (Fig. 4e, f). While this pattern was observed in postmolt and premolt crabs, the pore canals of premolt crabs had a greater size range. Within a given sectioning plane, smaller, crenated pore canals could be seen alongside very large, dilated pore canals (cf. 5a, b and 5c, d).

Small pore canals were round and completely surrounded by a pore canal sheath (Fig. 5e). Large pore canals were laterally compressed by adjacent bhf and assumed an oblong shape (Figs. 4f; 5f). Anaglyphs made from tangential sections near the hypodermis suggested that the lateral compression of pore canals occurred passively with the helical rotation of the bhf within successive planes. The anaglyph in figure 5g shows that pore canals in the plane near the surface of the section have their long axes oriented in the direction indicated by the arrow labeled “a” whereas at the bottom of the section, the long axes are oriented as indicated by the arrow labeled “b”. For larger pore canals, their long axes were adjacent to the bhf while their short axes abutted a pore canal sheath (pcs) (Fig. 5f). The triangular pcs constituted the fourth fiber type observed and was virtually indistinguishable from the vf (Fig. 5e; Table 2, Group B). Their designation as a separate type of fiber was based on their proximity to the pore canals.

Near the hypodermis, the pore canals reached their maximum size of about 500 nm by 900 nm (Figs. 4f; 5f). For some pore canals, there appeared a round electron dense vertical fiber closely associated with or attached to the exterior face of the pore canal membrane (Figs. 5f; 6a, b). This pore canal fiber (pcf) constituted the fifth fiber type observed (Table 2, Group B). Transverse sections revealed that these fibers originate from invaginations at the base of the pore canal (Fig. 6a). The invaginations were highly

Figure 6. TEM of fresh, standard fixed dorsal carapace. a, b, c. Cross-section (a) and tangential sections (b, c) showing the insertion of the pore canal fiber into the hypodermis. Note the ring of microtubules (arrowhead) surrounding the insertion point when cut in cross-section (b, c). Also note the appearance of the insertion point when sectioned superficially (arrowhead) and deeply (curved arrow) in c. d, e. Higher (d) and low (e) magnifications of cross-sections through the proximal exocuticle and tendinous epidermal cell at a region of muscle insertion. density, d; pore canal, pc; pore canal fiber, pcf; microtubule, mt; tendinous epidermal cell, TEC; tonofiber; tf

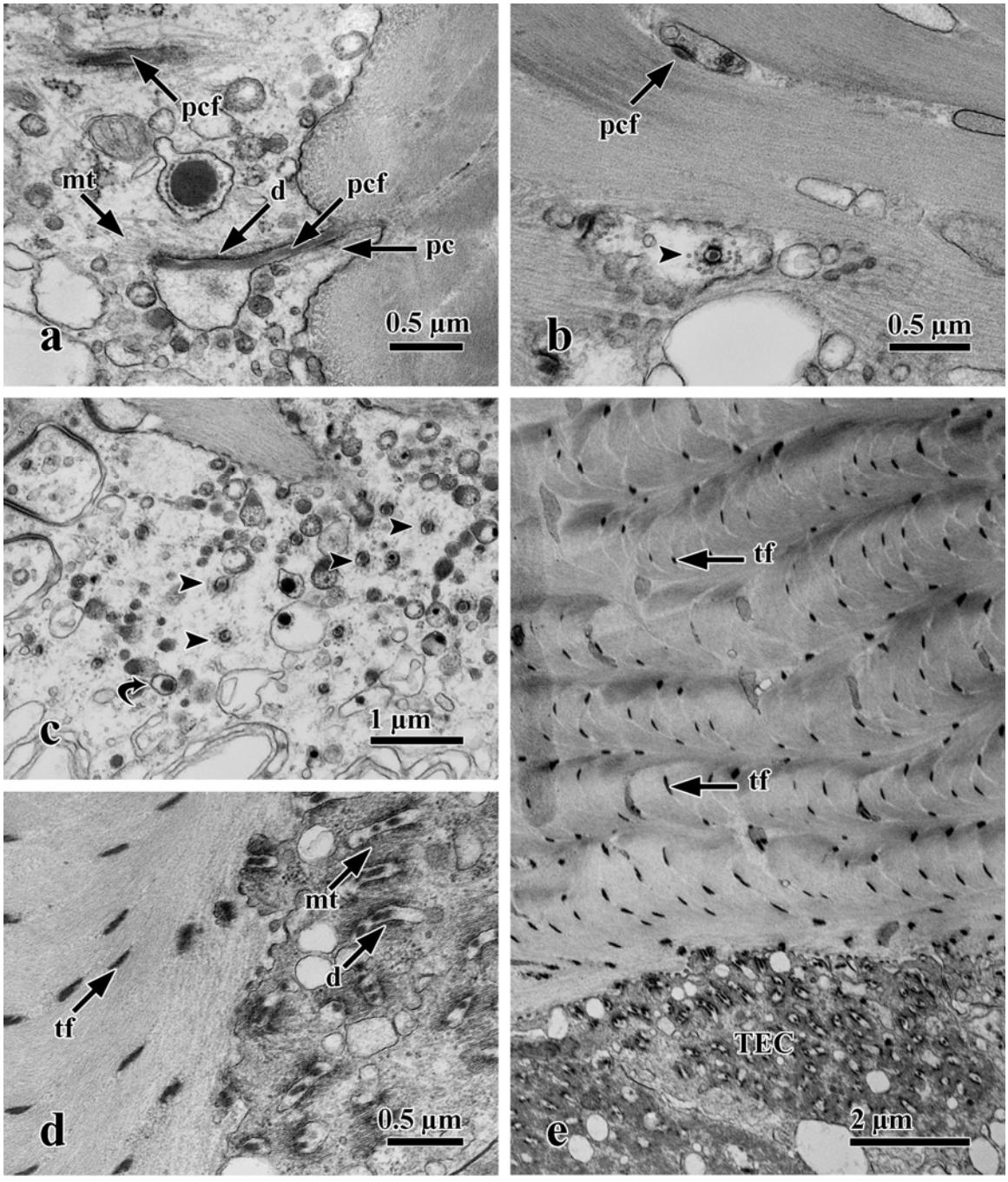
pcf
mt
d
pcf
pc
0.5 µm
a
pcf
0.5 µm
b
1 µm
c
tf
tf
TEC
2 µm
e
mt
d
tf
0.5 µm
d

abundant and localized to the surface of the hypodermal cell membrane (Fig. 6c). They appeared as a vesicle within the cell that extended to the surface by a long tubular process. The pcf ran through the tubular process and along one side of the vesicle and appeared to be attached to the extracellular face of the cell membrane. On the opposite, or cytoplasmic, face of the membrane was a dense region where bundles of microtubules were anchored (Fig. 6a). Cross-sections of this structure clearly showed that microtubules are attached around the entire circumference of the tubular process (Fig. 6b).

Pore canals near the hypodermis contained actin filaments and, in some instances, microtubules (Fig. 6a). At the base of some pore canals, the membrane formed microvilli with electron dense apical plaques (Fig. 3b). More distally, most pore canals contained granular cytoplasmic material or vesicle-like structures (Fig. 5f).

The sixth and final widespread fiber type observed were the vertical anchoring fibers (af) (Table 2, Group B). These thin (100 nm by 20 nm) fibers paralleled the pcf's but were clearly not associated with pore canals and passed through the middle of the bhf (Figs. 4f; 5e, f). The af became progressively smaller from the hypodermis (Fig. 5f) toward the epicuticle (Fig. 5e) and therefore were more easily seen in the proximal portions of the exocuticle. The af appeared to originate from the hypodermis, but no actual attachment was seen (Figs. 3b; 8a). The af were more prominent in the proximal exocuticle due to their close juxtaposition to the bhf and larger size (Figs. 2f; 3b; 4f; 5f) but could also be seen extending into the medial exocuticle (Fig. 5e).

Two additional fiber types were observed less frequently in part because they were associated with specialized portions of the cuticle (Table 2, Group C). Tonofibers (tf) were electron dense vertical fibers that projected from tendinous epidermal cells and traversed the

entire exocuticle (Fig. 6d, e). They arose from deep invaginations in the apical cell membrane of tendinous epidermal cells. The cytoplasmic face of the invagination bore hemidesmosome-like densities that appeared to anchor bundles of microtubules (Fig. 6d). The manner by which the tf attached to the cell membrane was similar to that of the pcf's but, unlike the rest of the hypodermis, the cytoplasm of the tendinous epidermal cell was filled with microtubules. The plasma membrane of the tendinous epidermal cell was extensively interdigitated with membranes of adjacent cells and connected with septate or intermediate junctions.

In tangential sections above the tendinous epidermal cell, tf occurred in groups approximately 6µm in diameter (Fig. 7a; bracket). Within the overall group, tf were subdivided into multiple round arrays, each forming a rosette-like pattern (Fig. 7a; circle). Pore canals were few or absent within the groups of tf. The tf were round or laterally compressed electron dense fibers approximately 60 nm by 100-200 nm. The margins of the tonofibers were fuzzy (Fig. 7b). When sectioned closer to the surface of the tendinous epidermal cell, bhf appeared to curve around tf (Fig. 7b). Pockets of granular material occurred in round patches within the groups of tf (Fig. 7a, b; arrowhead)

The second specialized fiber type was only found in the distal exocuticle, near the epicuticle. These fibers formed electron dense rods approximately 20 nm in diameter and oriented perpendicular to the surface of the cuticle (Fig. 7d). The rods most often were grouped into clusters between bhf (Fig. 7c, d). The clusters were further arranged into aggregates about 5-6 µm in diameter (Fig. 7c; bracket). Within the aggregate, many tf were also observed (Fig. 7d). Dense fibers were also seen extending into the outer epicuticle (Fig. 7e, f), but it was not possible to determine if they were continuations of the rods or tf.

Figure 7. TEM of fresh, standard fixed dorsal carapace. a, b. Low (a) and higher (b) magnifications of tangential sections through the proximal exocuticle above a tendinous epidermal cell. Note the groups of tonofibers (bracket) and circular arrays (circle). c, d. Low (c) and higher (d) magnifications of tangential sections through the distal exocuticle above a tendinous epidermal cell. Note the groups of electron dense rods (bracket). e, f. Low (e) and higher (f) magnifications of tangential section through the epicuticle showing the insertion of rods or tonofibers (arrows). bundles of horizontal fibers, bhf; epicuticular canal, ec; electron dense rods, r; granular material, arrowhead; pigment granule, pg; tonofiber, tf

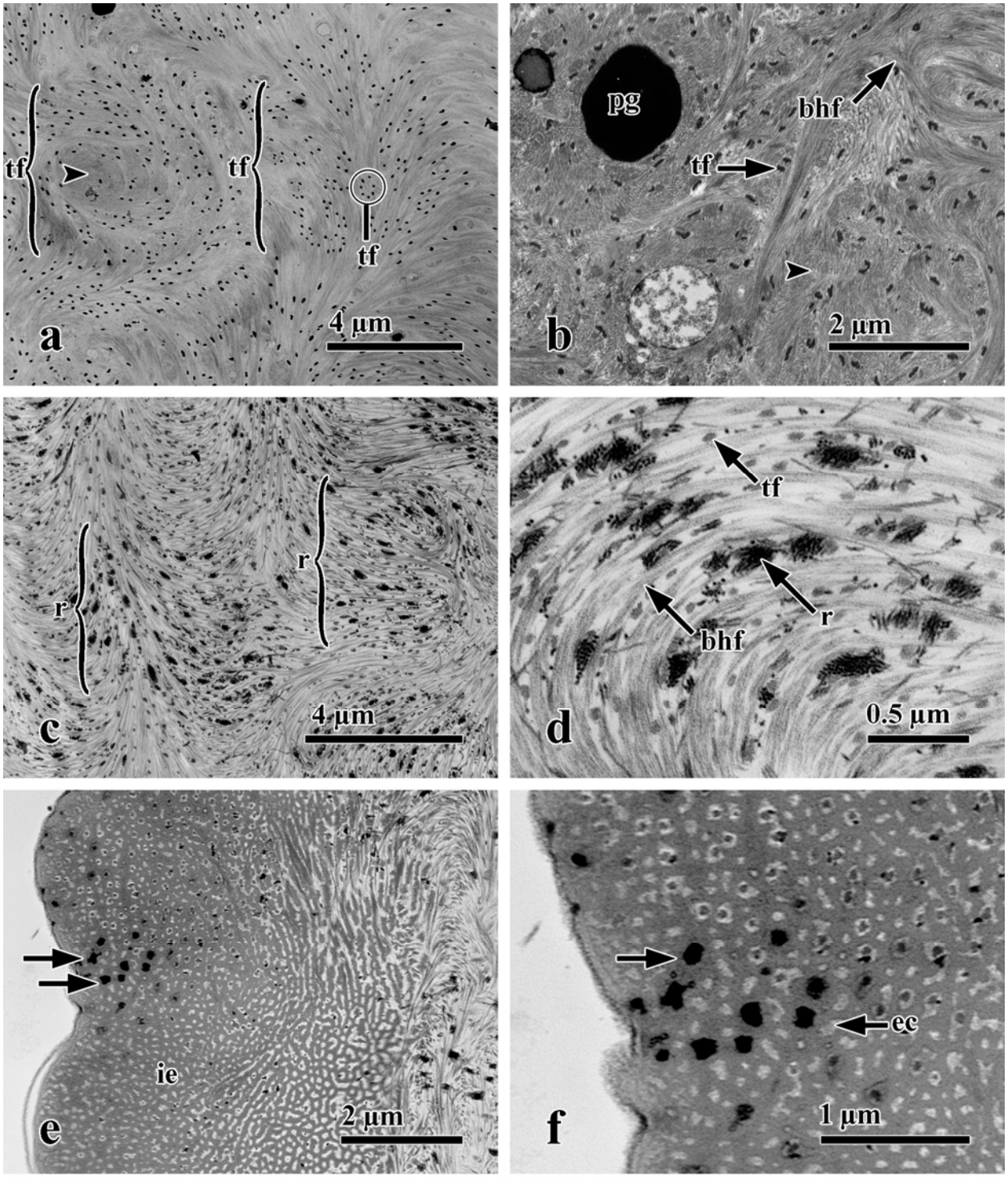
tf
tf
tf
4 µm
a
pg
bhf
tf
2 µm
b
r
r
4 µm
c
tf
r
bhf
0.5 µm
d
ie
2 µm
e
ec
1 µm
f

Standard fixation offered superior preservation of the hypodermis and connective tissue. The hypodermal cells had many features that supported their involvement in the deposition of chitin-protein fibers. In addition to giving rise to numerous pore canals, the apical membrane had numerous microvilli containing electron dense apical plaques (Figs. 3b; 8b). In tangential sections, the horizontal fibers of the exocuticle appeared to polymerize at or near the surface of the microvilli (Fig. 8a). Cross-sections (Fig. 8b) indicated the presence of an assembly zone above the tips of the microvilli where chitin fibrils were being initially polymerized and lengthened. Tangential sections near the surface of the hypdermis also revealed a transition zone within the newly synthesized fibers of the exocuticle (Fig. 8a). This region could be distinguished by the staining intensity and the formation of more dense fiber bundles.

The hypodermis also contained numerous apical vesicles, many containing electron dense material (Figs. 3a, b; 8a). At their apical borders, septate and intermediate junctions interconnected adjacent cells (Fig. 8c). Cells also contained large numbers of mitochondria, sometimes in clumps (Fig. 3a, 8f). The elaboration of the endomembrane system in the hypodermis and the complexity of connective tissue varied between premolt and postmolt samples. In general, the protein-synthesizing machinery was more extensive in premolt than in postmolt crabs. Rough endoplasmic reticulum, Golgi vacuoles, and the suite of hypodermal connective tissue cells were more complex in premolt than in postmolt crabs (cf. 8d, e and 8f). . Aside from the extensiveness of the endomembrane system and range in pore canal size, few other differences in cuticle structure between premolt and postmolt crabs were recognized.

Comparisons between premolt and postmolt crabs were complicated by a number of variables. First, the cuticle of premolt crabs was more highly folded than in postmolt crabs.

Figure 8. TEM of fresh, standard fixed dorsal carapace. a, b, c. Tangential (a, c) and cross-section (b) through the proximal exocuticle and hypodermis. Note the assembly zone (AZ) and transition zone (TZ) were fibrils are initially polymerized and organized into bundles. d, e, f. Comparison of premolt (d, e) and postmolt (f) hypodermis. anchoring fiber, af; apical electron dense plaque, arrowhead; clear vesicle, cv; electron dense vesicle, v; exocuticle, Exo; golgi vacuole, GV; highly interdigitated junction between cells, arrows; intermediate junction, j; microvilli, mv; mitochondria, mc; pore canal, pc; rough endoplasmic reticulum, rER

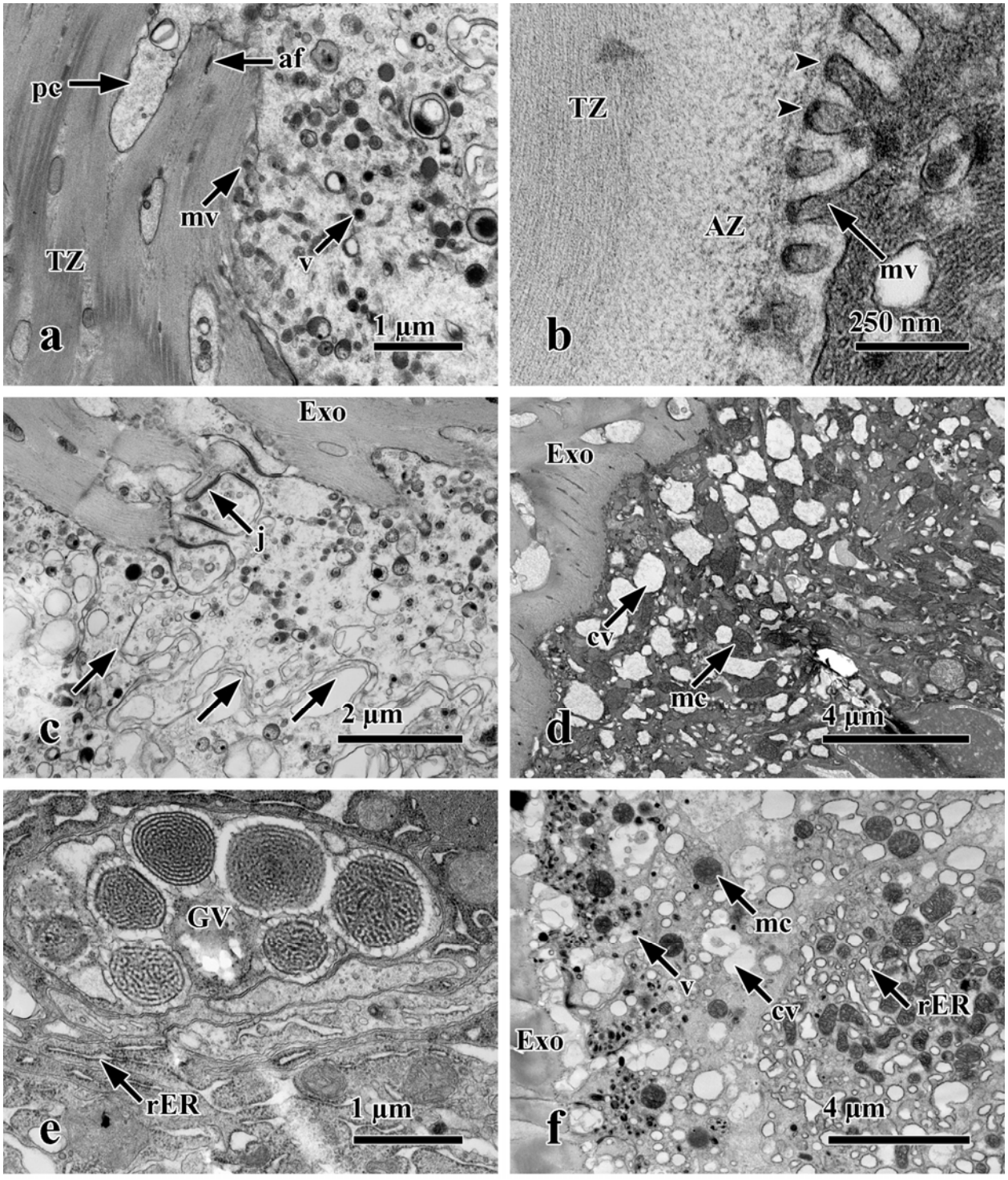
pc
af
mv
v
TZ
a
1 µm
TZ
AZ
mv
b
250 nm
Exo
j
c
2 µm
Exo
cv
mc
d
4 µm
GV
rER
e
1 µm
mc
v
cv
rER
Exo
f
4 µm

Therefore, obtaining tangential views of the cuticle was more difficult, and a given sectioning plane would pass through many different regions of the cuticle simultaneously and at various angles. Another factor was the variability in fixation among samples. When good fixation and embedding occurred, the standard fixation offered superior views of the cuticle and hypodermis. Unfortunately, the cuticle was often highly resistant toward infiltration, which resulted in poor preservation. In some samples, the hypodermis was not preserved and pore canals appeared dilated. Moreover, in those samples, bhf were highly disorganized, with no regular, periodic arrangement, and obscured by a hazy background staining (Fig. 9a). In other samples, the background had an irregular staining pattern such that in the distal exocuticle, the interprismatic septa (IPS) were visible (Fig. 9b). In all well fixed samples, the IPS were not apparent.

With standard fixation, good preservation of cuticle and hypodermis only occurred along the perimeters of the samples where the chemicals could diffuse into the tissue laterally through the cut edges (Fig. 9d). Unfortunately, this phenomenon was discovered *post hoc* when samples were prepared for observation with the SEM. In postmolt samples, the internal surface (Fig. 9c) of the cuticle appeared black, being completely osmicated. The external surface (Fig. 9d) was pale, with osmication only occurring 1 mm in from the cut edges. This was in stark contrast to premolt samples, which osmicated on both the internal and external faces of the cuticle (Fig. 9e, f).

Fresh, Uranyl Acetate Fixed Tissue

Samples fixed with uranyl acetate (UA) had the same basic structural patterns and fiber types as standard fixed cuticles. Whereas the hypodermis was very poorly preserved by UA, the

Figure 9. TEM of fresh, standard fixed dorsal carapace (a, b) and whole pieces of standard fixed cuticle (c, d, e, f). a, b. Tangential sections through the exocuticle demonstrating variable fixation. c, d. Inner (c) and outer (d) surface of postmolt cuticle. Note lack of osmication of the outer surface. e, f. Inner (e) and outer (d) surface of premolt cuticle. bundles of horizontal fibers, bhf; interprismatic septa, IPS; pore canal, pc

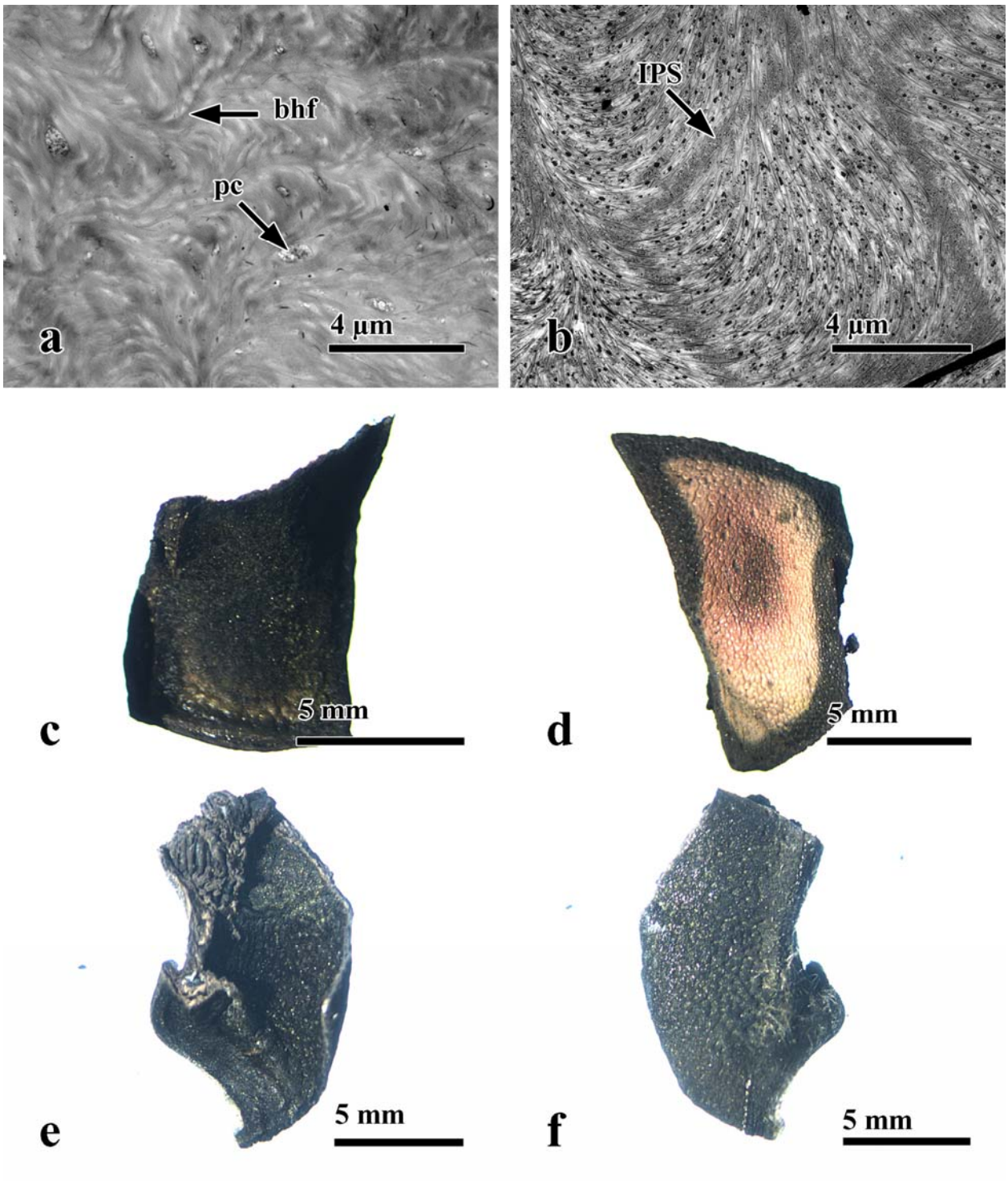
bhf
pc
4 µm
a
IPS
4 µm
b
5 mm
c
5 mm
d
5 mm
e
5 mm
f

preservation of cuticular fibers was much more consistent among samples than for standard fixation. Uranyl acetate fixation greatly increased the contrast of cuticular fibers, making them ideal for viewing anaglyphs, and it accentuated the IPS and the calcification initiation site at the epicuticle-exocuticle boundary (Figs. 10d, e, f; 11a, b; 13a).

The epicuticle of samples fixed by uranyl acetate appeared as two layers: a thin 70 nm outer epicuticle and a thick 2.5 μm inner epicuticle (Fig. 10a, b). The outer epicuticle was trilaminar, having an electron dense surface coat, a moderately staining middle layer, and an electron lucent inner layer (Fig. 10b). The inner epicuticle was comprised of vertical epicuticular roots that often appeared thinner and more discrete than those of standard fixed samples and contained parallel arrays of small constitutive fibers (Fig. 10a). Canal-like spaces between the roots extended through the entire inner epicuticle and frequently contained electron dense epicuticular fibers (Fig. 10a, b; ef). More proximally, the roots tapered conically and terminated amongst the horizontal fibers of the exocuticle (Fig. 10a).

In tangential sections, the inner epicuticle was similar in appearance to standard fixed samples. It consisted of a homogeneous matrix that was penetrated distally by pores, or epicuticular canals, that often contained electron dense ef's (Fig. 10c). These canals were more electron lucent than those seen in standard fixed samples. Adjacent to the exocuticle, the matrix of the epicuticle appeared to be fragmented into discrete aggregates that corresponded to cross-sections of the epicuticular roots (Fig. 10c).

At the interface between the epicuticle and exocuticle, an electron dense globular material was occasionally present (Figs. 10d; 11a; 13a). The globular material, referred to as the

Figure 10. TEM of fresh, uranyl acetate fixed dorsal carapace. a, b, c. Cross-sections (a, b) and tangential sections (c) through the epicuticle. d, e, f. Low (d) and higher (f) magnification of cross-sections and slightly oblique sections (e) through the cuticle. Note that interprismatic septa lose staining intensity with depth. dense vertical fibers, dvf; epicuticular canal, ec; epicuticular fiber, ef; epicuticular root, er; external zone, EZ; inner epicuticle, ie; interprismatic septa, IPS; outer epicuticle, oe; vertical fibers of IPS; arrowheads

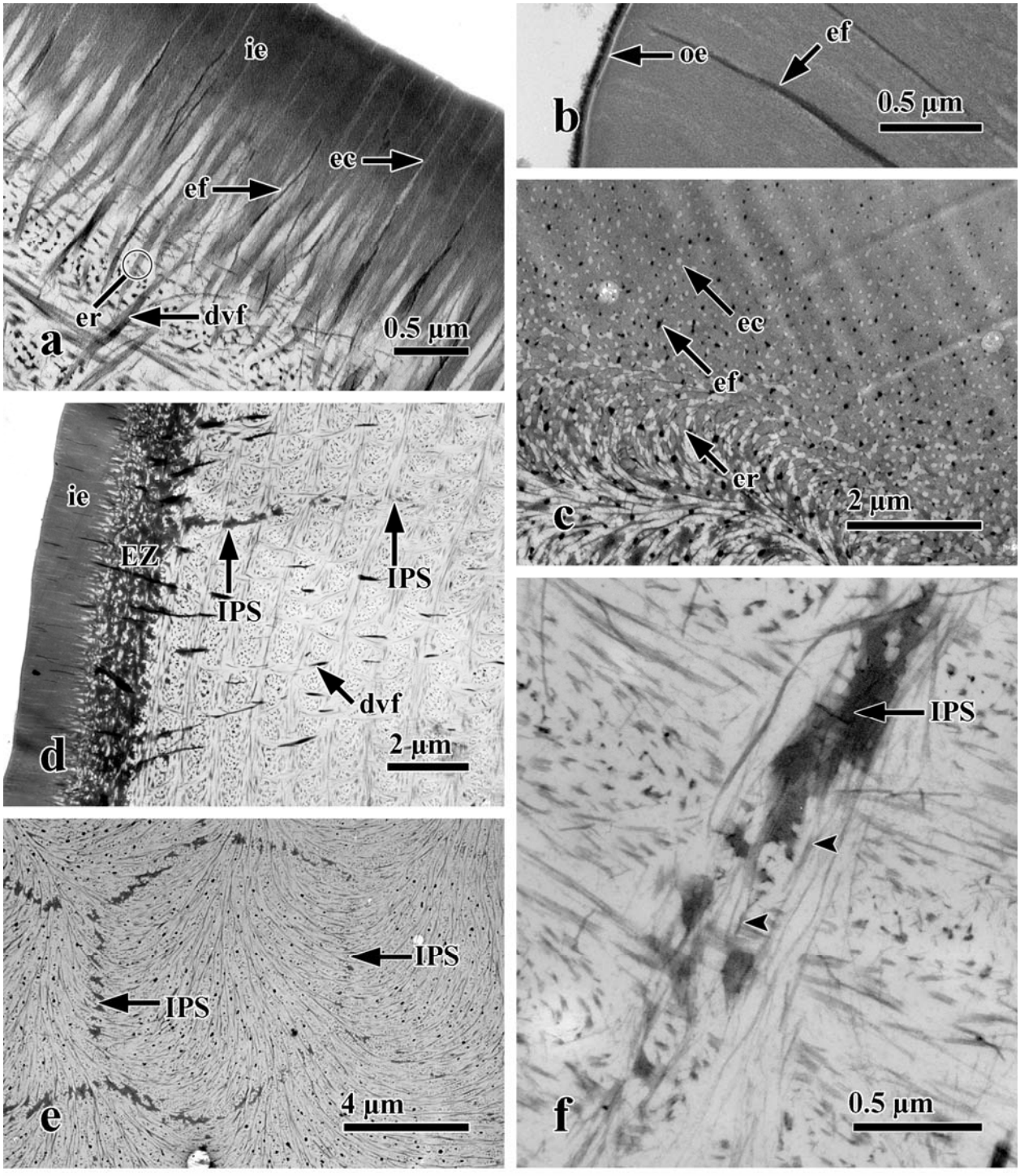
ie
ec
ef
er
dvf
0.5 µm
a
oe
ef
0.5 µm
b
ec
ef
er
2 µm
c
ie
EZ
IPS
IPS
IPS
dvf
2 µm
d
IPS
IPS
4 µm
e
IPS
0.5 µm
f

external zone (EZ) by Hegdahl et al. (1977) and Drach et al. (1939), was attached to the horizontal fibers and was so extensive at times that it obscured the first 2-3 lamellae of the exocuticle. The presence of the EZ was highly variable, being very prominent in some samples (Figs. 10d; 11a; 13a) while absent in others (Figs. 10a; 11b, c; 12a). Although not restricted to stage D_3, the EZ was most often observed in premolt crabs.

In the distal exocuticle, the IPS stained intensely in some, but not all, samples. The IPS were polygonal structures, appearing to be comprised of the same electron dense globular material that constituted the EZ (Figs. 10e, f; 11a, b). Since the globular material was observed in sections that were not post-stained with UA or lead citrate, its presence was a function of uranyl acetate *en bloc* fixation. In cross-sections, the IPS were 5-6 µm wide and formed electron dense vertical lines that extended from the epicuticle-exocuticle interface to 4-15 µm into the exocuticle (Fig. 10d). As the IPS extended deeper into the exocuticle, the globular material became finer. This was evident in both cross-sections (Fig. 10 d, f) and slightly oblique tangential sections (Fig. 10e).

The IPS varied considerably in staining intensity among samples in both premolt and postmolt crabs. The IPS sometimes stained very intensely (Figs. 10d, e; 11a, b; 13a) and sometimes faintly, if at all (Fig. 11c). In general, the IPS stained intensely for most premolt crabs and faintly for most postmolt crabs. Cross-sections (Fig. 10f) and anaglyphs (Fig. 11d) made from thick tangential sections revealed that the IPS were comprised of bundles of vertical fibers oriented perpendicular to the horizontal fibers. Due to their affinity for the globular material, these vertical fibers have been designated as another type of fiber in the exocuticle (Table 2, Group C).

Figure 11. TEM of fresh, uranyl acetate fixed dorsal carapace. a, b, c. Tangential sections through the inner epicuticle (ie) and distal exocuticle. Note the variation in the staining intensity of the external zone (EZ) and interprismatic septa (IPS). d. Anaglyph of a tangential section through the distal exocuticle. dense vertical fibers, dvf; external zone, EZ; interprismatic septa, IPS

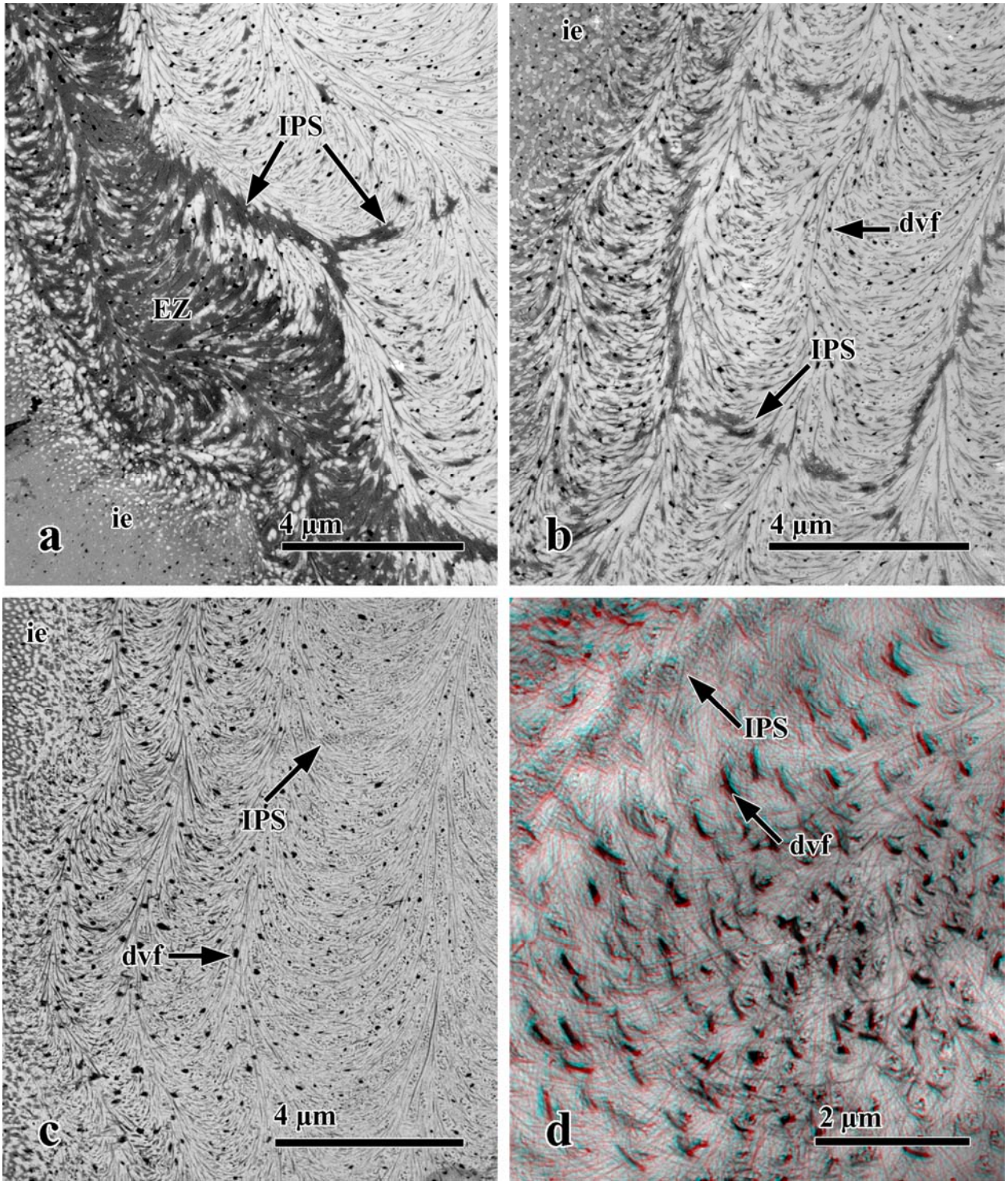
IPS
EZ
ie
4 µm
a
ie
dvf
IPS
4 µm
b
ie
IPS
dvf
4 µm
c
IPS
dvf
2 µm
d

Whenever an extensive EZ was present, the IPS in the distal exocuticle always stained intensely, appearing as an electron dense globular material (Figs. 10d; 11a; 13a). No samples had an EZ without IPS. However, samples were observed that lacked the EZ but had either intensely (Fig. 11b) or faintly stained IPS (Fig. 11c).

While both standard and UA fixations demonstrated the plywood-like arrangement of fibers, the UA fixation greatly improved the contrast of the fibers, making them more distinct and selectively visible against the background (Figs. 12a-d; 13a-d). Cross-sections of UA fixed samples sometimes yielded two disparate exocuticle morphologies. Samples differed in the thickness of the lamella (c.f. 12a-d and 13a-d), being three times thicker in one than the other at all comparable regions of the exocuticle. Furthermore, the size and packing density of the bhf also varied. In some, the bhf were so tightly packed that individual fibers were not seen, and the bhf formed discrete units that were separated by much empty space (Fig. 12a-d). In the other samples, the bhf were loosely packed so that individual fibers were more dispersed and easily resolvable (Fig. 13a-d). Morphologies appearing intermediate to these two extremes were also observed. In all cases, the first few lamellae adjacent to the epicuticle were the most narrow, with lamellae becoming wider more proximally (Figs. 12a; 13a). The variations in cross-sectional morphology may be attributed to the sectioning angle or distortions in the cuticle caused by folds.

Tangential sections through the cuticle revealed the same general patterns and fiber types observed in standard fixed samples, but all fiber types had more contrast than those in standard fixations and, consequently, anaglyphs revealed more information about the three-dimensional arrangement of fibers. As in standard fixations, the horizontal fibers occurred individually

Figure 12. TEM of fresh, uranyl acetate fixed dorsal carapace. Low (a, c) and higher (b, d) magnifications of cross-sections through the distal (a, b) and medial (c, d) exocuticle. Note that lamellae width and the density of horizontal fibers increases from the distal to proximal exocuticle. bundles of horizontal fibers cut longitudinally, arrowhead; dense vertical fibers, dvf; exocuticle, Exo; inner epicuticle, ie; lamella, L; pore canal, pc; vertical fibers, vf

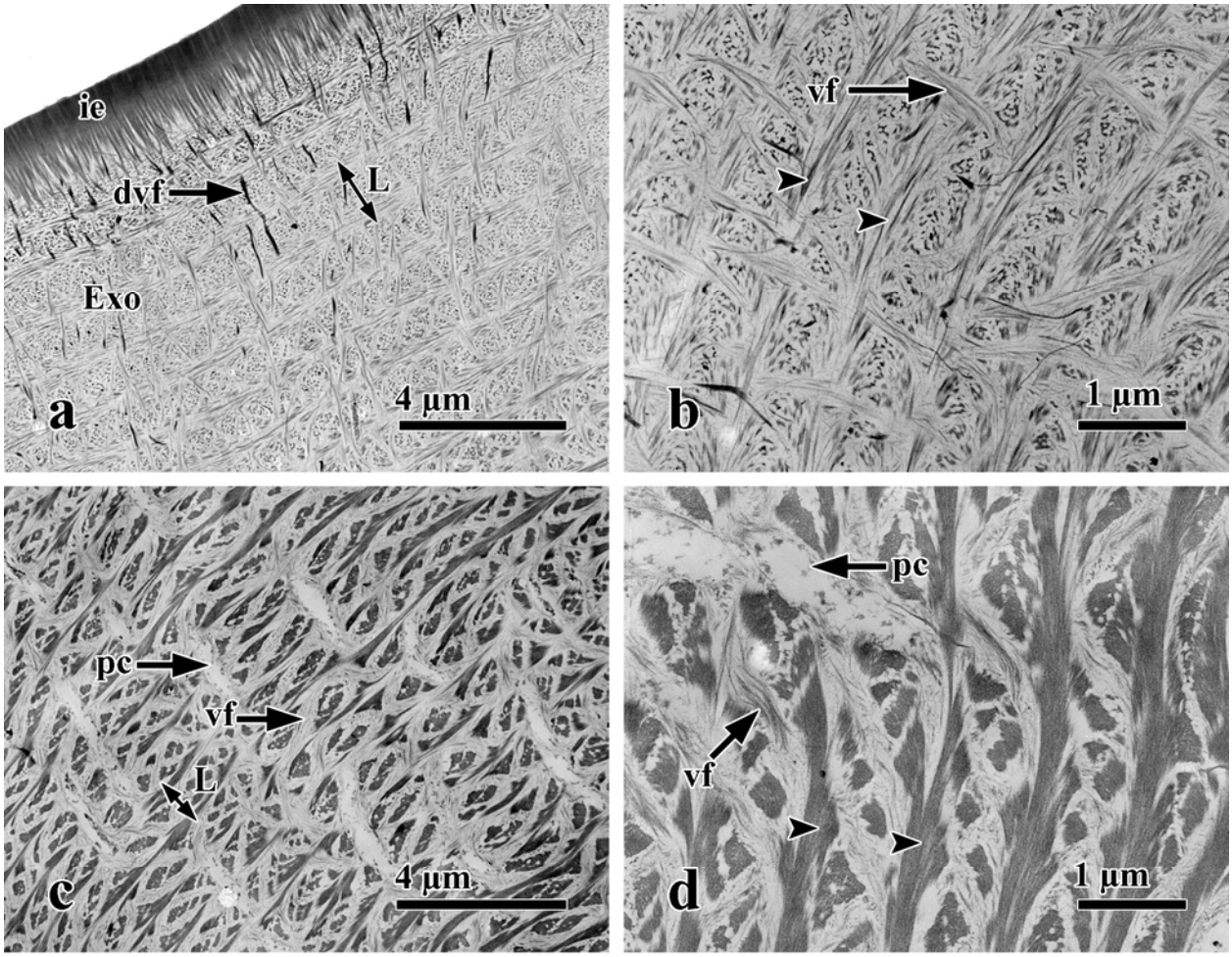
ie
dvf
L
Exo
a
4 µm
vf
b
1 µm
pc
vf
L
c
4 µm
pc
vf
d
1 µm

Figure 13. TEM of fresh, uranyl acetate fixed dorsal carapace. Low (a, c) and higher (b, d) magnifications of cross-sections through the distal (a, b) and medial (c, d) exocuticle. Note that lamellae width and the density of horizontal fibers increases from the distal to proximal exocuticle. bundles of horizontal fibers cut longitudinally, arrowhead; dense vertical fibers, dvf; exocuticle, Exo; external zone, EZ; inner epicuticle, ie; interprismatic septa, IPS; lamella, L; pore canal, pc; vertical fibers, vf

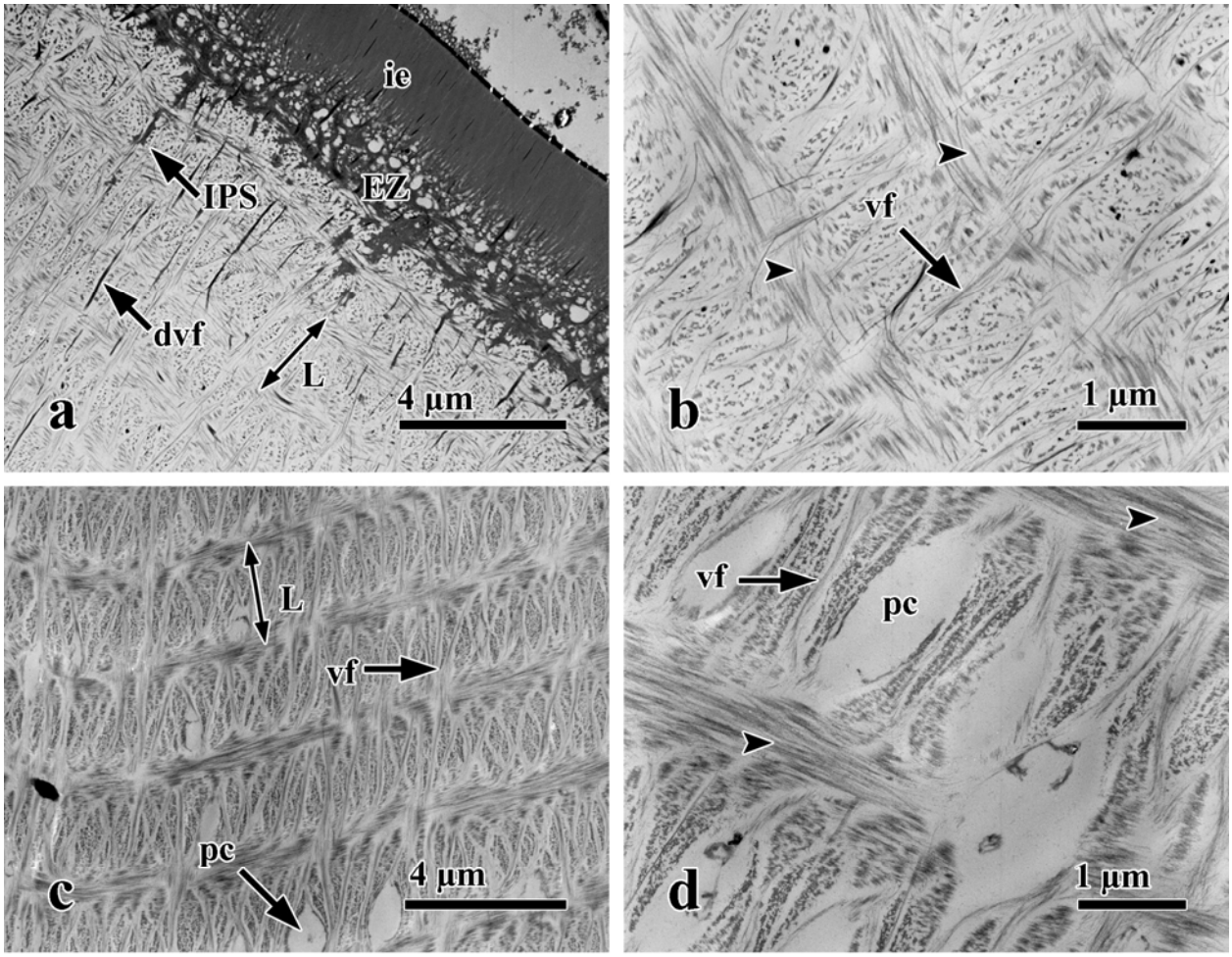
ie
IPS
EZ
dvf
L
4 µm
a
vf
1 µm
b
L
vf
pc
4 µm
c
vf
pc
1 µm
d

adjacent to the epicuticle (Fig. 14a, b) but became organized into small bundles in the medial exocuticle (Fig. 14 c, e). The bhf became progressively larger in diameter, reaching a maximum thickness adjacent to the hypodermis (Fig. 14d, f). The change in bundle thickness was also seen in cross-sections. Lamellae near the epicuticle contained discrete fibers (Figs. 12a, b; 13a, b) while those closer to the hypodermis were packaged into larger bundles and appeared more electron dense (Figs. 12 c, d; 13c, d). Although the bhf increased in diameter for all samples, bhf from premolt crabs often were not as large as those from postmolt crabs near the hypodermis (c.f. 14c to 14e and 14d to 14f).

Anaglyphs of tangential sections confirm Bouligand's twisted plywood model of the cuticle. The bhf in adjacent planes rotated relative to one another so as to create a helicoidal structure (Fig. 15a, b). In more truly tangential anaglyphs, only two planes of fibers could be seen in the section (Fig. 15a). However, anaglyphs of slightly oblique areas allowed for multiple planes to be observed simultaneously. In such sections, bhf formed a pattern of arcs. Anaglyphs showed that these arcs actually consist of overlapping fibers in successive planes (Fig. 15b). While one complete arc is created by a 180˚ rotation of bhf, the bhf did not rotate continuously around an axis but, rather, were displaced in discrete steps of approximately 30˚.

Emanating from within or near the epicuticle were dvf oriented perpendicular to the cuticle surface. Tangential sections near the epicuticle-exocuticle interface in crabs that lacked the EZ revealed many uniformly distributed electron dense vertical fibers within the most distal portions of the exocuticle, which may be extensions of both ef's and dvf (Fig. 14a; arrows). Slightly below this plane, the dvf became organized into discrete round groups (Fig. 14b; bracket) located within the center of the prisms defined by the IPS (Fig. 11b, c). As seen in

Figure 14. TEM of fresh, uranyl acetate fixed dorsal carapace. Tangential sections through the distal (a, b), medial (c, e) and proximal (d, f) exocuticle of postmolt (a, b, c, d) and premolt (e, f) crabs. Note the groups of dense vertical fibers (b; bracket) and pore canals (c, e; bracket). Note that the bundles of horizontal fibers (bhf) increase in width from the distal (a, b) to the medial (c, e) to the proximal (d, f) exocuticle. dense vertical fibers, dvf; epicuticular fibers and dense vertical fibers, arrows; inner epicuticle, ie; pore canal, pc

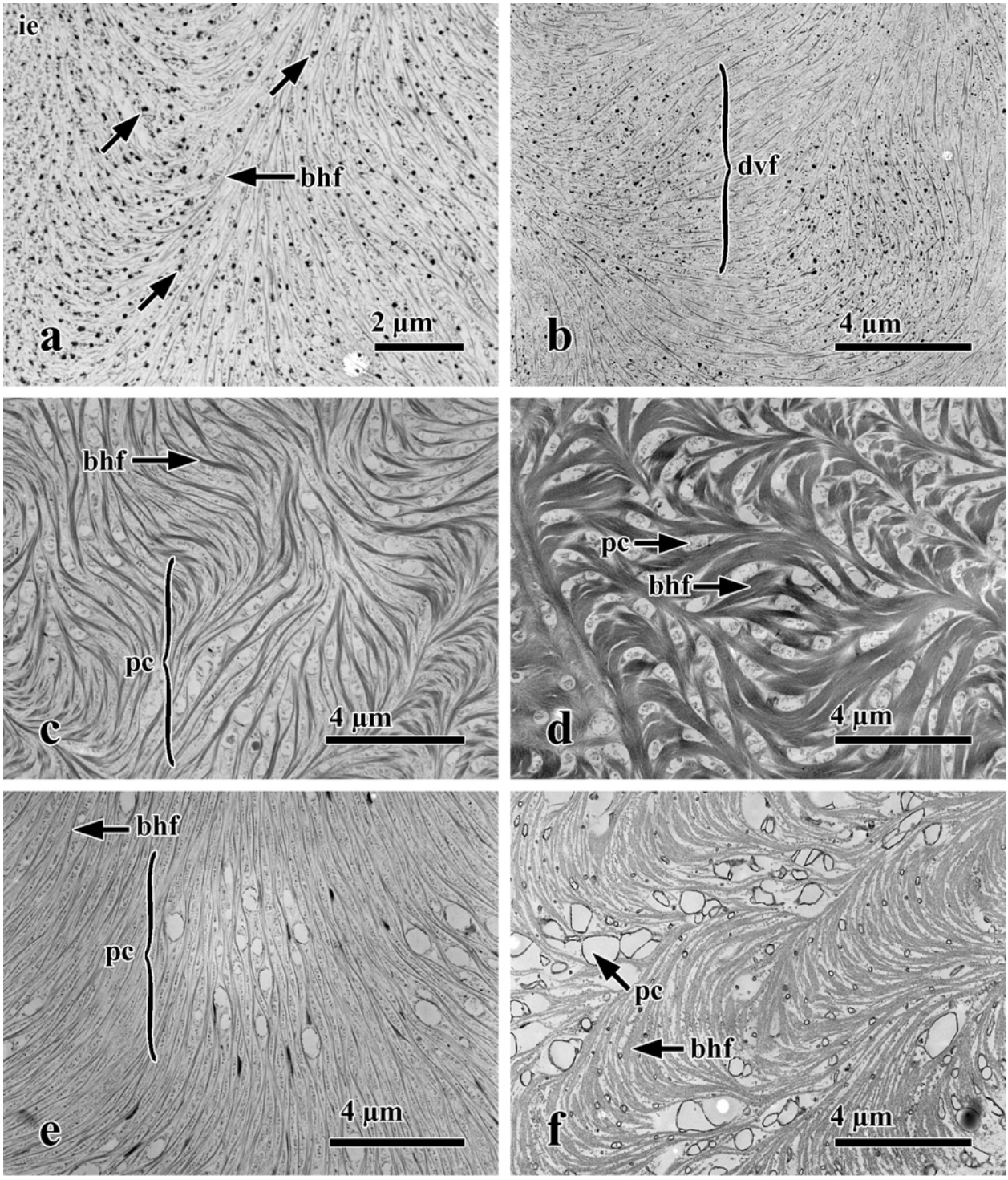
ie
bhf
2 µm
a
dvf
4 µm
b
bhf
pc
4 µm
c
pc
bhf
4 µm
d
bhf
pc
4 µm
e
pc
bhf
4 µm
f

Figure 15. TEM of fresh, uranyl acetate fixed dorsal carapace. a, b. Anaglyphs of tangential (a) and oblique (b) sections showing the rotation of bundles of horizontal fibers (arrows). c, d. Tangential thin section (c) and anaglyph (d) showing vertical fibers (vf). e, f. Tangential section showing variation in preservation of the pore canal membrane (arrowhead). g, h. Tangential thin section (g) and anaglyph (h) showing anchoring fibers (af). bundles of horizontal fibers, bhf; dense vertical fibers, dvf; pore canal, pc; pore canal sheath, pcs; vertical fibers, vf

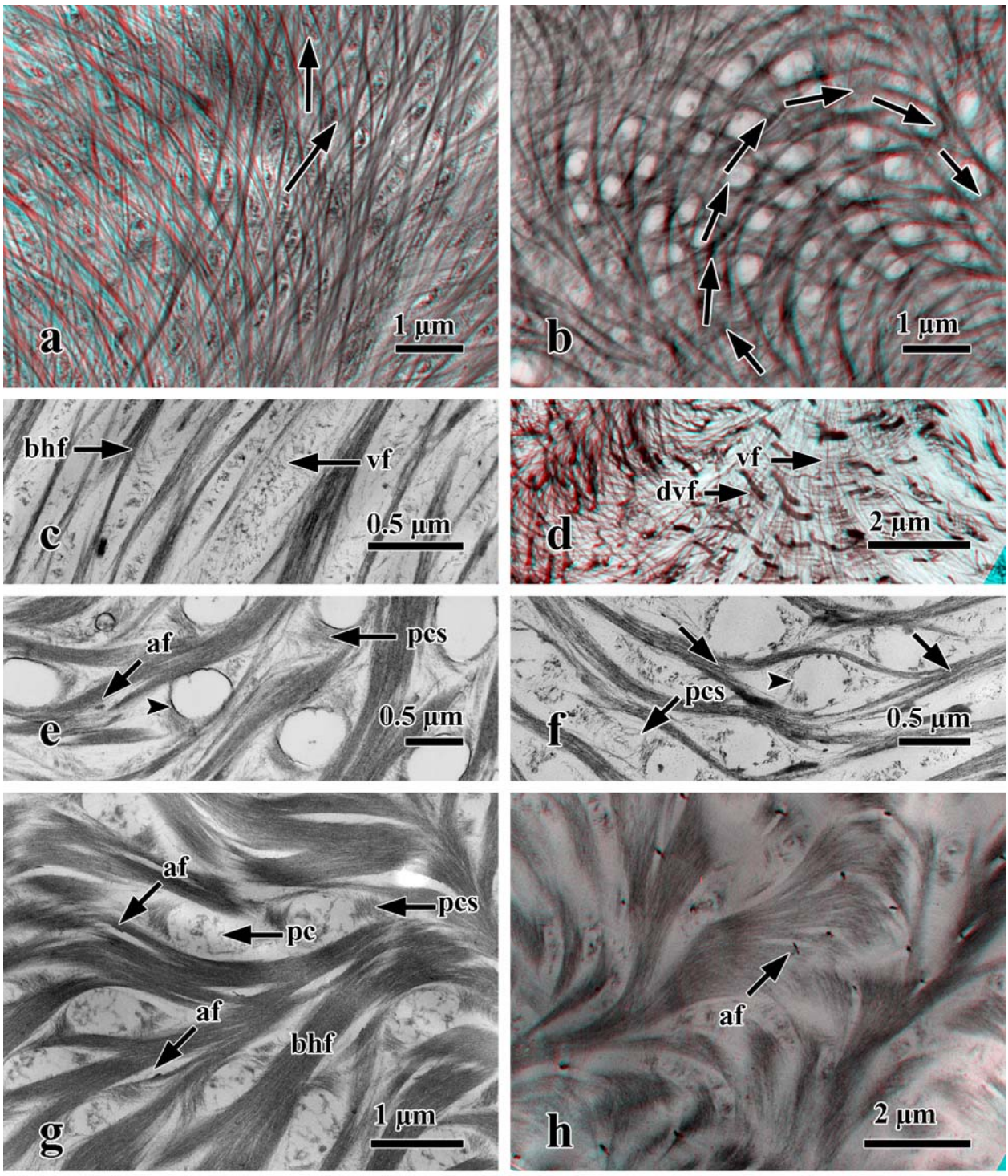
a
1 µm
b
1 µm
bhf
vf
c
0.5 µm
vf
dvf
d
2 µm
af
pcs
e
0.5 µm
pcs
f
0.5 µm
af
pcs
pc
af
bhf
g
1 µm
af
h
2 µm

cross-sections, these dvf did not traverse the entire width of the cuticle but only occurred in the distal third of the exocuticle (Figs. 12a; 13a).

The vf had the same electron density as the horizontal fibers but were oriented perpendicular to the cuticle surface (Fig. 15c). These vf were more numerous than the dvf coming from the epicuticle. Based on cross-sections, they were present across most of the exocuticle (Figs. 12b, d; Fig. 13b, d) but, in tangential sections, could only be identified in the distal and medial exocuticle. These fibers appeared as short fibrous segments or granular material between the bhf (Fig. 15c). Upon closer inspection, the larger bhf actually split to bypass the vf and pore canals, thereby forming a spindle-shaped compartment containing the vf or pore canals (Fig. 15f; arrows). Anaglyphs of thick sections revealed that the horizontal fibers in conjunction with the vertical fibers create an extensive interwoven network in the distal exocuticle (Fig. 15d).

Pore canals were absent in the distal lamellae of the exocuticle. They first became visible either within or slightly below the groupings of dvf (Fig. 14c, e). In cross-sections of the cuticle, the pore canals formed either continuous or discontinuous vertical channels that crossed lamellae (Figs. 12c, d; 13c, d). As in standard fixations, the pore canals initially were arranged in small groups (Fig. 14c, e; brackets), and the size of the groups and the number of pore canals increased from the medial to proximal exocuticle. Near the hypodermis, the pore canals reached a maximum size and became very abundant, acquiring a uniform distribution (Fig. 14d, f). In premolt crabs, the pore canals were often much larger than those from postmolt crabs and had a distended, dilated appearance (c.f.14c to 14e and 14d to 14f).

Unlike standard fixations, the pore canals in UA fixations lacked any cytoplasmic contents, and the preservation of the pore canal membrane varied from sample to sample. In some, the phospholipid membrane was well fixed, creating a defined boundary (Fig. 15e; arrowhead) while in others, the membrane was absent or only partially fixed so that the pore canal was difficult to identify, appearing as a round void defined by a pcs (Fig. 15f). The pore canals were bounded by bhf and a wedge-shaped aggregation of vertical fibers of the pcs (Fig. 15e, f).

In tangential sections obtained from the medial to proximal exocuticle, the fibers described as af in standard fixations were also seen in tangential sections (Fig. 15e, g). These obscure fibers crossed lamellae by intersecting bhf and were more clearly seen in anaglyphs (Fig. 15h).

The tf were not sampled in freshly fixed tissue but were observed in quick-frozen samples fixed in UA. In tangential sections, the appearance and arrangement of tf were similar to those seen in standard fixations but having much higher contrast (c.f. Fig. 16a and 7a). The tf tended to be laterally compressed with a fuzzy outline (Fig. 16a, c) and were thicker than the af described previously. Anaglyphs of tangential sections clearly showed that tf were arranged in pairs or small groups near the surface of the tendinuous epidermal cell (Fig. 16b, c) but become more dispersed distally (Fig. 16d). In standard fixations, the bhf appeared to curve around the groups of tf (Fig. 7b), but anaglyphs of UA fixed samples showed that the curvature was an optical illusion created by the overlap of short fibers in successive planes (Fig. 16c; arrow).

Figure 16. TEM of quick-frozen, uranyl acetate fixed dorsal carapace. a. Tangential section above a site of muscle insertion. b, c, d. Anaglyphs of tangential sections through the proximal (b, c) and medial (d) exocuticle above a tendinous epidermal cell at a site of muscle insertion. Note the overlap of bundles of horizontal fibers (arrows) in c. bundles of horizontal fibers, bhf; exocuticle above tendinous epidermal cell, TEC; granular material, arrowhead; tonofiber, tf

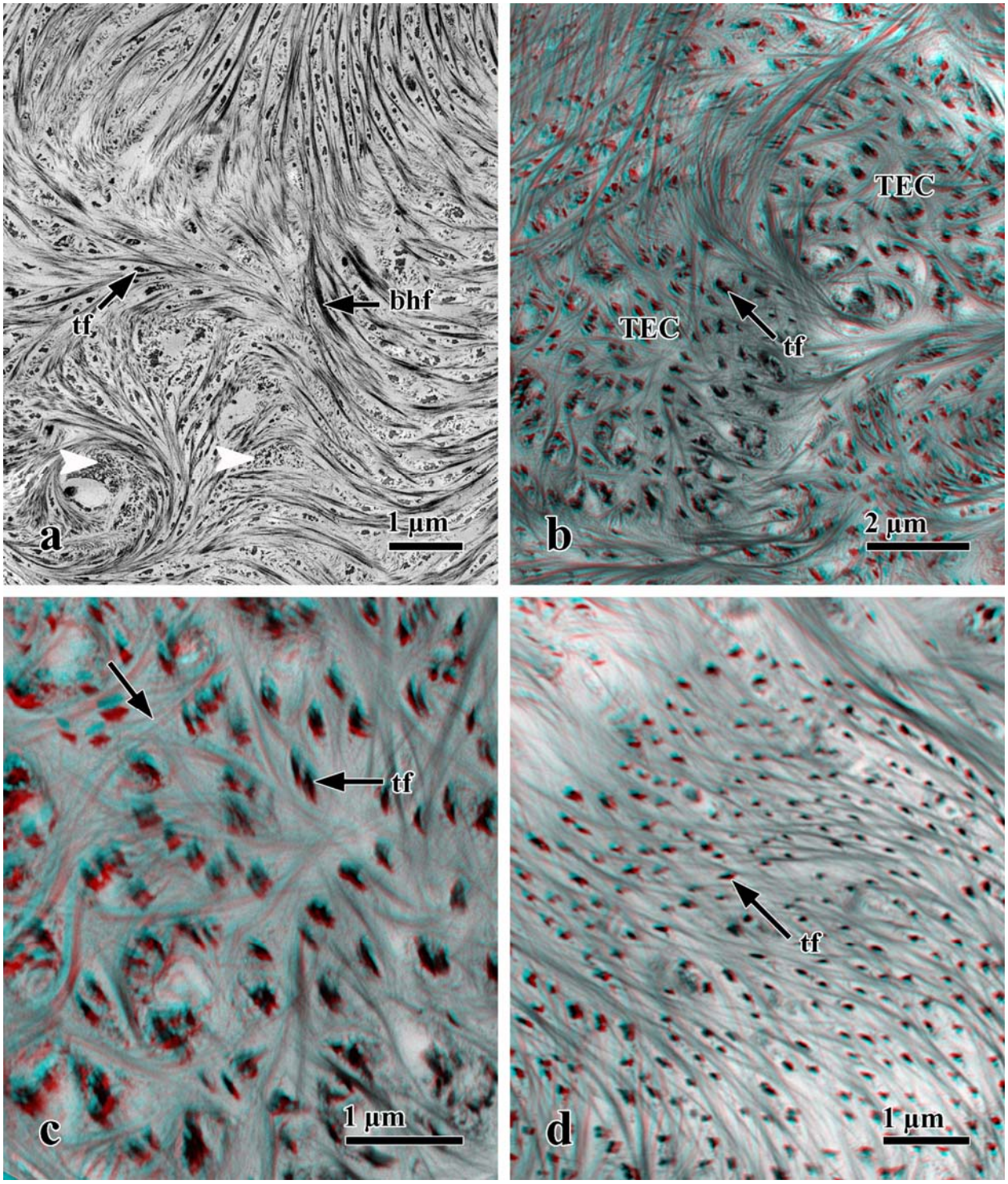
tf
bhf
1 µm
a
TEC
TEC
tf
2 µm
b
tf
1 µm
c
tf
1 µm
d

Quick-Frozen, Standard Fixed Tissue

All samples that were quick-frozen in liquid nitrogen and preserved by either standard or UA fixation yielded morphologies inferior to fresh tissue. Frozen samples treated by standard fixation produced much more variable results, partly as a result of poor infiltration. For example, the morphology of the hypodermis was variable, appearing well preserved in some preparations and poorly in others. However, some consistent freeze artifacts were observed. The most common artifact was the formation of voids in the ground substance between bhf. The voids were seen in both cross-sections (Fig. 17a, b) and tangential sections (Fig. 17c), but their size varied among samples and even within a single sample. Some voids were relatively minor and appeared as areas of lower electron density between bhf (Fig. 17a). However, others were extensive and consequently displaced fibers, disrupting their normally well ordered, periodic arrangement (Fig. 17b, c) and transforming the cuticle into an extensive latticework. Voids followed the rotation of successive planes of bhf, being cut in cross-section in the center of lamellae and in longitudinal section at the interface between adjacent lamellae (Fig. 17c).

There was poor preservation of cellular components, with pore canals being considerably shriveled, becoming small vesicular structures (Fig. 17a, d). In some instances, pore canals were only seen in sections taken close to the hypodermis.

Quick-Frozen, Uranyl Acetate Fixed Tissue

Quick-frozen samples fixed by UA were less adversely impacted than those fixed by standard methods and results were more consistent. Small elongate voids were seen between bhf, causing the fibers to be displaced (Fig. 18a, b). The size of the voids varied among samples. In some instances, the voids were so minor that the cuticle appeared virtually identical to freshly

Figure 17. TEM of quick-frozen, standard fixed dorsal carapace. a, b. Cross-sections showing minor (a) and severe (b) freeze artifacts. c. Oblique section through the exocuticle showing severe freeze artifact. d. Tangential section through proximal exocuticle. Note the poor preservation of pore canals (pc). bundles of horizontal fibers, bhf; inner epicuticle, ie; exocuticle, Exo; pore canal, pc; voids, asterix

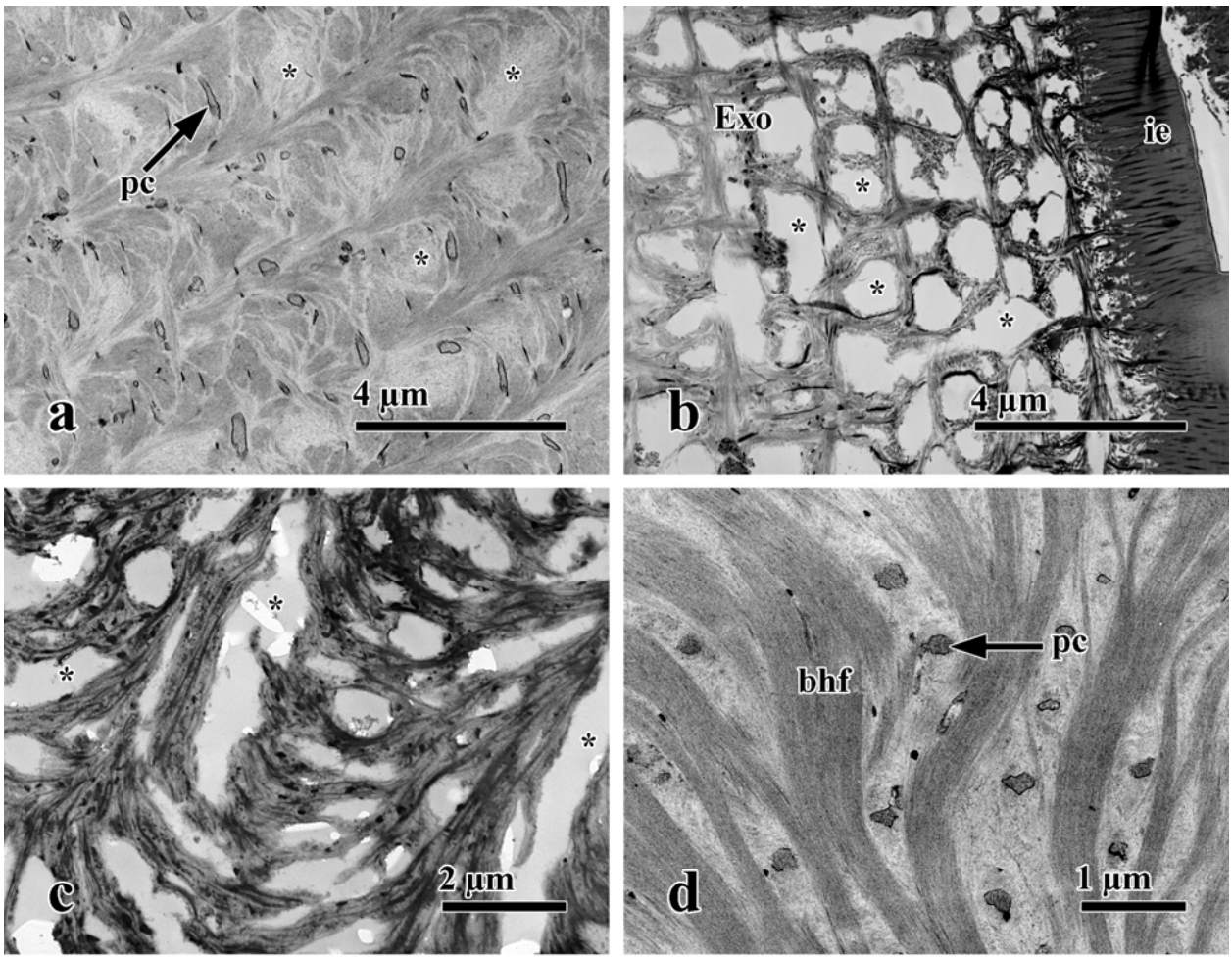
pc
4 µm
a
Exo
ie
4 µm
b
2 µm
c
bhf
pc
1 µm
d

Figure 18. TEM of quick-frozen, uranyl acetate fixed dorsal carapace. a. Cross-section through the exocuticle. b, c, d. Tangential sections through the distal exocuticle (b), inner epicuticle (c), and proximal exocuticle (d). bundles of horizontal fibers, bhf; pore canal, pc; void, asterix; voids in inner epicuticle, arrowheads

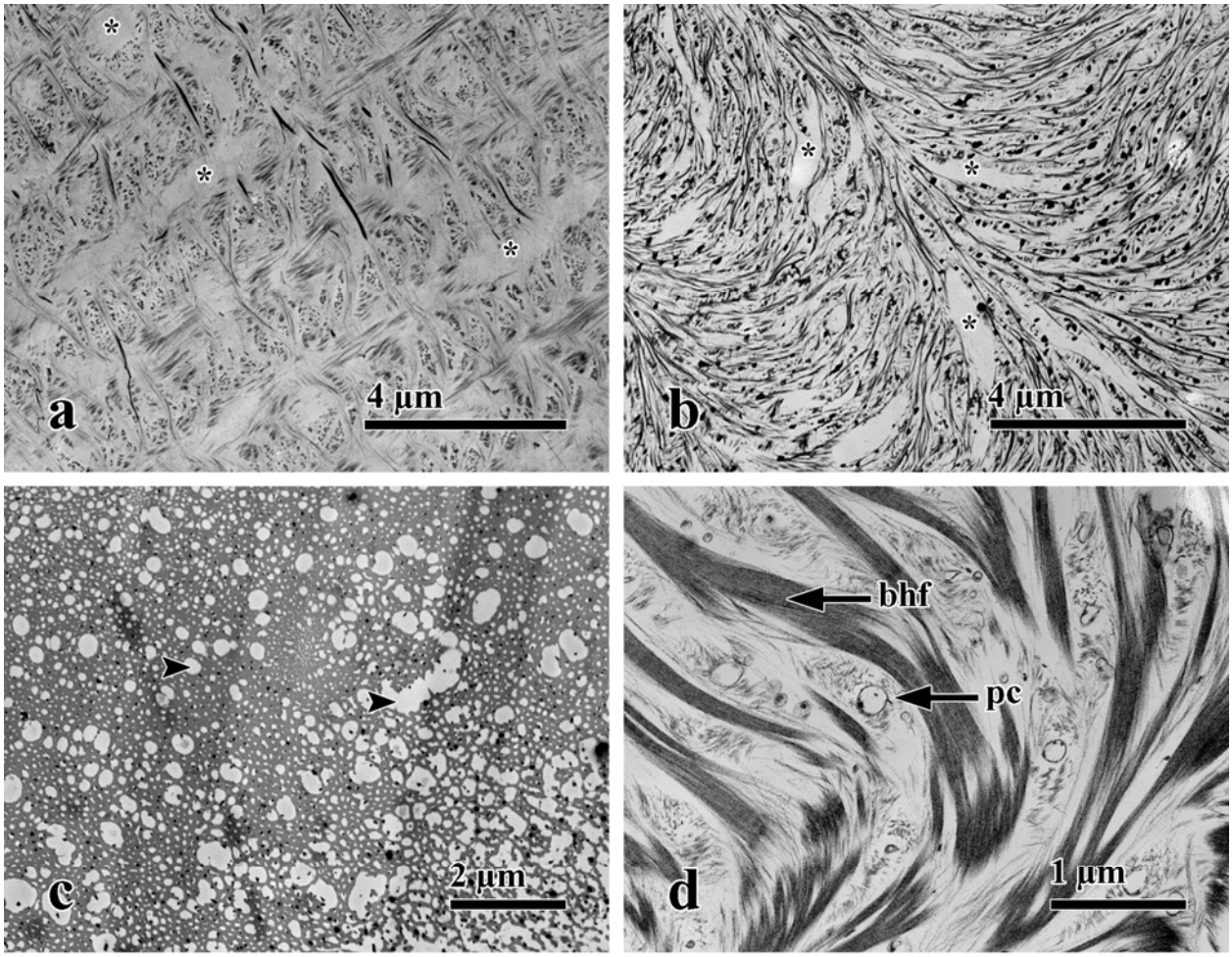
a
4 µm
b
4 µm
c
2 µm
d
bhf
pc
1 µm

fixed samples. In other instances, the voids were more noticeable, but they never reached the same magnitude as those seen in some standard fixed samples. In addition to the elongate voids between fibers, voids were also observed in tangential sections through the inner epicuticle (Fig. 18c).

Freezing also deteriorated the pore canals. In most samples, pore canals were only observed in the lamellae of the proximal exocuticle, near the hypodermis (Fig. 18d) and, when present, they were smaller than those freshly fixed and defined either by a membrane or an empty canal bordered by a pcs.

Lyophilized, Standard Fixed Tissue

For both standard and UA fixations, lyophilization greatly disrupted the arrangement of fibers in the exocuticle by amplifying the artifacts produced by quick-freezing. In standard fixations, lyophilization created an extensive network of voids between the fibers of the exocuticle (Fig. 19a, c). The voids were not restricted to specific regions but, rather, extended throughout the exocuticle and were more numerous and larger than in most quick-frozen samples. In cross-sections, lyophilization caused the cuticle to be transformed into a latticework containing a lamellar periodicity (Fig. 19a). The voids displaced the adjacent fibers, causing them to condense so that individual bhf could not be resolved (Fig. 19b). Most of the voids were empty but some contained a fine granular material.

Although the epicuticle remained relatively unaffected by lyophilization, the hypodermis and associated pore canals were greatly altered (Fig. 19d). Pore canals were shrunken and localized to the lamellae near the hypodermis. The cytoplasm of the hypodermis was highly vesiculated and organelles could not be recognized.

Figure 19. TEM of lyophilized, standard fixed dorsal carapace. a, b, d. Low (a) and higher (b, d) magnifications of cross-sections through the exocuticle. c. Tangential section through the exocuticle. exocuticle, Exo; hypodermis, H; pore canal, pc; microvilli, mv; voids, asterix

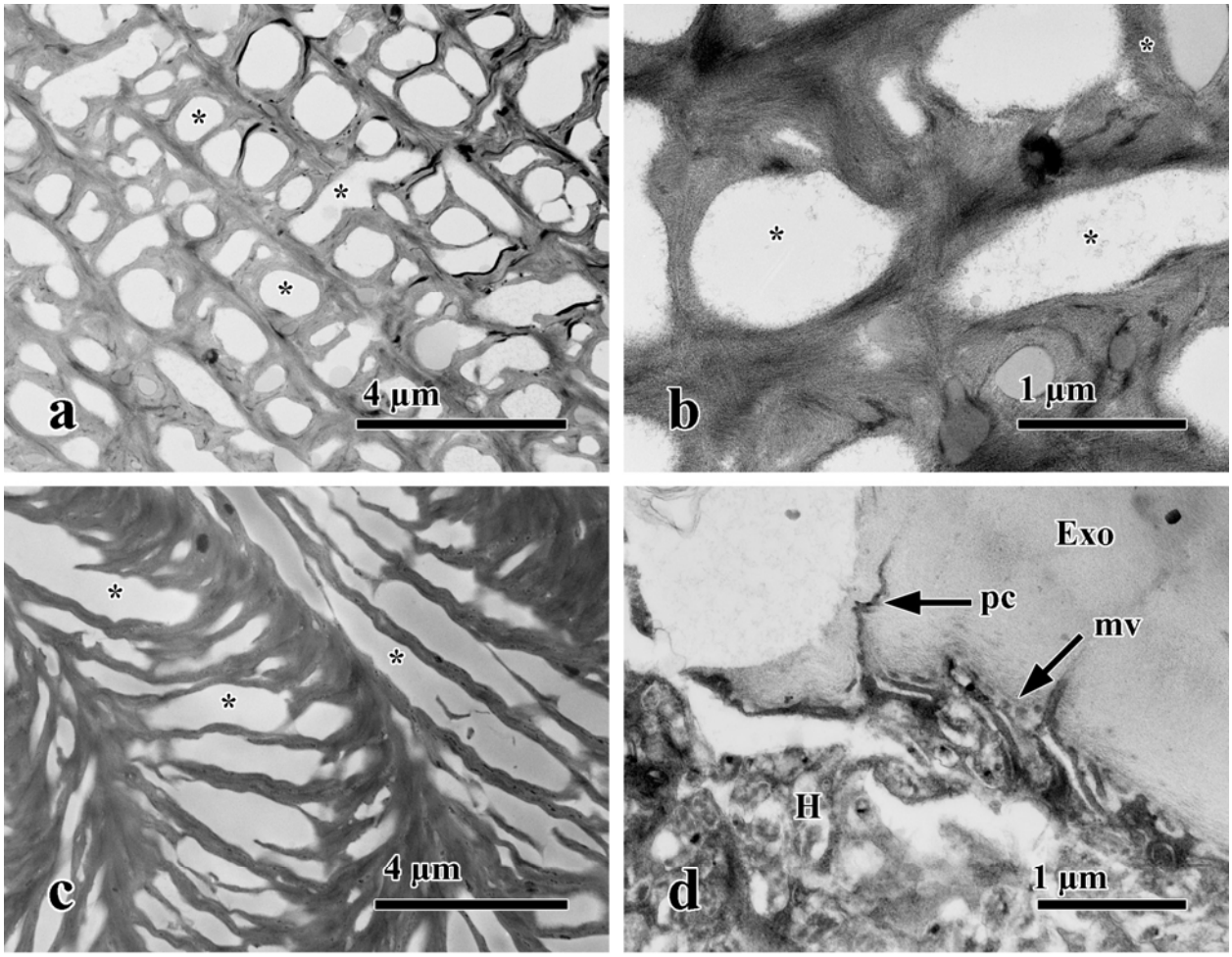
a
4 µm
b
1 µm
c
4 µm
d
Exo
pc
mv
H
1 µm

Lyophilized, Uranyl Acetate Fixed Tissue

In UA fixation, lyophilization intensified the artifacts caused by quick-freezing. Lyophilized samples were characterized by a series of round or elongate voids occurring inner epicuticle (Fig. 20c). The exocuticular voids were more extensive than those seen in quick-frozen samples fixed by UA but not as severe as the ones occurring in lyophilized samples subsequently treated by the standard fixation. Anaglyphs revealed that the voids followed the helicoidal geometry of the bhf (Fig. 20e). Unlike standard fixations, the voids created by lyophilization of UA fixed samples did not compress the bhf to the same extent and, due in part to the higher contrast, bhf could be recognized. The appearance of voids varied slightly from one sample to another, with some having a well defined boundary (Fig. 20a) while others lacked a distinct margin (Fig. 20b). In cross-sections, the cuticle did not have an extensive latticework morphology as in lyophilized samples treated by standard fixation and retained most of the characteristics of a fibrous matrix (Fig. 20d) despite having voids throughout the lamellae.

Lyophilized, Embedded Tissue

Lyophilized, unfixed samples had a unique morphology unlike those frozen or lyophilized and then treated with standard or UA fixation. The fibrous matrix normally observed in fixed samples was virtually absent, and the exocuticle was transformed into an intricate latticework, resembling a section through cellular foam (Fig. 21a, b, c). Overall, the exocuticle morphology was dominated by continuous tubes that appeared as circular voids when cut in cross-section or as elongate cylinders when cut in longitudinal section. In cross-sections of the cuticle, the circular profiles dominated except where the bhf were in the plane of the section (Fig. 21a; arrowhead) while, in tangential sections of the cuticle, the cylindrical profiles dominated

Figure 20. TEM of lyophilized, uranyl acetate fixed dorsal carapace. a, b, c. Tangential sections through the exocuticle (a, b) and inner epicuticle (c). Note that voids appear well defined in some instances (a) and poorly defined in others (b). d. Cross-section through the exocuticle. e. Anaglyph of tangential section through the exocuticle showing the rotation of voids in successive planes (arrows). bundles of horizontal fibers, bhf; inner epicuticle, ie; voids, asterix

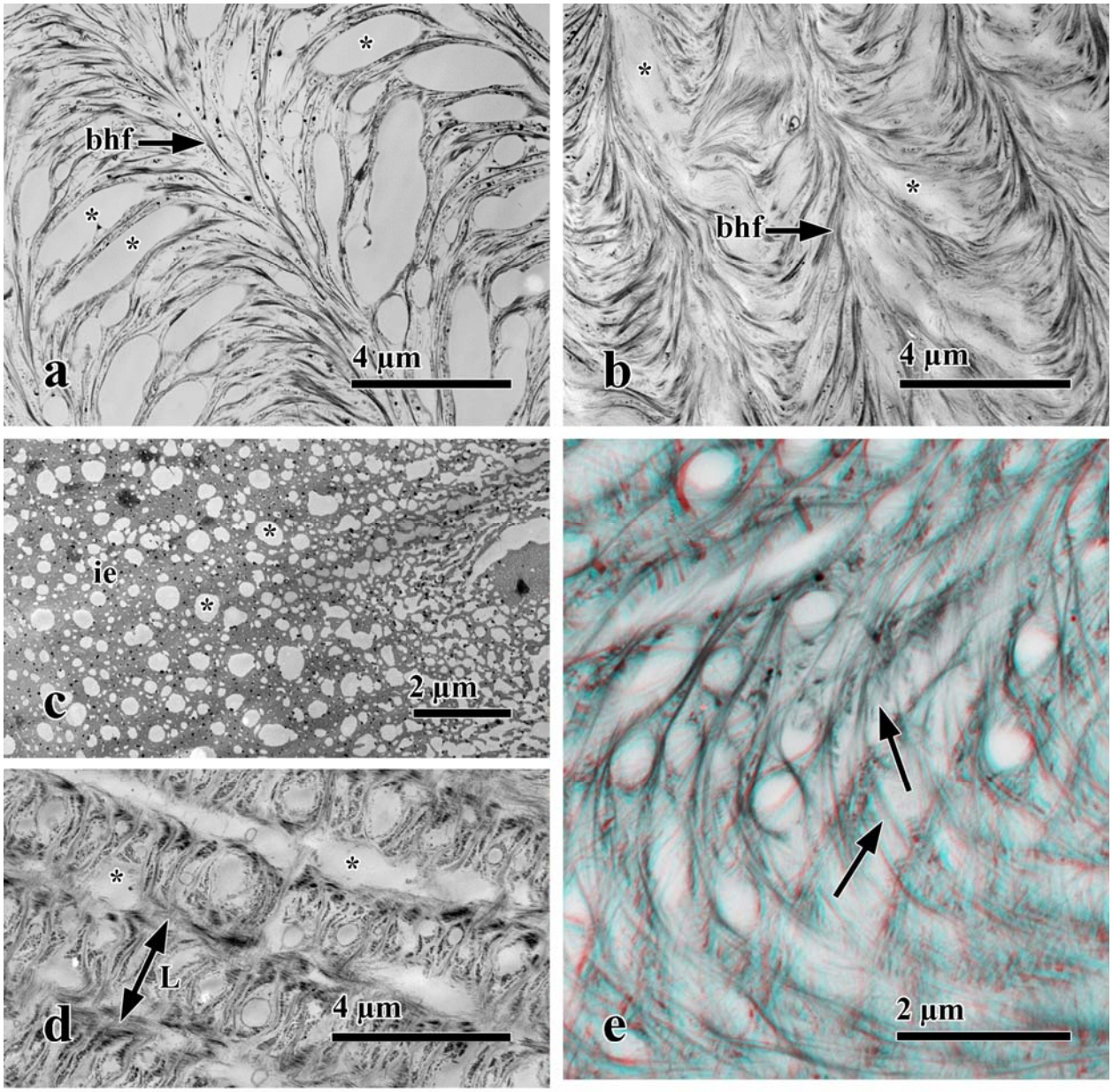
bhf
4 µm
a
bhf
4 µm
b
ie
2 µm
c
L
4 µm
d
2 µm
e

Figure 21. TEM of lyophilized, embedded dorsal carapace. a. Cross-section through the cuticle. b, c, d, e. Tangential sections through the medial exocuticle (b, c, d) and inner epicuticle (e). Note the fine fibers within the amorphous material (curved arrow) f. Thick tangential section through the exocuticle. Note the discrete groups of vertical tubes (bracket). epicuticular canals, ec; epicuticular roots, er; inner epicuticle, ie; tubes cut longitudinally, arrowhead; walls of tubes, arrow

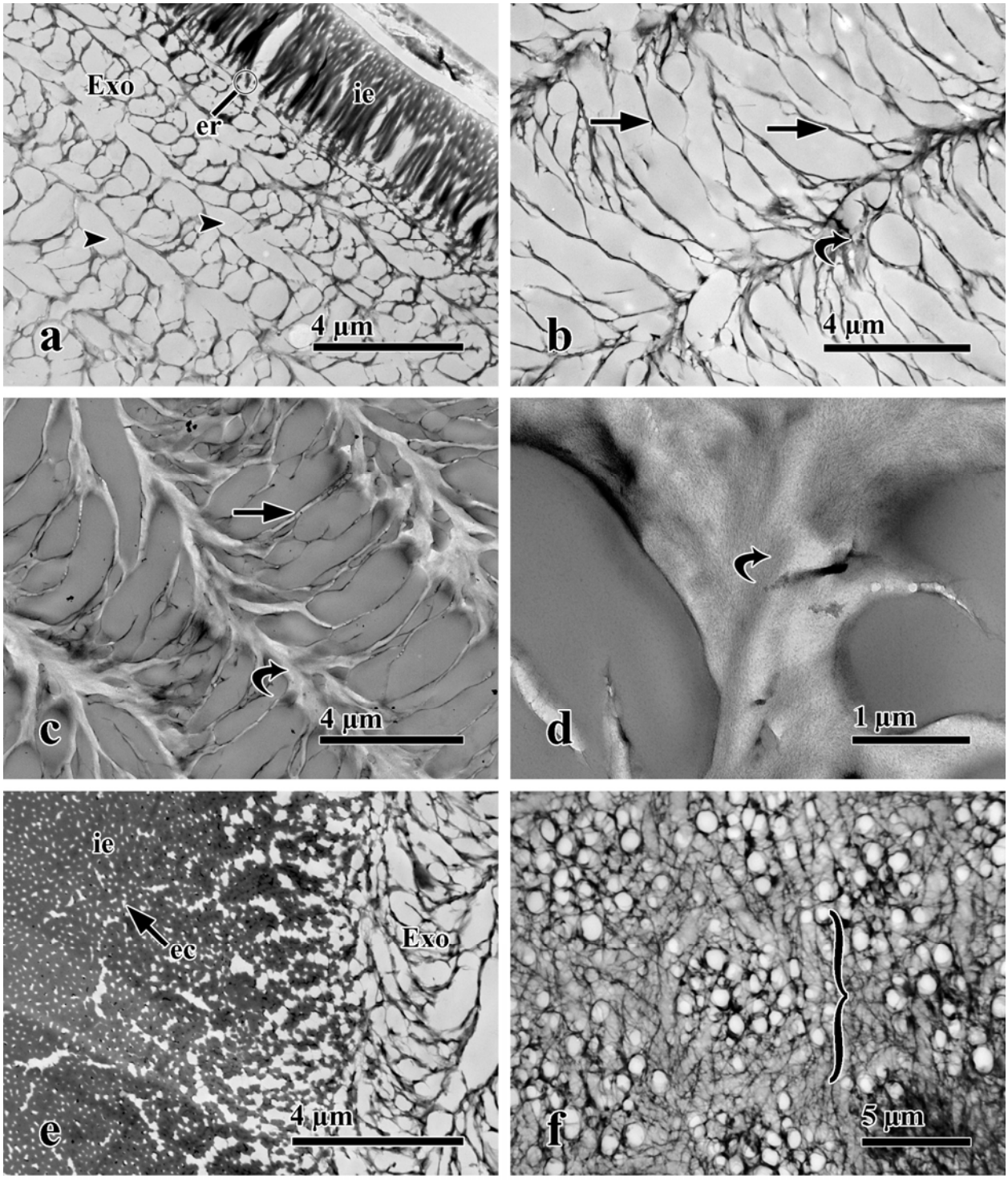
Exo
er
ie
a
4 µm
b
4 µm
c
4 µm
d
1 µm
ie
ec
Exo
e
4 µm
f
5 µm

(Fig. 21b, c). The walls of the tubes were formed by either thin, electron dense filaments (Fig. 21b) or a slightly thicker electron lucent material (Fig. 21c). The electron lucent material appeared to be areas that excluded resin upon embedding but whose contents were subsequently extracted during sectioning. Often attached to the walls of the tubes was an amorphous material, sometimes occurring in dense aggregates (Fig. 21b, c, d). Very fine fibers were seen within the amorphous material and electron lucent walls of the tubes when examined at high magnifications (Fig. 21d).

Although unfixed lyophilized cuticle possessed a morphology completely unlike fresh tissue treated by standard fixation, some similarities were observed. First, the epicuticle was clearly recognizable. As in fixed samples, the epicuticle was made up of vertical roots that terminated within the matrix of the exocuticle (Fig. 21a) and contained epicuticular canals (Fig. 21e). Next, the plywood-like geometry was maintained in lyophilized, unfixed samples. In cross-sections, the exocuticle appeared as an intricate latticework composed of round tubes of varying sizes that exhibited a lamellar periodicity resulting from the continual rotation of tubes through successive planes (Fig. 21a). Moreover, when the cuticle was sectioned obliquely, the tubes created an arcing pattern, reminiscent of patterns for fibers seen in fixed samples (Fig. 21b, c). A final congruency was the observation of round groups of vertical tubes in thick, tangential sections (Fig. 21f). The round groups seemed similar to the discrete groups of pore canals seen in the medial exocuticle of fixed samples.

Lyophilized, Rehydrated Tissue

Finally, lyophilized samples were examined that had been rehydrated in water then dehydrated in acetone. This treatment reconstituted the fibrous matrix absent in lyophilized and

Figure 22. TEM of lyophilized, rehydrated dorsal carapace. Low (a, c) and higher (b, d) magnifications of cross-sections through the distal exocuticle (a), epicuticle (a, b), and proximal exocuticle (c, d). bundles of horizontal fibers cut longitudinally, arrowhead; dense vertical fibers, dvf; epicuticular fibers, ef; epicuticular roots, er; exocuticle, Exo; pore canal, pc; vertical fibers, vf; voids, asterix

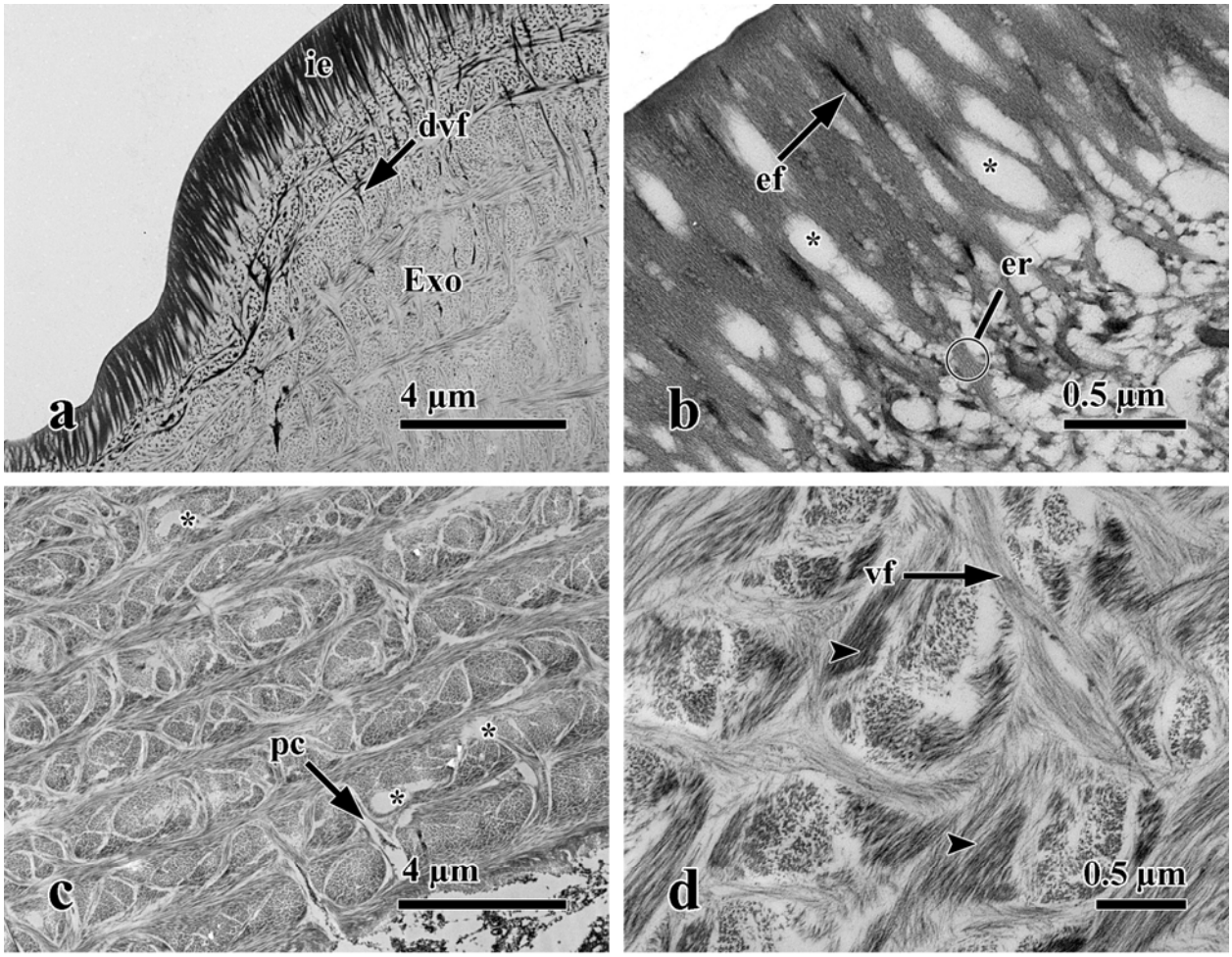
ie
dvf
Exo
4 µm
a
ef
*
*
er
0.5 µm
b
*
pc
*
*
4 µm
c
vf
0.5 µm
d

embedded sampled such that it most closely resembled the morphology of UA fixed samples. This was most obvious in cross-sections (Fig. 22a-d). Similar to UA fixations, bhf rotated in successive planes; however, the fibers in lyophilized and rehydrated samples, while highly contrasted, were not as condensed and appeared more uniformly dispersed than in UA fixations (cf. 22a, c, d and 12a, c, d). Perhaps as a consequence, less space was seen surrounding the vertical fibers that crossed lamellae, and the lumens of pore canals were less prominent (Fig. 22c, d). The morphology of the epicuticle was similar to uranyl acetate fixed samples, being composed of vertical roots (Fig. 22b). The filaments comprising the vertical roots were more apparent in rehydrated samples than UA fixed samples (c.f. 22b and 10a). Voids similar to those seen in frozen or lyophilized samples fixed in UA were present within or between lamellae in cross-section (Fig. 22c) and in the inner epicuticle (Figs. 22b; 23a) and between bhf in tangential section (Fig. 23b, c).

Tangential sections of lyophilized, rehydrated samples displayed most of the fiber types and fiber arrangements as those seen in UA fixation, such as ef, bhf, vf, pcs, and af (Fig. 23b, c, d). A notable exception were the IPS and EZ, which were completely absent in lyophilized and rehydrated samples. Furthermore, the bhf in lyophilized and rehydrated samples were less compact than in UA fixed samples. Whereas in UA fixation, bhf were clearly separated from one another by much free space containing few vf, in lyophilized, rehydrated samples, the space between bhf was completely filled with vf that stained with the same intensity as the bhf (cf. 23c and 15c). Consequently, vf occupied a larger fraction of space in lyophilized, rehydrated samples than UA fixed samples. The pore canals were only apparent in the proximal exocuticle where their lumen was filled by an expanded pcs (Fig. 23d). This expanded pcs filled the spindle

Figure 23. TEM of lyophilized, rehydrated dorsal carapace. Tangential sections through the inner epicuticle (a), distal exocuticle (b), medial exocuticle (c), and proximal exocuticle (d). anchoring fibers, af; bundles of horizontal fibers, bhf; dense vertical fibers, dvf; exocuticle, Exo; inner epicuticle, ie; pore canal sheath, pcs; vertical fibers, vf; voids; asterix

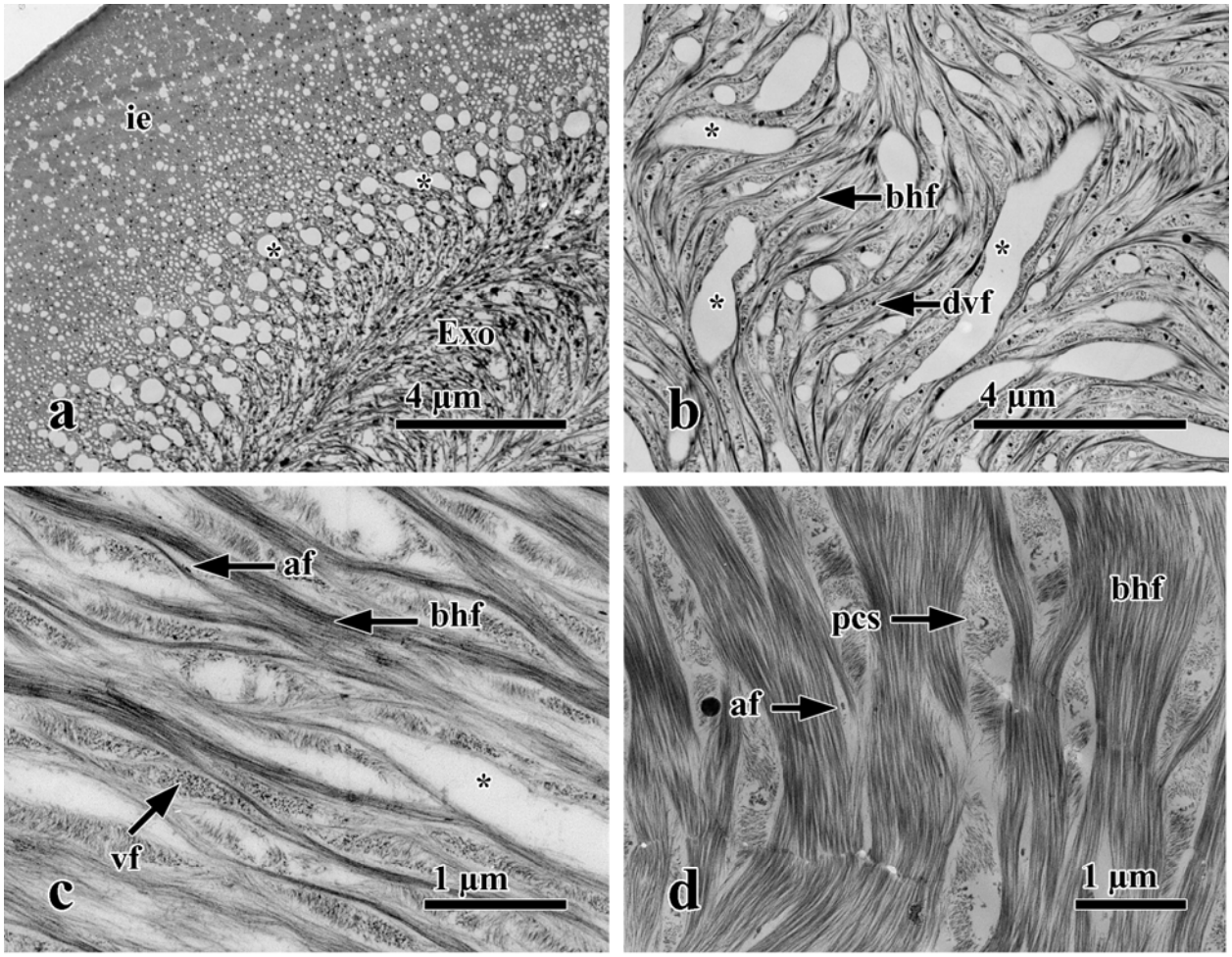
ie
Exo
4 µm
a
bhf
dvf
4 µm
b
af
bhf
vf
1 µm
c
pcs
af
bhf
1 µm
d

shaped compartment bounded by the bhf (cf. 23d and 15e, f). As expected, neither the membranes of the pore canals nor the hypodermis were preserved in this treatment.

SEM Observations

Fresh, Standard Fixed Tissue

Standard fixed samples and lyophilized, unfixed samples were examined by scanning electron microscopy. The morphology of standard fixed samples was consistent with those seen in the TEM. The appearance of premolt cuticle was the same as postmolt crabs, the exception being that premolt cuticle was highly convoluted (Fig. 24a). The epicuticle was comprised of closely apposed vertical elements while the exocuticle consisted of a fibrous matrix (Fig. 24b, c). The fibers near the epicuticle were morphologically distinct from those in the medial to proximal exocuticle. Whereas fibers in the distal exocuticle were more diffuse (Fig. 24b, c), those in the medial and proximal exocuticle formed horizontal sheet-like lamellae of tightly packed fibers (Fig. 24b, d, e). Fibers within a lamella appeared to rotate relative to one another so that a single sheet was composed of fibers rotating through a 180˚ angle (Fig. 24d, e). Tangential fractures through the exocuticle preferentially exposed horizontal fibers oriented in the same direction (Fig. 25a). Consequently, horizontal fibers in adjacent sheets frequently appeared parallel to one another. Tangential fractures also showed numerous pore canals with their associated pcs embedded within the fibrous sheet (Fig. 25a, b). Horizontal fibers of the fibrous sheet were closely apposed to one another but became displaced to either side in regions containing pore canals (Fig. 25b; arrowheads).

Figure 24. SEM of fresh, standard fixed dorsal carapace treated with HMDS and fractured. a. Highly folded premolt cuticle. b. Overview of the cuticle. Note that horizontal fibers appear more diffuse near the epicuticle than more proximally. c. Higher magnification of epicuticle and distal exocuticle. d, e. Higher magnification of medial exocuticle. Note that horizontal fibers are arranged in sheet-like lamellae (sl) and rotate in successive planes (e; arrows). diffuse horizontal fibers, dhf; epicuticular root, er; exocuticle, Exo; inner epicuticle, ie; sheet-like lamella, sl.

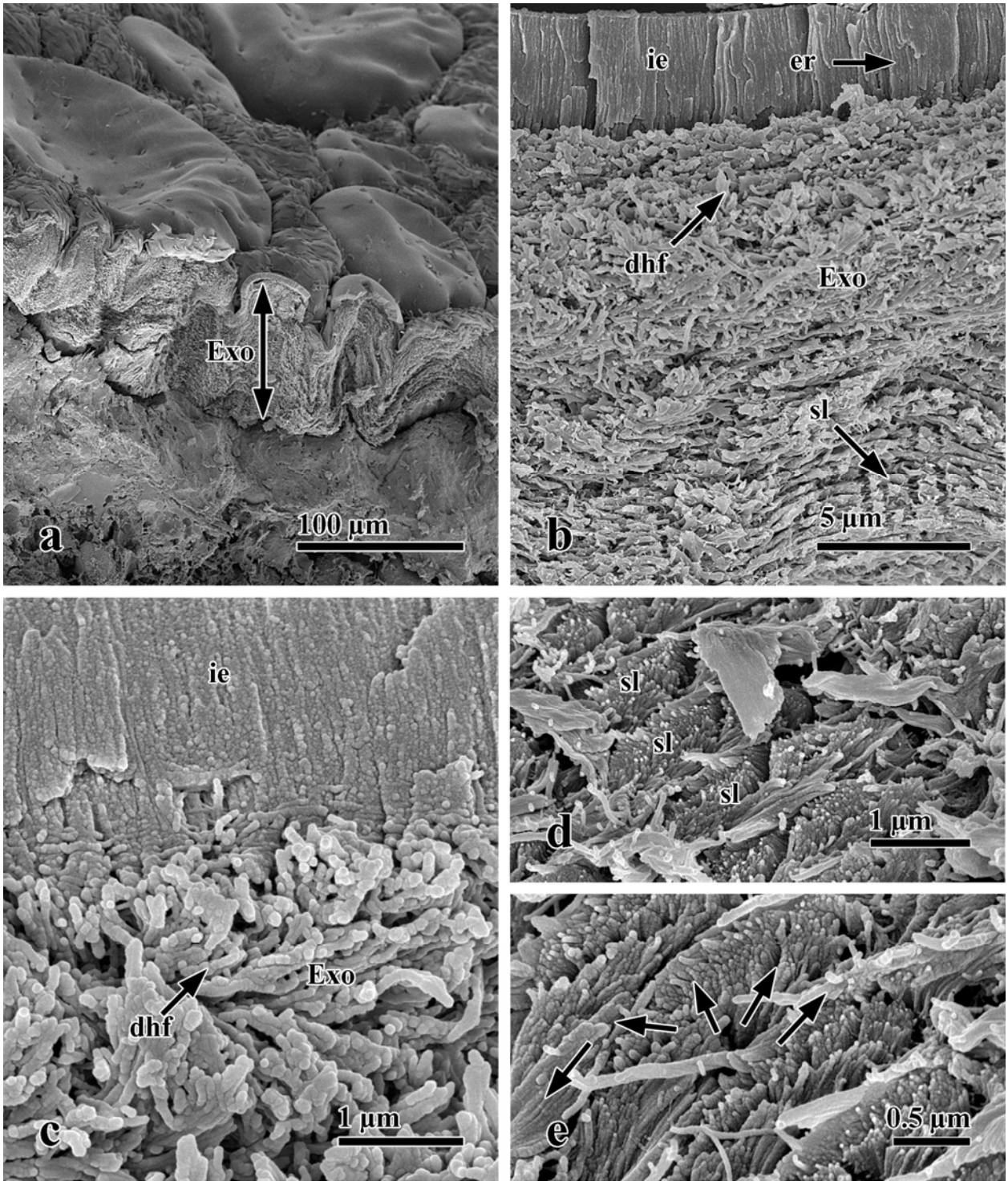
a
Exo
100 µm
b
ie
er
dhf
Exo
sl
5 µm
c
ie
Exo
dhf
1 µm
d
sl
sl
sl
1 µm
e
0.5 µm

Figure 25. SEM of fresh, standard fixed dorsal carapace treated with HMDS and fractured. a, b. Tangential fractures through the exocuticle. Note how the fracture preferentially exposes horizontal fibers oriented in the same direction (sl1-4; a). Note the rotation of horizontal fibers (b; arrow) and the displacement of horizontal fibers around a pore canals (b; arrowheads). pore canal, pc; pore canal sheath, pcs; successive sheet-like lamellae, sl1-4.

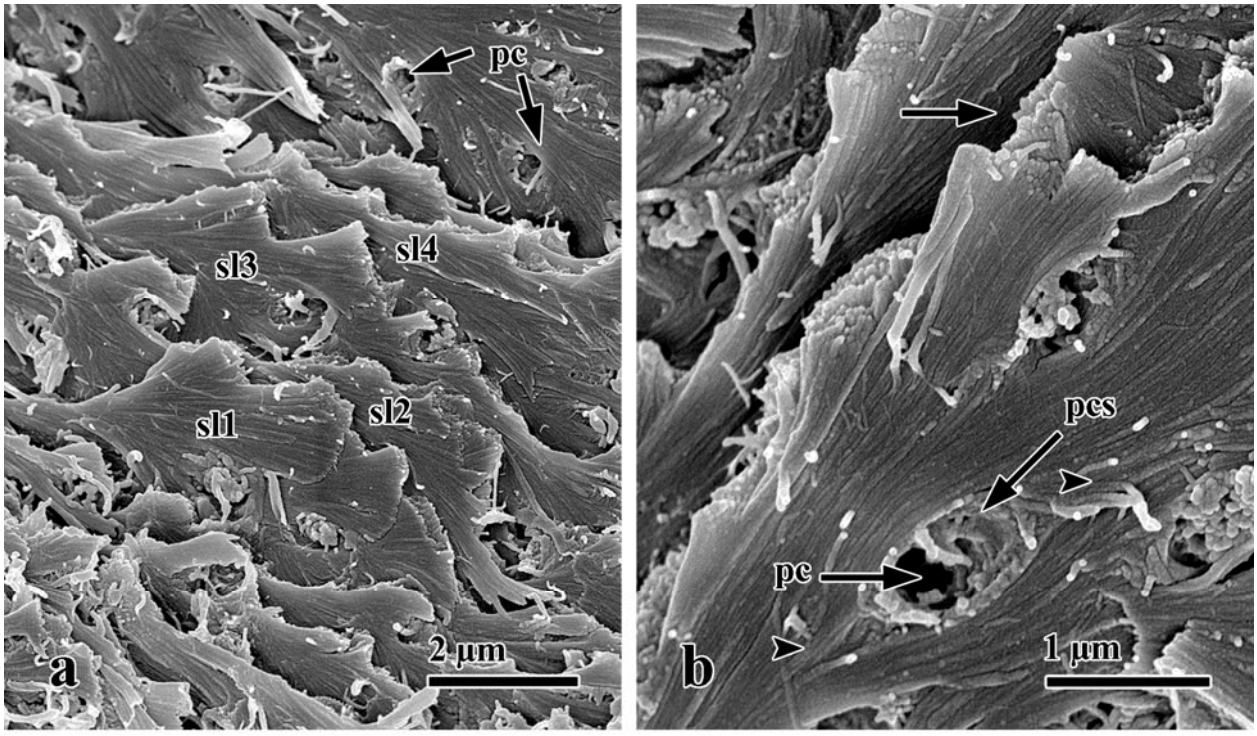
pc
sl3
sl4
sl1
sl2
2 µm
a
pcs
pc
1 µm
b

Lyophilized, Unfixed Tissue

When lyophilized samples were compared to those viewed with the TEM, the epicuticles were similar, but the fibrous matrix was transformed into rows of tubes having a lamellar aspect (Fig. 26a, b, c). In fractures that broke the cuticle tangentially (Fig. 26e) or slightly obliquely (Fig. 26d), the tubes within a given plane were oriented parallel to one another while tubes in adjacent planes were successively rotated. Although the tubes were hollow, the inside surface of the lumen contained a few stray fibers, giving it a faint striated appearance (Fig. 26f). Pore canals were greatly reduced in both size and abundance and were only evident in some tangential fractures (Fig. 26e). Although tubes were present in all unfixed lyophilized tissue, some regions within samples had a more fibrous morphology (Fig. 26g).

DISCUSSION

Comments on General Fixation

This project examined the effects of both physical (quick-freezing and lyophilization) and chemical (standard and UA) fixation on the morphology of the late premolt and early postmolt cuticle, and results demonstrate that the appearance of the crustacean cuticle is highly dependent upon the mode of specimen handling and preservation. For instance, in lyophilized, unfixed samples, the cuticle is transformed into a highly intricate latticework of tubes whereas in chemically fixed samples, the cuticle appears as a dense fibrous matrix. These two diametrically apposed morphologies brought into question the true nature of the crustacean cuticle. Since some constituents of the dorsal carapace have been implicated in controlling biomineralization, knowing their morphology and distribution, especially near the time of ecdysis, is of utmost importance in identifying those fibers that may inhibit, nucleate, and regulate the growth of calcium carbonate crystals.

Figure 26. SEM of lyophilized, unfixed and fractured dorsal carapace. a, c. Transverse fracture through the epicuticle (a) and exocuticle (a, c). b. Anaglyph of transverse fracture through the exocuticle. d. Oblique fracture through the exocuticle. Note the rotation of tubes (arrows). e, f. Tangential fractures through exocuticle. Note the rotation of tubes (arrows in e) and the fibers compressed along the walls of the tubes (arrowhead in f). g. Location in exocuticle exhibiting a more fibrous morphology. exocuticle, Exo; inner epicuticle, ie; pore canal, pc; tubes fractured longitudinally, ls; tubes fractured transversely; xs

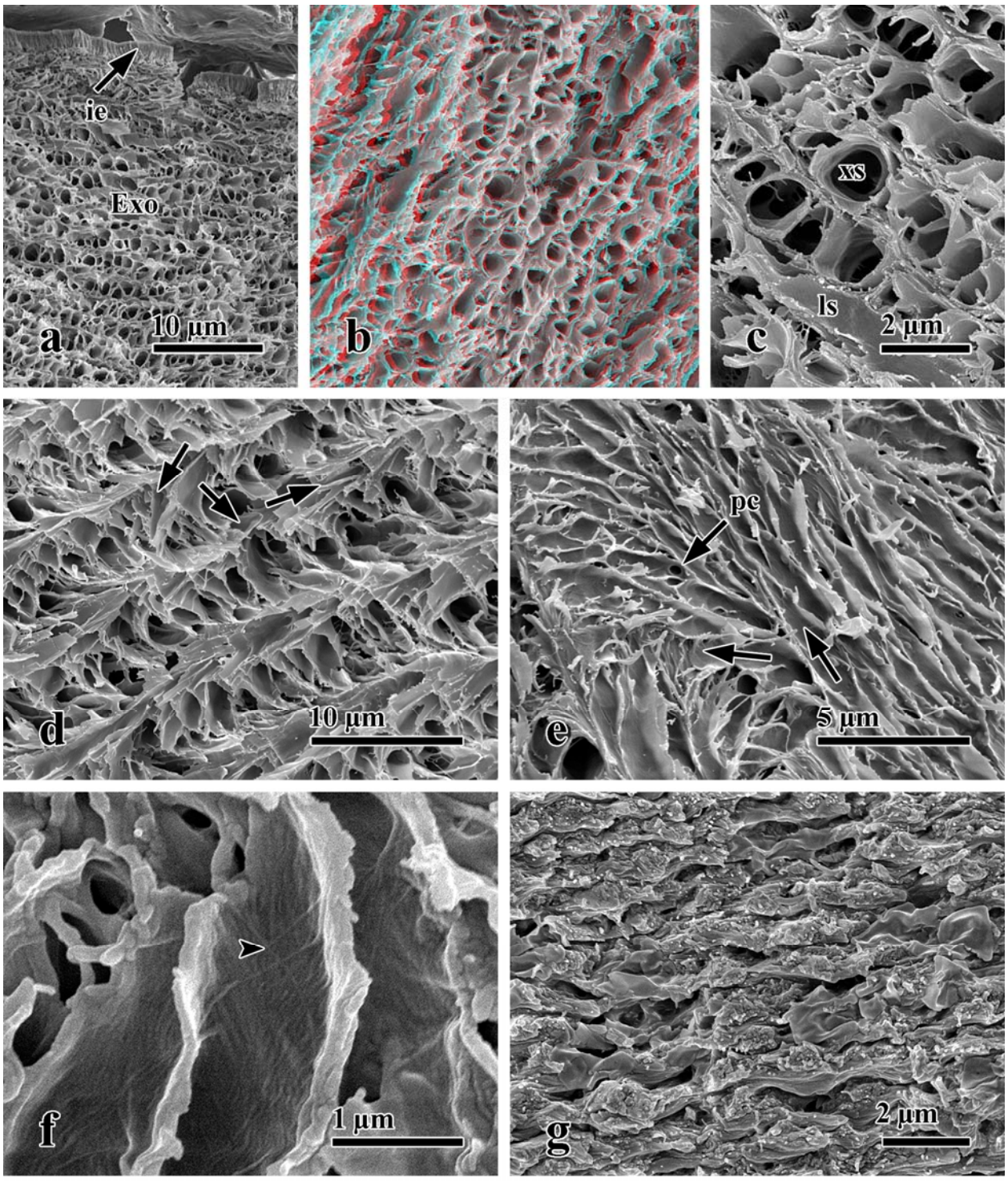
ie
Exo
10 µm
a
b
xs
ls
2 µm
c
10 µm
d
pc
5 µm
e
1 µm
f
2 µm
g

Chemical fixation, quick-freezing, and lyophilization can introduce a number of artifacts that distort the actual structure of a living specimen in its native state. In ideal chemical fixations, the fixative should penetrate the specimen rapidly to prevent post-mortem changes and protect against extraction, distortion, or shrinkage during subsequent stages of dehydration, infiltration, sectioning, and viewing with the electron beam (Bozzola & Russell, 1999). Unfortunately, no chemical fixative can fully meet the ideal requirements. Many fixatives, including glutaraldehyde, osmium tetroxide, and tannic acid, penetrate tissues slowly, and the subsequent reactions that cross-link and stabilize the organic components do not occur instantaneously. Moreover, chemical fixatives are not multipotent and cannot stabilize every chemical constituent of the tissue (Gilkey and Staehelin, 1986; Hayat, 2000). Glutaraldehyde effectively cross-links proteins while osmium tetroxide fixes lipids. Various other factors such a pH, osmolarity, temperature, ionic composition, duration of fixation, concentration of the fixative, buffer choice, embedding medium, and the type of tissue to be processed can all impact the quality of specimen preservation (Hayat, 2000).

To circumvent a number of problems that may occur during chemical fixation, a specimen can be rapidly frozen. Ultra-rapid freezing stops cell physiological processes more quickly than chemical fixatives and retains a greater proportion of molecules that would otherwise be extracted during chemical processing. However, just as with chemical fixation, rapid freezing also has a number of disadvantages. True vitrification of biological tissues is often not possible and, consequently, inadequate freezing or vitrification followed by thawing and recrystallization can introduce ice crystals that cause structural damage. The use of cryoprotectants can minimize ice crystal formation, but these chemicals can also introduce

artifacts such as osmotic shrinkage or displacement of intracellular structures (Gilkey and Staehelin, 1986; Hayat, 2000).

Since most embedding media for the TEM are immiscible with water, frozen specimens must be lyophilized to sublimate ice. Lyophilization can also be problematic. The temperatures and times required to sublimate the ice with minimal artifacts vary from one sample to the next and must be determined experimentally. Moreover, the size, structure, and composition of the frozen specimen can impede the diffusion of water vapor. Chemically bound water does not freeze, making it impervious to removal by lyophilization (Edelmann, 1986). Additionally, lyophilization of certain buffer, sugar, and salt solutions has been shown to generate an artifactual latticework of filamentous structures that can be mistaken for biological material (Miller et al., 1983). Sublimation of ice can also cause dimensional changes due to significant tissue shrinkage or collapse (Edelmann, 1986; Hayat, 2000).

From the above discussion, it is clear that a wide range of artifacts can be generated at any stage of specimen preparation. Therefore, to understand the true structure of the crustacean cuticle, it was paramount to determine whether the fibrous or tubular morphologies were an artifact of chemical fixation or freezing and lyophilization, respectively. To accomplish this task, samples were subjected to various combinations of chemical and physical treatments and examined to isolate specific variables and assess their contribution to the observed morphology.

Freeze Artifacts

In fresh tissue treated by standard and UA fixations, the cuticle appeared as a complex network of horizontal and vertical fibers. This fibrous morphology was also present in both quick-frozen and lyophilized samples subsequently treated with fixatives. However, quick-frozen samples also contained a number of voids between and parallel to the bundles of

horizontal fibers. Since voids were present in quick-frozen samples but absent in freshly fixed samples, they most likely represent an artifact caused by ice formation. Samples had been quick-frozen by placing the tissue into cryovials and dropping them in a dewar filled with liquid nitrogen. Liquid nitrogen is a poor cryogen for quick-freezing due to its low specific heat constant. It forms an insulating layer of nitrogen gas around the tissue and slows freezing (Hayat, 2000; Scouten & Cunningham, 2006). Consequently, ice crystals probably arose from the ground substance and grew in a direction parallel to that of the bundles of horizontal fibers. As the water in the cuticle changed phase, the ice excluded any ground materials and pushed the fibers to the side, generating voids.

The location and shape of the voids were uncharacteristic of typical freeze artifacts. Interestingly, voids only occurred in the plane parallel to the cuticle surface and none were observed perpendicular to the cuticle surface, suggesting that ice preferentially formed between horizontal fibers rather than vertical fibers and pore canals. Horizontal fibers may be more hydrated than vertical fibers. Alternatively, vertical fibers and pore canals may be associated with more ions than horizontal fibers and, consequently, the freezing point is depressed around their vicinity. Indeed, calcium ions have been localized to the pore canal lumen (Dillaman et al., 2005). Moreover, the voids were rounded, yielding circular profiles in cross-sections, and no needle-like profiles were observed. This may be attributed to the high degree of glycosylation of cuticular proteins, which may allow the proteins to control the shape and orientation of ice crystals (Marlowe et al., 1994; Shafer et al., 1994, 1995; Compère et al., 2002).

The voids appearing in quick-frozen samples were substantially larger and more widespread in lyophilized samples processed by standard or UA fixations. Amplification of the voids most likely reflects the degree of rehydration of the cuticle matrix. When the tissue is

placed in the chemical fixative, cross-linking reactions do not occur instantaneously. Therefore, in quick-frozen samples, the ice that formed between fibers had an opportunity to melt and partially reconstitute the fibrous matrix before being fixed in place. However, in lyophilized samples, sublimation removed ice prior to fixation. As a result, the fibers could only become rehydrated by the aqueous buffer that carried the fixative. Fibers in lyophilized samples would have less opportunity to rehydrate before becoming stabilized by the chemical fixative.

The effect of water on reforming the fibrous matrix was clearly seen when lyophilized, unfixed samples were compared to lyophilized samples rehydrated in water and dehydrated in acetone. Since lyophilized, unfixed samples were devoid of water and did not have an opportunity to rehydrate, they demonstrated the extreme consequences of ice formation due to inadequate freezing. Tubes appeared where ice severely displaced the surrounding fibers. Fibers could be seen pressed along the walls of the tubes in both the TEM and SEM. Interestingly, discrete regions of lyophilized, unfixed samples exhibited a more fibrous matrix when examined with both the TEM and SEM. Such fibrous areas could be locations where either some vitrification occurred, or ice crystals were too small to significantly cause structural modifications. Rehydration of lyophilized samples reconstituted the fibrous matrix so that it more closely resembled samples treated by standard or UA fixatives. Consequently, the true morphology of the crustacean cuticle appears to be that of a fibrous matrix while the tubular morphology is an artifact of quick-freezing.

Since lyophilization and freezing generate tubular artifacts, the fibrous morphologies seen by chemical fixations probably provide a close representation of the cuticle in its native state. Chemical fixatives are capable of cross-linking specific components of tissues and can therefore make certain structures selectively visible. Moreover, combinations of fixatives can

have agonistic or antagonistic effects. In some instances, fixatives or stains can interact and mask a particular component of a specimen whereas in other cases, they can have a mordanting effect and enhance contrast (Hayat, 1993). Due to this property, using different chemical regimes can prove useful when trying to elucidate all the morphological features of a specimen. In this study, cuticle was processed by either a standard fixation consisting of sequential fixation in 2.5% glutaraldehyde, 0.5% osmium tetroxide, 1.5% tannic acid, and 2% aqueous UA or by a fixation in 2% aqueous UA.

Differences between Standard and UA Fixations

Both standard and UA fixations yielded the same basic morphological patterns in terms of the types of fibers and their orientations and locations. However, the standard fixation differed greatly in overall appearance from UA fixation, and the two treatments could easily be differentiated primarily in five ways: (1) contrast of fibers, (2) preservation of cellular features, (3) preservation of IPS and EZ, (4) packing density of fibers, and (5) uniformity of fixation. First, UA fixation greatly enhanced the contrast of cuticle fibers, making them stand out against the background. Consequently, UA fixation was ideal for creating anagylphs. This was consistent with the contrast and preservation afforded by UA when it was used as a primary fixative for muscle (Fassel & Greaser, 1997) and as a secondary fixative to aldehyde-treated tissues (Locke, 1994).

Contrary to UA fixation, standard fixation caused the cuticle to appear as varying shades of gray and no one feature stood out against the rest. This was most likely attributed to the use of more fixatives, which, in addition to preserving a greater fraction of organic components, would also enhance the staining of those components. For instance, osmium tetroxide, tannic acid, and UA are capable of imparting electron density (Hayat, 1993). Moreover, both osmium

and tannic acid can function as mordants: osmium enhances lead staining while tannic acid can act as a mordant between osmicated structures and lead or for UA (Hayat, 1993). Additionally, tannic acid, followed by UA fixation was shown to have a selective affinity for both charged and neutral complex carbohydrates (Sannes et al., 1978). Since crustacean cuticle contains abundant glycoproteins, tannic acid likely contributed significantly to the staining pattern (Marlowe et al., 1994; Shafer et al., 1994, 1995; Compère et al., 2002). Therefore, since more cuticle features are preserved and stained by standard fixation, no one component could appear contrasted against the others.

As a corollary to the enhanced preservation offered by standard fixation, the voids appearing in lyophilized and quick-frozen samples fixed in UA were less extensive than those found in lyophilized and quick-frozen standard fixed samples. This observation points to the different cross-linking abilities of the two techniques. Standard fixations can preserve many more components and, therefore, create a more rigid structure than UA alone. Consequently, when fibers are displaced by ice, standard fixation will hold them in place more effectively and cause quick-frozen and lyophilized samples to appear more distorted in standard than in UA fixations.

A second difference between standard and UA fixations was the preservation of cellular features. UA did not retain pore canals and hypodermis, and standard fixations offered superior preservation and visualization of these cellular constituents. Consequently, standard fixations reveal information about the physiological state of the hypodermis based on the number and types of organelles present. It also provides insights into how the chitin-protein fibers interact with the cellular components.

Third, UA fixations preserved the IPS and EZ, which were absent from standard-fixed samples. Interestingly, IPS were observed in early postmolt cuticle from *Carcinus maenas* when it was fixed in 3% glutaraldehyde, post-fixed in 1% OsO_4, and post-stained with UA and lead citrate (Giraud-Guille, 1984). This discrepancy can probably be attributed to the use of tannic acid in the present study. Although tannic acid can act as a mordant for UA, it has also been shown to inhibit the staining of sites that would otherwise react with UA alone (Afzelius, 1992). Moreover, Locke (1994) found that the treatment of tissues fixed with aldehyde and UA revealed structures not seen in osmicated tissues.

Fourth, in addition to enhancing contrast, UA caused fibers to appear more densely packed relative to standard fixation and lyophilized, rehydrated tissue. In UA preparations, the epicuticular roots appeared thinner and more distinct than in standard fixations. Moreover, in cross-sections, the vertical fibers often occupied electron lucent channels that were absent in standard fixations. The tight aggregation of fibers could be easily visualized when UA fixation was compared to lyophilized, rehydrated tissue. Fibers of lyophilized, rehydrated cuticle were much more dispersed than those of UA fixations, with the pcs's filling the pore canal lumens.

The final difference between UA and standard treatments was the uniformity of fixation. Cuticle fixed with UA yielded much more repeatable results with less variation. Although the appearance of the IPS and pore canals differed between samples, the morphology of the fibers was highly consistent. This suggests that UA may readily penetrate the cuticle. Alternately, UA may complex only a few components of the cuticle (ie. IPS, EZ, pore canal membranes) and therefore exert weak fixative abilities relative to its strong staining abilities. Moreover, since UA fixation closely resembled lyophilized, rehydrated cuticle, the quality of infiltration may be more difficult to discern than in standard fixation.

In contrast, the quality of fixation by standard treatments was highly variable depending on where the sample was sectioned, with edge pieces having better preservation than those from the interior. This phenomenon might be accounted for in at least three ways. First, the standard fixatives are large molecules that penetrate tissues very slowly. Next, the crustacean cuticle is very resistant to fixation due to its highly impenetrable lipo-protein epicuticle (Lindley, 1992). Consequently, the pieces of cuticle used in this study were probably too large to allow for complete infiltration. Finally, a change in the permeability of the outer epicuticle occurs between premolt and postmolt to create a closed microenvironment for calcification (Williams, 2000). This change was exemplified when premolt and postmolt cuticles were compared after being processed for the SEM. The outer surfaces of all premolt cuticles osmicated completely while those of postmolt cuticles only osmicated near the cut edges where the fixatives could diffuse laterally into the tissue. This change in permeability was not paralleled in ultrastructural investigations of the epicuticle. The morphology of the outer epicuticle varied between a trilaminar or pentalaminar structure but neither coincided exclusively to premolt or postmolt stages. It is possible that the variations in the outer epicuticle represent discrete snapshots into an ongoing structural modification. For instance, Compère et al. (1995) observed minor changes in the pentalaminar outer epicuticle in *Carcinus maenus* after exuviation.

Cuticle Fiber Types

The different appearances of UA and standard fixed cuticles along with the comparison of tangential sections, cross-sections, and anaglyphs permitted a more thorough understanding of the morphology of the late premolt and early postmolt dorsal carapace. From this analysis, a diversity of fiber types were described including horizontal fibers, various vertical fibers, and more specialized fibers associated with muscle insertions (Table 2). The more common vertical

Figure 27. a-d. Diagrams illustrating the various vertical fiber types and features within the cuticle as well as their distribution in tangential sections near the epicuticle, medial exocuticle, and proximal exocuticle. Each hexagonal prism represents the cuticle overlying a single hypodermal cell. a. Diagram showing the pore canals (pc) extending from hypodermal cells (H) and dense vertical fibers (dvf) extending down from the epicuticle (epi). b. Diagram showing the distribution of vertical fibers (vf) and the pore canal sheath (pcs). Note that vertical fibers are distal extensions of the more proximally located pore canal sheaths. c. Diagram showing the distribution of pore canal fibers (pcf). d. Diagram showing the distribution of anchoring fibers (af).

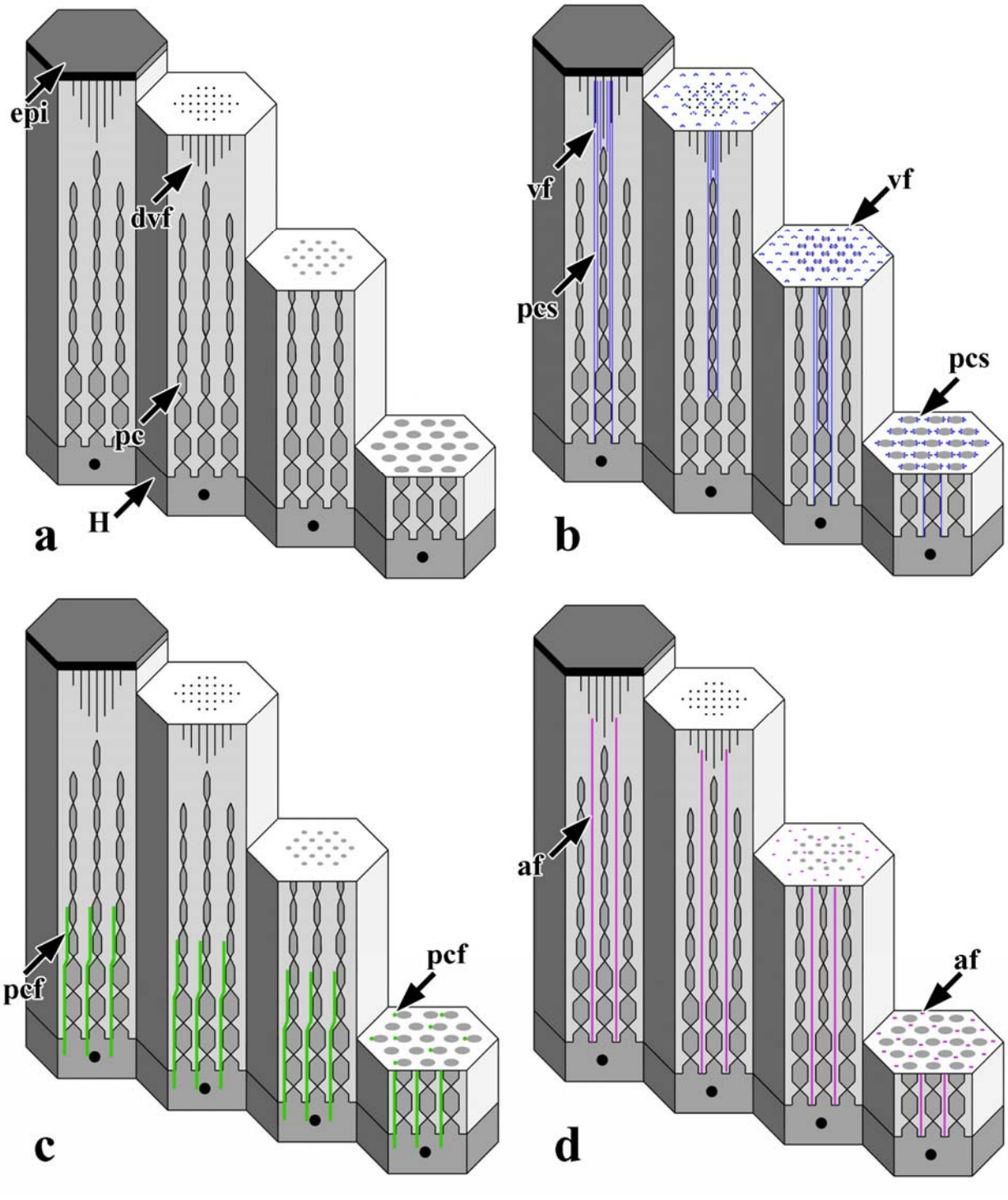
epi
dvf
pc
H
a
vf
pcs
vf
pcs
b
pcf
pcf
c
af
af
d

fiber types are illustrated in figure 27. The horizontal fibers, oriented parallel to the cuticle surface, both increased in diameter and changed orientation as one progressed from the epicuticle toward the hypodermis. Anaglyphs showed that these fibers rotate relative to one another in successive planes as described by Bouligand (1972). Unfortunately, anaglyphs in this study were only 800 nm thick and required magnifications that showed a rather small field of view. Consequently, the organization of horizontal fibers on a larger scale could not be determined and requires further investigation. In the TEM, the horizontal fibers were organized into discrete bundles that were laterally displaced by pore canals or vertical fibers. Such parting was also observed in the SEM, but the fibers appeared to be organized into continuous sheets rather than discrete bundles.

In addition to horizontal fibers, the cuticle was traversed by several types of vertical fibers. Among these were dvf that emanated from the lower boundary of the epicuticle and extended through only the distal portion of the exocuticle (Fig. 27a). Based on the location of these fibers and their intense staining with UA, which has a high affinity for charged sites (Hayat, 1993), they may play a role in the second phase of calcification. In the first phase beginning 3 hr after the molt, calcification of the exocuticle occurs at the epicuticle-exocuticle and exocuticle-endocuticle interface and then extends along the IPS. Calcium is originally deposited in the form of amorphous calcium carbonate. In the second phase, the prisms in-fill with calcium, with the distal regions of the exocuticle becoming more calcified than the proximal regions. The final phase, occurring at about 12 hr postmolt, involves the conversion of amorphous calcium carbonate into calcite along a front that mimics the initial calcification pattern (Dillaman et al., 2005). Since the dvf only occurred in the distal exocuticle within the

center of the prisms, they could possibly play a role as a secondary nucleator for calcification and allow the distal exocuticle to become more calcified than the proximal exocuticle.

Other fibers observed were the abundant, less electron dense vf and the pcs. The vf appeared to traverse most of the exocuticle in cross-sections but were only observed in the distal and medial exocuticle in tangential sections. Near the hypodermis, the vf were not observed but were instead replaced by numerous pore canals and their associated pcs's. Such an overlapping distribution suggests that the vf and the pcs's are probably the same structure. In *Carcinus maenas*, the pore canal processes undergo a periodic growth and degeneration during the molt cycle (Compère & Goffinet, 1987). Beginning at stage D_2, pore canals retract from the distal exocuticle as new lamellae are deposited. During postmolt, the pore canals degenerate at their distal ends, and the fibers of the pcs's fill the vacant lumen. The vf observed in the exocuticle in this study are probably the product of pore canal regression with the subsequent dissociation of the pcs's. The vf would therefore be contiguous with pore canals located more proximally (Fig. 27b).

Of the remaining vertical fibers observed, many appeared to partake in an anchoring function. The tf arose from depressions on the apical surface of muscle-associated tendinous epidermal cells and traversed the entire cuticle. They appeared consistent with fibers used for muscle attachment in the insects *Calpodes ethlius* and *Rhodnius prolixus* (Lai-Fook, 1967) and the larval brown shrimp, *Penaeus aztecus* (Talbot et al., 1972). Intracellularly, the tf were anchored by an extensive network of microtubules. Within the upper exocuticle, clusters of electron dense rods were observed in conjunction with tf. In the brown shrimp, tf (referred to as intracuticular fibers), were found associated with tendinous epidermal cells and supporting cells that form a bridge between the outer cuticle and inner cuticle lining the branchial chamber. The

rods, however, were only observed in the outer cuticle and were not restricted to sites of muscle insertion. The tf were proposed to function in attachment while the rods were presumed to offer additional support to discrete areas of the cuticle subjected to stress (Talbot et al., 1972). Nevertheless, such an extensive extracellular arrangement of fibers and rods and intracellular bundles of microtubules must provide associated muscles with a substantial amount of leverage by which to contract and transmit force.

While the tf were localized to regions of muscle attachment, af were more uniformly distributed. These fibers first appeared near the hypodermis as thin electron dense vertical fibers and were observed extending throughout a large portion of the exocuticle (Fig. 27d). If these fibers are the cuticle-secreting cell analog of tf, it is possible that the af may also span the epicuticle, perhaps being contiguous with the fibers residing in the epicuticular canals. The af most likely provide discrete attachment sites that connect the hypodermis to the overlying cuticle. Such fibers could be critical during ecdysis and prevent the newly synthesized cuticle from peeling away from the underlying epithelium.

Finally, some pore canals were associated with a pcf. The pcf's appeared similar to tf in that they arose from depressions in the hypodermal cell membrane and were anchored intracellularly by a ring of microtubules. The fiber was closely associated with or attached to the extracellular face of the pore canal membrane. Such an arrangement likely provides support to growing pore canals. In conjunction with the pcs, the pcf's may also maintain pore canal structure after ecdysis when the highly folded cuticle expands.

Pore Canals

Although pore canal distribution was studied by Compère & Goffinet (1987) for *Carcinus maenas* across the entire molt cycle, the use of tangential sections in this project

revealed additional information about pore canal distribution in the cuticle of the blue crab around the time of ecdysis. Pore canals were completely absent in the distal exocuticle. Small pore canals initially appeared at the level where the dvf diminished. The pore canals first arose in small discrete groups located within the center of the prisms defined by the IPS (Fig. 27a). Since the IPS are considered to be the outlines of the underlying hypodermal cells, these pore canals would have arisen from the centers of the underlying cells. Both the groups and diameter of the pore canals themselves became increasingly larger more proximally (Fig. 27a). Near the hypodermis, pore canals were so numerous that no discrete groups are observed, and they assumed a more uniform distribution. The ordered spatial organization of the pore canals suggests that the cytoplasmic processes undergo a degenerative process that follows a specific temporal sequence.

According to Compère and Goffinet (1987) in *Carcinus maenas*, pore canals initially extend up to the epicuticle in early D_2 but, in subsequent stages, degenerate. It appears that pore canal degeneration also occurs in the blue crab, but with an added dimension. Based on pore canal distribution, the first pore canals to degenerate are those located along the lateral margins of each underlying hypodermal cell. Over time, pore canals sub-adjacent to the lateral margins degenerate next followed by those located even more medially. Pore canals, therefore, degenerate in a step-wise fashion from the edge to the middle of the cell, forming a tiered structure similar to a wedding cake (Fig. 27a). This pattern of pore canal regression is mirrored by the distribution of dense vertical fibers extending from the epicuticle (Fig. 27a). The distribution of pore canals and dense vertical fibers suggests that the hypodermal cells exhibit a lateral polarity across their apical membrane. This polarity may account for the early calcification pattern that occurs along the IPS.

Both premolt and postmolt crabs exhibited this tiered arrangement of pore canals, but the pore canals of premolt crabs appeared to have a greater size variation. For within a given sectioning plane, pore canals of premolt crabs ranged in size from large, dilated cytoplasmic processes to those having a small and shriveled appearance whereas those of postmolt crabs exhibited a more uniform appearance. Such a discrepancy could be attributed to several possible factors. First, it is possible that more pore canals were observed in a degenerative state in the premolt than in the postmolt samples. Alternatively, pore canals of premolt crabs may contain a more variable ionic content than postmolt crabs. Since pore canals have been shown to act as conduits for calcium ions (Dillaman et al., 2005), the dilated or crenated appearance of pore canals may be attributed to osmotic swelling or shrinking. As a final possibility, the dilated appearance of premolt pore canals may be a function of the highly folded state of the cuticle before ecdysis. Upon ecdysis and expansion of the cuticle, the pore canals may become stretched causing their diameters to decrease and become more uniform in postmolt crabs.

Interprismatic Septa (IPS)

In UA fixations, the EZ and the IPS were visible. The IPS were polygonal structures that stained intensely in the distal exocuticle but gradually faded with depth until becoming entirely absent in the proximal exocuticle. Since the initial deposition of calcium occurs along the EZ and IPS, discovering the composition of these structures is critical to understanding the processes controlling calcification in the crab (Dillaman et al., 2005).

By knowing the staining and fixative properties of UA, one could postulate a number of components that may be present in the EZ and IPS. UA has a high affinity toward molecules rich in phosphates, but it will also complex with cationic or anionic proteins. The staining intensity appears to be related to the amount of charge carried by the molecule (Hayat, 1993).

UA has also been shown to strongly complex with carbonate ions (Piron et al., 1997). Moreover, the IPS and EZ were not apparent in lyophilized, rehydrated tissue, suggesting they were either extracted by water or simply not stained. Consequently, the EZ and IPS are likely to contain highly charged, water-soluble molecules.

Although the complete chemical makeup of the IPS is not known, efforts had been made to reveal its constituents. Studies by Giraud-Guille (1984) and Tweedie et al. (2004) found that the IPS have a high protein content. Moreover, anionic glucosaminoglycans were found to be present in the EZ and distal portions of the IPS while carbonic anhydrase was also localized in the IPS by the Hansson reaction (Giraud-Guille, 1984). Studies have also shown differential binding to the IPS by α-D-mannose specific lectins (ConA). Near the epicuticle, the IPS, but not the prisms, bound the lectin while more proximally, the prisms, rather than the IPS, exhibited ConA affinity (Marlowe et al., 1994). Together these investigations would suggest that the IPS contain multiple constituents whose combined actions may contribute to both the inhibition and nucleation of calcium carbonate crystals.

In fact, earlier studies by Hegdahl et al. (1977) found that the EZ was more heavily calcified than the rest of the exocuticle. Their study also reported variations in the radiodensity for both the IPS and prisms of intermolt crabs. Some IPS exhibited a radiodensity greater than that of the prisms while others failed to diffract X-rays. Later work concluded that the EZ and IPS are sites that initially deposit stable amorphous calcium carbonate and subsequently transform the mineral into calcite (Dillaman et al., 2005). Since amorphous calcium carbonate is transparent to X-rays (Prenant, 1927 cited from Addadi et al., 2003), the variations in IPS radiodensity reported by Hegdahl et al. (1977) may be attributed to the presence of amorphous calcium carbonate in certain regions of the IPS of fully calcified intermolt crabs. These previous

investigations suggest that the IPS exhibit both a functional and chemical polarity whereby IPS preferentially deposit amorphous calcium carbonate in some regions and calcite in others. Fixation by UA in this study also revealed a morphological polarity of the IPS whereby only the IPS in the distal exocuticle stained.

UA staining has been highly correlated with the phosphate content of proteins, nucleic acids, and inorganic deposits (Brodie et al., 1982). Moreover, those macromolecules that participate in mineralization are highly acidic, with aspartic acid, glutamic acid, or phosphorylated residues (Lowenstram & Weiner, 1989). Consequently, the intensely staining distal IPS and EZ may contain proteins or glycoproteins with a high phosphate composition. Indeed, alkaline phosphatase activity has been localized to the junction between the inner epicuticle and exocuticle during late premolt and early postmolt (Travis, 1963). The presence of phosphates may have important implications in both the inhibition of calcite mineralization and nucleation of the amorphous phase. Both organic macromolecules and inorganic ions such as magnesium and phosphate have been implicated in the stabilization of amorphous phases (Levi-Kalisman et al., 2000; Raz et al., 2002; Addadi et al., 2003). Moreover, these same ions also inhibit calcite mineralization and allow calcium and carbonate ions to reach supersaturated levels favorable to the formation of amorphous minerals (Reddy, 1977; Raz et al., 2002). Therefore, inorganic constituents of the IPS in addition to associated glycoproteins may act in conjunction to control calcification.

Even more intriguing than the appearance of the EZ and IPS by UA fixation was the variation in staining intensity among samples. In some samples, both the IPS and EZ stained intensely, being comprised of an electron dense globular material attached to the fibers. Meanwhile, in other samples, the EZ was absent and the IPS either stained faintly or very

prominently. Although both variations occurred in premolt and postmolt crabs, premolt crabs, in general, exhibited a stronger staining pattern than postmolt crabs. Such variation could be attributed to poor infiltration and the formation of a permeability barrier in the outer epicuticle at postmolt, which was a common problem for standard fixations. However, the appearance of the fibers in UA fixations was highly consistent among samples, suggesting that UA may penetrate the cuticle more easily than glutaraldehyde and osmium tetroxide. Moreover, if infiltration were an issue, one would not expect to see intensely staining IPS in the absence of an EZ.

Consequently, the variation in staining of the IPS and EZ may represent a significant biochemical change that is occurring in the cuticle around the time of ecdysis. Previous work by Shafer et al. (1995) revealed a post-ecdysial cuticle alteration (PECA) that occurred 1-3 hours postmolt. The PECA involved the disappearance of a 69 kDa and 71 kDa glycoprotein band with an accompanying loss of PAS and ConA reactivity. These changes correlated with the ability of cuticle to nucleate calcite crystals. Subsequently, cuticle proteins were isolated at numerous times post-ecdysis by various extraction methods, and their ability to bind calcium carbonate crystals was assessed. Some small crystal associated proteins (CAPs) persisted throughout the molt and were proposed to function as nucleators. Other large CAPs, identical in molecular mass to those described in the PECA, persisted until one hour post-ecdysis. The larger CAPs were considered to act as inhibitors of nucleation until being modified by proteolytic cleavage or deglycosylation (Coblentz et al., 1998). One of the inhibitory CAPs was purified by Tweedie et al. (2004) and an antibody was raised against it for immunohistochemistry. Results showed that the protein was uniformly present throughout the cuticle until 2 hr postmolt whereupon the IPS exhibited decreased antigenicity toward the antibody.

These previous studies suggest that a series of deglycosylations or proteolytic cleavages may be occurring prior to the onset of mineralization. Consequently, the variation in staining intensity of the EZ and IPS by UA may reflect these changes. If nothing else, the decreased staining intensity suggests that specific regions of the exocuticle are losing a substantial amount of charge and, hence, decreased affinities for UA. It is interesting to note that the loss of intense staining of the EZ seemed to precede the loss of staining in the IPS. This sequence parallels the early calcification pattern described by Dillaman et al. (2005).

As a final note on the morphology of the cuticle, lyophilization clearly caused the appearance of tubular artifacts throughout the exocuticle due to the formation of ice crystals that displaced the surrounding ground substance and fibers. Although this artifact is not a true structure, it reveals important information about the state of the cuticle as it would exists *in vivo*. The formation of the tubes in lyophilized samples suggests that the cuticle contains a very high water content during late premolt and early postmolt. With the use of a cryo-TEM, Levi-Kalisman et al. (2001) were able to examine the nacreous layer of a decalcified mollusk in a hydrated state. From their observations, they postulated that the organic matrix existed as a hydrated gel. A similar hydrated gel may also occur in the matrix of the crab cuticle and could have important functional implications. A hydrated gel could create pathways for the diffusion of calcium and bicarbonate ions. Moreover, a gel-like matrix may be conducive to the formation of stable amorphous calcium carbonate. Stable amorphous calcium carbonate exists in a hydrated form and would likely crystallize when placed in an aqueous compartment (Addadi et al., 2003). The deglycosylations associated with the onset of mineralization may not only reveal nucleation sites but they may also liberate bound water from the gel and promote the conversion of amorphous calcium carbonate into calcite.

Summary

In summary, the observed morphology of dorsal carapace is highly dependent upon physical and chemical fixations. Standard fixation preserved the cuticle matrix and the hypodermis. However, it offered inadequate contrast for making anaglyphs and yielded variable results due to poor infiltration. The large molecular size of chemical fixatives, the impervious nature of the cuticle, and the formation of a permeability barrier by 1 hr postmolt contributed to suboptimal fixation. UA fixation, on the other hand, greatly improved the visualization of fibers, allowing their three-dimensional arrangement to be investigated with anaglyphs, but it did not preserve the hypodermis. Moreover, UA exposed the IPS and EZ, both key features likely to be involved with controlling calcification, which were not apparent in standard fixations. Examination of cuticle using both techniques revealed a diverse collection of horizontal fibers, oriented parallel to the cuticle surface, and vertical fiber types, oriented perpendicular to the cuticle surface. Horizontal fibers rotated in successive planes. Of the vertical fiber types observed, some were associated with pore canals, others were not, and certain ones were restricted to specialized regions of the cuticle. Quick-freezing caused tubular voids to appear in the epicuticle and between the horizontal fibers of the exocuticle due to the formation of ice crystals. Such freeze artifacts were accentuated by lyophilization. Distortion of horizontal fibers was more pronounced in quick-frozen and lyophilized cuticles treated by standard fixation than in quick-frozen and lyophilized cuticles fixed in UA alone. Lyophilized, unfixed samples had an intricate, nonfibrous latticework morphology consisting of rows of tubes rotating in successive planes. Tubular voids were rounded and elongate in shape and paralleled the horizontal fibers. Rehydration of lyophilized cuticles reconstituted the fibrous matrix. This treatment caused the cuticle to most closely resemble UA fixation but made fibers more

dispersed. All fiber types described in chemically fixed samples were present in lyophilized, rehydrated samples except the IPS and EZ. Although the tubular morphology is an artifact caused by ice formation, it alludes to the highly hydrated state of the late premolt and early postmolt cuticle. This study has demonstrated that applying multiple fixation procedures allows a more thorough understanding of cuticle structure. This information will provide opportunities for future immunocytochemical and functional studies to correlate specific cuticle features with the physiological and biochemical processes controlling cuticle deposition and mineralization.

LITERATURE CITED

Addadi, L, Raz, S, Weiner, S. 2003. Taking advantage of disorder: Amorphous calcium carbonate and its role in biomineralization. Adv Mater 15: 959-970.

Afzelius, BA. 1992. Section staining for electron microscopy using tannic acid as a mordant: A simple method for visualization of glycogen and collagen. Microsc Res Tech 21: 65-72.

Andrews, SC, Dillaman, RM. 1993. Ultrastructure of the gill epithelium in the crayfish *Procambrus clarkia* at different stages of the molt cycle. J Crust Biol 13 77-86.

Blackwell, J, Weih, MA. 1980. Structure of chitin-protein complexes: Ovipositor of the ichneumon fly *Megarhyssa*. J Mol Biol 137: 49-60.

Bouligand, Y. 1972. Twisted fibrous arrangements in biological materials and cholesteric mesophases. Tissue Cell 4: 189-217.

Bozzola, JJ, Russell, LD. 1999. Electron microscopy: Principles and techniques for biologists, 2nd ed. Sudbury: Jones and Bartlett Publishers, Inc. p 15-38.

Brodie, DA, Huie, P, .Locke, M, Ottensmeyer, FP. 1982. The correlation between bismuth and uranyl staining and phosphorus content of intracellular structures as determined by electron spectroscopic imaging. Tissue Cell 14: 621-627.

Coblentz, FE, Shafer, TH, Roer, RD. 1998. Cuticular proteins from the blue crab alter *in vitro* calcium carbonate mineralization. Comp Biochem Physiol B 121: 349-360.

Compère, P. 1995. Fine structure and morphogenesis of the sclerite epicuticle in the Atlantic shore crab *Carcinus maenas*. Tissue Cell 27: 525-38.

Compère, P, Goffinet, G. 1987. Elaboration and ultrastructural changes in the pore canal system of the mineralized cuticle of *Carcinus maenas* during the moulting cycle. Tissue Cell 19: 859-875.

Compère, P, Jaspar-Versali, M, Goffinet, G. 2002. Glycoproteins from the cuticle of the Atlantic shore crab *Carcinus maenas*: I. Electrophoresis and western-blot analysis by use of lectins. Biol Bull 202: 61-73.

Compère, PA, Goffinet, TG. 1998. Fine structural survey of old cuticle degradation during pre-ecdysis in two European Atlantic crabs. Tissue Cell 30: 41-56.

Dillaman, RM, Hequembourg, S, Gay, M. 2005. Early pattern of calcification in the dorsal carapace of the blue crab, *Callinectes sapidus*. J Morphol 263: 356-374.

Drach, P. 1939. Mue et cycle d'intermue chez les crustacés décapodes. Annls Inst oceanogr, Monaco 19: 103-391.

Edelmann, L. 1986. Freeze-dried embedded specimens for biological microanalysis. Scan Electron Microsc 4: 1337-1356.

Elliot, EA, Dillaman, RM. 1999. Formation of the inner branchiostegite cuticle of the blue crab, *Callinectes sapidus*. J Morph 240: 267-281.

Fassel, TA, Greaser, ML. 1997. Uranyl acetate as a primary fixative for skeletal muscle. Microsc Res Tech 37: 600-601.

Gilkey, JG, Staehelin, A. 1986. Advances in ultrarapid freezing for the preservation of cellular ultrastructure. J Electron Microsc Tech 3: 177-210.

Giraud-Guille, M. 1984. Calcification initiation sites in the crab cuticle: The interprismatic septa. Cell Tissue Res 236: 413-420.

Giraud-Guille, M. 1994. Liquid crystalline order of biopolymers in cuticles and bones. Microsc Res Tech 27: 420-428.

Giruad-Guille, M. 1984. Fine structure of the chitin-protein system in the crab cuticle. Tissue Cell 16: 75-92.

Green, JP, Neff, MR. 1972. A survey of the fine structure of the integument of the fiddler crab. Tissue Cell 4: 137-171.

Greenway, P, Dillaman, RM, Roer, RD. 1995. Quercitin-dependent ATPase activity in the hypodermal tissue of *Callinectes sapidus* during the moult cycle. Comp Biochem Physiol A 111: 303-312.

Hayat, MA. 1993. Stains and cytochemical methods. New York: Plenum Press. p 23-31; 336-346; 353-362.

Hayat, MA. 2000. Principles and techniques of electron microscopy: Biological applications, 4th ed. Cambridge: Cambridge University Press. p 4-62; 334-350; 400-421.

Hegdahl, T, Gustavsen, F, Silness, J. 1977. The structure and mineralization of the carapace of the crab (*Cancer pagarus* L.). Zool Scr 6: 101-105.

Inoue, H, Ozaki, N, Nagasawa, H. 2001. Purification and structural determination of a phosphorylated peptide with anti-calcification and chitin-binding activities in the exoskeleton of the crayfish, *Procambarus clarkii*. Biosci Biotechnol Biochem 65: 1840-1848

Inoue, H, Ohira, T, Ozaki, N, Nagasawa, H. 2003. Cloning and expression of a cDNA encoding a matrix peptide associated with calcification in the exoskeleton of the crayfish. Comp Biochem Physiol B Biochem Mol Biol 136: 755-765.

Inoue, H, Ohira, T, Ozaki, N, Nagasawa, H. 2004. A nocel calcium-binding peptide from the cuticle of the crayfish, *Procambarus clarkia*. Biochem Biophys Res Commun 318: 649-654.

Lai-Fook, J. 1967. The structure of developing muscle insertions in insects. J Morphol 123: 503-528.

Levi-Kalisman, Y, Falini, G, Weiner, S. 2001. Structure of the nacreous organic matrix of a bivalve mollusck shell examined in the hydrated state using cryo-TEM. J Struct Biol 135: 8-17.

Levi-Kalisman, Y, Raz, S, Weiner, S, Addadi, L, Sagi, I. 2000. X-ray absorption spectroscopy studies on the structure of a biogenic "amorphous" calcium carbonate phase. J Chem Soc Dalton Trans 21: 3977-3982.

Lindley, VA. 1992. A new procedure for handling impervious biological specimens. Microsc Res Tech 21: 355-360.

Locke, M. 1961. Pore canals and related structures in insect cuticle. J Biophys Biochem Cytol 10: 589-618.

Locke, M. 1994. Preservation and contrast without osmication or section staining. Micros Res Tech 29: 1-10.

Lowenstam, HA, Weiner, S. 1989. On biomineralization. New York: Oxford University Press. p 25-50.

Marlowe, RL, Dillaman, RM, Roer, RD. 1994. Lectin binding by crustacean cuticle: The cuticle of *Callinectes sapidus* throughout the molt cycle, and the intermolt cuticle of *Procambrus clarki* and *Ocypode quadrata*. J Crust Biol 14: 231-246.

Merzendorfer, H, Zimoch, L. 2003. Chitin metabolism in insects: structure, function and regulation of chitin synthases and chitinases. J Exp Biol 206: 4393-4412.

Miller, KR, Prescott, CS, Jacobs, TL, Lassingnal, NL. 1983. Artifacts associated with quick-freezing and freeze-drying. J Ultrastruct Res 82: 123-133.

Mutvei, H. 1974. SEM studies on arthropod exoskeletons. Part. I. Decapod crustaceans, *Homarus gammarus* and *Carcinus maenas.* Bull Geol Instr 45:73–80.

Mykles, DL. 1980. The mechanism of fluid absorption at ecdysis in the American lobster, *Homarus americanus*. J Expt Biol 84: 89-101.

O'Brien, JJ, Skinner, DM. 1987. Characterization of enzymes that degrade crab exoskeleton: I. Two alkaline cysteine proteinase activities. J Exp Zool 243: 389-400.

O'Brien, JJ, Skinner, DM. 1988. Characterization of enzymes that degrade crab exoskeleton: II. Two acid proteinase activities. J Exp Zool 246: 124-131.

Prenant, M. 1927. Les formes minéralogiques du calcaire chez les êtres vivants, et le probléme de leur déterminisme. Biol Rev 2: 365-394.

Prion, E, Domard, A. 1997. Interaction between chitosan and uranyl ions: Part 1. Role of physicochemical parameters. Int J Biol Macromol 21: 327-335.

Raz, S, Testeniere, O, Hecker, A, Weiner, S, Luquet, G. 2002. Stable amorphous calcium carbonate is the main component of the calcium storage structures of the crustacean *Orchestia cavimana*. Biol Bull 203: 269-274.

Reddy, MM. 1977. Crystallization of calcium carbonate in the presence of trace concentrations of phorphorous-containing anions. J Cryst Growth 41: 287-295.

Reynolds ES. 1963. The use of lead citrate at high pH as an electron opaque stain in electron microscopy. J Cell Biol 17: 208-212.

Roer RD, Dillaman R M. 1993. Molt-related changes in integumental structure and function. In: Horst MN, editor. The crustacean integument: morphology and biochemistry. Boca Raton: CRC Press. pp 2-37.

Roer, R D, Bugess, SK, Miller, CB, Dail, MB. 1988. Control of calcium carbonate nucleation in pre- and postecdysial crab cuticle. *In*: C S Sikes and A P Wheeler, eds., Chemical aspects

of regulation of mineralization. Mobile: University of South Alabama Publication Service. p 21-24.

Roer, R. 1980. Mechanisms of resorption and deposition of calcium in the carapace of the crab *Carcinus maenas*. J Exp Biol 88: 205-218.

Sannes, PL, Katsuyama, T, Spicer, SS. 1978. Tannic acid-metal salt sequences for light and electron microscopic localization of complex carbohydrates. J Histochem Cytochem 26: 55-61.

Scouten, CW, Cunningham, M. 2006. Freezing biological samples. Microscopy Today 14: 48.

Shafer, T, Roer, RD, Miller, CG, Dillaman, RM. 1994. Postecdysial changes in the protein and glycoprotein composition of the cuticle of the blue crab, *Callinectes sapidus*. J Crust Biol 14: 210-219.

Shafer, TH, Roer, RD, Midgette-Luther, C, Brookins, TA. 1995. Postecdysial cuticle alteration in the blue crab, *Callinectes sapidus*: Synchronous changes in glycoprotein and mineral nucleation. J Exp Zool 271: 171-182.

Spurr RA. 1969. A low-viscosity epoxy resin embedding medium for electron microscopy. J Ultrastruct Res 26: 31-43.

Talbot, P, Clark, WH, Lawrence, AL. 1972. Ultrastructural observations of the muscle insertion and modified branchiostegite epidermis in the larval brown shrimp, *Penaeus aztecus*. Tissue Cell 4: 613-628.

Taylor, RA, Kier, WM. 2003. Switching skeletons: Hydrostatic support in molting crabs. Science 301: 209-210.

Tchernigovtzeff C. 1965. Multiplication celulaire et régénération au cours du cycle d'intermue des crustacés décapodes. Arch Zool Exp Gen 106: 377-529.

Travis, D, Friberg, U. 1963. The deposition of skeletal structures in the crustacea. VI. Microradiographic studies of the exoskeleton of the crayfish *Orconectes virilis* Hagen. J Ultrastruct Research 9: 285-301.

Travis, DF. 1963. Structural features of mineralization from tissue to macromolecular levels of organization in the decapod crustacea. Ann NY Acad Sci 109: 117-245.

Tweedie, EP, Coblentz, FE, Shafer, TH. 2004. Purification of a soluble glycoprotein from the uncalcified ecdysial cuticle of the blue crab *Callinectes sapidus* and its possible role in initial mineralization. J Exp Biol 207: 2589-2598.

Weis-Fogh, T. 1970. Structure and formation of insect cuticle. Roy Entomol Soc Lond 5: 165-185.

Williams, DL. 2000. The formation of a permeability barrier within the crab cuticle after the molt. Master's Thesis, The University of North Carolina at Wilmington.

Williams, CL, Dillaman, RM, Elliot, EA, Gay, DM. 2003. Formation of the arthrodial membrane in the blue crab, *Callinectes sapidus*. J Morph 256: 260-269.